

CHARACTERISATION OF HIGH TEMPERATURE SUPERCONDUCTING COMPOUND BY X-RAY AND OTHER TECHNIQUES

**THESIS
SUBMITTED TO
THE UNIVERSITY OF KERALA
IN PARTIAL FULFILMENT
OF THE REQUIREMENTS
FOR THE DEGREE OF
DOCTOR OF PHILOSOPHY IN PHYSICS**

**BY
SIMON AUGUSTINE**

REGIONAL RESEARCH LABORATORY (CSIR)

**THIRUVANANTHAPURAM LIBRARY & INFORMATICS 95 019
CENTRE FOR DOCUMENTATION AND INFORMATION SCIENCE (CSIR) TRIVANDRUM**



G1605

NOVEMBER 1992

Dedicated to

My Parents & Uncle

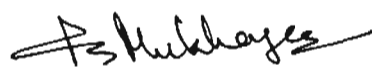
DECLARATION

I, SIMON AUGUSTINE, hereby declare that this thesis entitled "Characterisation of High Temperature Superconducting Compound by X-ray and other Techniques" is a bonafide record of research work done by me and that no part of this thesis has been presented earlier for any degree or diploma of any other Universities.


SIMON AUGUSTINE

CERTIFICATE

This is to certify that the thesis entitled "Characterisation of High Temperature Superconducting Compound by X-ray and other Techniques" is an authentic record on the research work carried out by Mr. Simon Augustine, M.Sc. under my supervision in partial fulfilment of the requirement for the Degree of Doctor of Philosophy of the University of Kerala and further that no part of this thesis has been presented before for any other degree.



*Dr. P.S. Mukherjee
Scientist, BSMR Division
Regional Research Laboratory (CSIR)
Thiruvananthapuram 695 019 (India)*

C O N T E N T S

	Page
ACKNOWLEDGEMENTS	i
PREFACE	iii
LIST OF PUBLICATIONS	v
LIST OF FIGURES	viii
LIST OF TABLES	xiii
CHAPTER 1	
1 GENERAL INTRODUCTION	1
1.1 Superconductivity, The phenomenon	1
1.2 High temperature superconductors	1
1.2.1 Superconductivity in Y-Ba-Cu-O system	2
1.2.2 Superconducting bismuth cuprates	2
1.2.3 Thallium cuprate superconductors	3
1.2.4 Other high temperature superconducting phases	3
1.3 Structure of $\text{YBa}_2\text{Cu}_3\text{O}_{7-\delta}$	5
1.4 Anisotropy in YBCO	5
1.5 Phase transformation in YBCO	10
1.6 Oxygen stoichiometry, oxygen ordering and superconducting properties	13
1.7 Phase diagram of Y_2O_3 -BaO-CuO system	15
1.8 Preparative methods	17
1.8.1 Ceramic route	17
1.8.2 Chemical route	17

CHAPTER	Page
1.9 Fabrication of YBCO for practical applications	18
1.9.1 Powder process	18
1.9.2 Melt process	19
1.9.3 Thin films and thick films	19
1.10 Single crystal growth	20
1.11 Some basic properties of $\text{YBa}_2\text{Cu}_3\text{O}_{7-\delta}$	20
1.12 Difficulties for practical applications and solutions	21
1.12.1 Low critical current density	21
1.12.2 Reaction with water	23
1.12.3 Brittleness	24
1.12.4 Possible solutions	24
1.13 Structure of bismuth cuprates	25
1.14 Aim, scope and objective of the present work	27
References	31
2 EXPERIMENTAL METHODS AND INSTRUMENTAL TECHNIQUES	42
2.1 Introduction	42
2.2 Transition temperature (T_c) measurement	42
2.3 Critical current density measurements	44
2.4 XRD analysis	44
2.5 Microscopic techniques	48
2.6 Thermal methods of analysis	49
2.7 Determination of oxygen stoichiometry by iodometric titration	51
References	53

PART A

CHAPTER		Page
3	STUDIES ON TEXTURED GRAIN GROWTH IN YBCO UNDER DIFFERENT OXYGEN PARTIAL PRESSURES AND TEMPERATURES	
		54
3.1	Introduction	54
3.2	Experimental	54
3.2.1	Measurement of textured grain growth	58
3.3	Results and discussion	64
3.3.1	Effect of oxygen partial pressure	64
3.3.2	Effect of temperature	71
3.3.3	Effect of oxygen partial pressure and temperature	76
3.3.4	Effect of soaking period	80
3.4	Conclusion	80
	References	84
4	STUDIES ON TEXTURED GRAIN GROWTH IN $\text{YBa}_2\text{Cu}_3\text{O}_{7-\delta}$ BY ALKALI METALS SUBSTITUTION	
		87
4.1	Introduction	87
4.2	Experimental	89
4.3	Result and discussion	89
4.4	Conclusion	97
	References	98
5	MECHANISM FOR ENHANCED TEXTURED GRAIN GROWTH UNDER DIFFERENT OXYGEN PARTIAL PRESSURES, TEMPERATURES AND SUBSTITUTIONS	
		99
5.1	Introduction	99
5.2.	Description of the model	102
5.2.1	Effect of Po_2 on textured grain growth	102
5.2.2	Effect of alkali metals substitutions on textured grain growth	102

CHAPTER		Page
PART B		
7	SYNTHESIS OF PHASE PURE $Y_1Ba_2Cu_3O_{7-\delta}$ BY DYNAMIC VACUUM CALCINATION AND ITS CHARACTERISATION	136
	7.1 Introduction	136
	7.2 Experimental	138
	7.2.1 Experimental set up	138
	7.2.2 Processing of YBCO by dynamic vacuum calcination	138
	7.3 Results and discussion	140
	7.4 Conclusion	147
	References	149
PART C		
8	VARIATION OF STRUCTURAL AND SUPERCONDUCTING PROPERTIES WITH INITIAL STOICHIOMETRY VARIATION IN (Bi,Pb)-Sr-Ca-Cu-O BULK SUPERCONDUCTOR	150
	8.1 Introduction	150
	8.2 Experimental	151
	8.3 Results and discussion	153
	8.3.1 Effect of Pb-doping	153
	8.3.2 Effect of Sr, Ca and Cu variations	155
	8.3.3 Effect of impurity phases on J_c	159
	8.3.4 Best initial stoichiometry	163
	8.3.5 Effect of soaking period HTf	163
	8.3.6 Effect of soaking period on T_{001}	165
	8.4 Conclusion	167
	References	168

CHAPTER		Page
9	STUDIES ON TEXTURED GRAIN GROWTH IN BPSCCO AND PREPARATION AND CHARACTERISATION OF TEXTURED SINTERED BULK BPSCCO BY SUSPENSION METHOD	169
	9.1 Studies on textured grain growth in BPSCCO	169
	9.1.1 Introduction	169
	9.1.2 Experimental	169
	9.1.3 Results and discussions	170
	9.2 Preparation and characterisation of textured sintered BPSCCO bulk by suspension method	172
	9.2.1 Introduction	172
	9.2.2 Experimental	177
	9.2.3 Results and discussion	179
	9.3 Conclusions	181
	References	182
10	SUPERCONDUCTING AND MECHANICAL PROPERTIES OF (Bi,Pb)-Sr-Ca-Cu-O/Ag COMPOSITE	183
	10.1 Introduction	183
	10.2 Experimental	184
	10.3 Results and discussion	184
	10.3.1 Superconducting properties of BPSCCO/Ag composite	184
	10.3.2 Mechanical properties of BPSCCO/Ag composite	192
	10.4 Conclusion	194
	References	197
	SUMMARY	198

ACKNOWLEDGEMENTS

I wish to express my deep sense of gratitude and indebtedness to Dr. P.S. Mukherjee, Scientist, Regional Research Laboratory, Thiruvananthapuram (RRL-T) for his constant encouragement, valuable guidance and continual support given to me throughout the course of this work.

I am extremely grateful to Dr. A.D. Damodaran, Director, RRL-T, for his keen interest, suggestions and encouragement during the period of this research. I am also thankful to him for extending all the facilities to carry out the work.

I am indebted to Mr. M. Sankara Sarma, RRL-T for his timely help and friendship and my sincere thanks are due to Mr. P. Guruswamy, RRL-T for his help throughout the work.

I take this opportunity to thank Dr. C. Pavithran, Prof. J. Koshy and Dr. K. Ravindran Nair of RRL-T, Dr. U. Balachandran, Argonne National Laboratory, USA, Dr. T.R.N. Kutty, IISc, Bangalore, Dr. B.V. Mohan, BHEL, Bangalore, and Dr. P. Murugaraj, CEMET, Trichur, for their useful discussions and suggestions during this work.

I thank Dr. K.G. Satyanarayana and Dr. (Mrs.) M. Lalithambika of RRL-T for all the help rendered to me when I was in their respective Divisions.

My sincere thanks are due to Mr. Peter Koshy, Dr. K.G.K. Warriar, Mr. K. Sukumaran, Mr. V.S. Prasad, Mrs. Prasanna Kumari, Mr. S.G.K. Pillai, Mr. K.K. Ravikumar, Mr. Krishna Pillai,

Mrs. Rugmini Sukumar of RRL-T and Prof. K.C. Patil of IISc, Bangalore, and Dr. A. Sequeira of BARC, Bombay, for their help in different instrumental methods used in this study.

I acknowledge with thanks Dr. C.S. Narayanan and Mr. K.P. Sadasivan of RRL-T and Prof. V.K. Vaidyan, Dept. of Physics, University of Kerala, Thiruvananthapuram, for their help during this work.

I have great pleasure to acknowledge the friendship and support of Mr. George John during the entire research period.

I acknowledge the affectionate friendship of Mr. K.P. Kumar, Mr. H.K. Varma, Mrs. P. Umadevi, Mr. K.V. Paulose, Mr. Anil Kumar, Mr. C. Mohan Kumar and Dr. George Thomas in the course of this work.

I make use of this opportunity to express my heartfelt thanks to Mr. M. Brahmakumar for making my stay at Thiruvananthapuram a pleasant one.

Help rendered by Messers P. Vijayakumar, R. Babu and N. Gopinathan in the preparation of this thesis is duly acknowledged.

I acknowledge with thanks staff of RRL-T for their kind cooperation and support at various stages of my dissertation work.

I acknowledge the Council of Scientific and Industrial Research (CSIR), New Delhi, for the financial support during the course of this work.

There still remains many other names to be remembered. I extend my heartfelt thanks to one and all of them.


SIMON AUGUSTINE

PREFACE

The discovery of high temperature superconductors has generated great interest all over the world because of its immense practical importance. From the initial stages of development itself, it has become clear that these new brand of ceramic materials exhibit a number of difficulties for practical applications. The main hurdles were the low transport critical current density (J_c) in bulk and brittleness. Efforts to overcome these hurdles have been initiated based on the observation of high J_c of the order of $10^6 - 10^7$ A/cm² in single crystals and epitaxially grown thin films. Also, from the single crystal studies it was found that J_c along ab-planes is at least one order of magnitude higher than that along c-axis. This anisotropy of J_c and the weak nature of grain connectivity have been identified as the major reasons for the large difference between the inter-grain and intra-grain J_c . The weak nature of grain connectivity arises mainly because of the impurity layers at the grain boundary. Thus it is clear that the application of high temperature superconductors in their bulk form requires:

- i. alignment or texture of grains so that their ab-planes lie in the direction of current,
- ii. absence of impurities at the grain boundary, and
- iii. better mechanical properties, perhaps by the incorporation of ductile metals in the superconductor matrix.

It is also known that J_c is enhanced if fine particles of "flux pinning materials", can be distributed uniformly throughout the bulk of the superconductors.

There are several different ways of introducing texture in the bulk polycrystalline ceramics. One of the important techniques is aligning grains by mechanically or magnetically and sintering it without disturbing the alignment achieved. The key to this technique is the grains with anisotropic morphology. Thus it is imperative to study textured grain growth in high temperature superconductors.

In the present work, the textured grain growth in $Y_1Ba_2Cu_3O_{7-\delta}$ (YBCO) under different oxygen partial pressures, temperatures and substitution during the calcination stage has been investigated for the first time. Also a mechanism has been suggested for explaining the enhanced textured grain growth arising under the experimental conditions mentioned above. Moreover, the effect of cold pressing and heat treatment on the alignment of platy YBCO grains and the alignment of platy grains of BPSCCO $[(Bi,Pb)_2Sr_2Ca_2Cu_3O_{10}]$ by suspension through a dense liquid have been studied. The correlation between the J_c and the texture has been investigated.

Conventional method of preparation of YBCO induces formation of nonsuperconducting phases due to the higher processing temperature and the presence of CO_2 in the processing environment. During the present study an experimental set up has been fabricated and the processing parameters have been standardized to yield phase pure YBCO.

Synthesis of the pure 2223 phase (with $T_c = 110$ K) in the (Bi,Pb)-Sr-Ca-Cu-O system is very difficult and a lot of controversy is still there regarding the initial stoichiometry to be taken so as to result in a sintered bulk material with higher J_c . Thus work has been carried out to study the effect of initial stoichiometry variation and processing conditions on the structural and superconducting properties of this system.

In the case of YBCO it is well established that ductility can be imparted by fabricating YBCO/Ag composites. Also its processing can be done in air without affecting the superconducting properties. But in the case of Bi-based superconductor, silver addition has a poisoning effect when processed in air. In the present work BPSCCO/Ag composite was synthesized by adding $AgNO_3$ and processing in air. Studies on the various superconducting and mechanical properties of these composites have also been done.

List of publications

1. Effect of oxygen partial pressure on oriented grain growth of $YBa_2Cu_3O_{7-\delta}$ superconductor, Solid State Commun., 72, 93 (1989).
2. Oriented grain growth of $YBa_2Cu_3O_{7-\delta}$ in different oxygen partial pressures and temperatures, Superconductor Science & technology, 5, 54 (1992).
3. Oriented grain growth in $YBa_2Cu_3O_{7-\delta}$ by alkali metals (Li, Na and K) substitution, Solid State Commun., 81, 253 (1992).

4. Study of single phase $\text{YBa}_2\text{Cu}_3\text{O}_{7-\delta}$ compound around 1-2-3 stoichiometry,
Pramana - J. Phys., 31, L 427 (1988).
5. Orientation in $\text{YBa}_2\text{Cu}_3\text{O}_{7-\delta}$ by cold pressing and heat treatment,
Solid State Commun., 71, 287 (1989).
6. Oriented grain growth in Bi-Pb-Sr-Ca-Cu-O superconductor,
Solid State Commun., 74, 477 (1990).
7. Superconductivity in Ag-added Bi-Pb-Sr-Ca-Cu-O system,
Solid State Commun., 76, 659 (1990).
8. Mechanical properties of (Bi, Pb)-Sr-Ca-Cu-O/Ag superconducting composite,
J. Mat. Sci. Lett., 11, 1437 (1992).
9. X-ray diffraction of Y-Ba-Cu-O superconductor,
J. Mat. Sci. Lett., 8, 981 (1989).
10. Variation of structural and superconducting properties with initial stoichiometry variation in (Bi,Pb)-Sr-Ca-Cu-O bulk superconductor (Manuscript under preparation).
11. Oxygen vacancies and oriented grain growth in $\text{YBa}_2\text{Cu}_3\text{O}_{7-\delta}$. (Manuscript under preparation).

Conference presentations

1. Preparation and processing of textured YBCO compound for enhancing J_c value,
1st Japan International SAMPE Symposium and Exhibition, Nov.28-Dec. 1, 1989.
2. X-ray diffraction study of Y-Ba-Cu-O superconductor,
XIX National Seminar on Crystallography, December 18-20, 1987,
Changanacherry, Kerala.

3. Superconductivity - A Review,
One-day Seminar of Kerala Academy of Science, 29th June 1990,
Regional research Laboratory, Trivandrum.

Patent

1. A process for the preparation of oriented powder of superconducting $\text{YBa}_2\text{Cu}_3\text{O}_{7-\delta}$ (YBCO) compound,
(ref. No.415/Del/88 dt. 3.10.1988).

LIST OF FIGURES

<u>Figure No.</u>	<u>Title</u>	<u>Page No.</u>
1.1	Typical structure of $\text{YBa}_2\text{Cu}_3\text{O}_7$	6
1.2	Typical structure of orthorhombic and tetragonal phase	11
1.3	Typical XRD patterns of orthorhombic and tetragonal YBCO	12
1.4	Typical plot of T_c vs oxygen stoichiometry	14
1.5	Compatibility regions in the pseudoternary Y_2O_3 -BaO-CuO system as determined at 950°C	16
1.6	Typical structure of $\text{Bi}_2\text{Sr}_2\text{CaCu}_2\text{O}_{8+\delta}$	26
2.1	Four-probe contacts	43
2.2	Sample holder for the measurement of J_c	45
2.3	X-ray diffraction in crystals	47
3.1	Experimental set up for the processing of YBCO under different oxygen partial pressures and temperatures	59
3.2	Typical SEM fractograph of samples having grain sizes $5\ \mu\text{m}$ and $15\ \mu\text{m}$	60
3.3	SEM photograph of the separated grains of sample S2	62
3.4	XRD patterns of (a) sample S1, and (b) sample S2	63
3.5	XRD patterns of samples S1, S2 & S3	66
3.6(a)	SEM photograph of fracture and powder of sample S1	67
3.6(b)	SEM photograph of fracture and powder of sample S2	68
3.6(c)	SEM photograph of fracture and powder of sample S3	69

<u>Figure No.</u>	<u>Title</u>	<u>Page No.</u>
3.7	Plots of grain size vs Po_2 of the samples processed at different temperatures	70
3.8(a)	SEM photograph of fracture and powder of sample S4	73
3.8(b)	SEM photograph of fracture and powder of sample S5	74
3.8(c)	SEM photograph of fracture and powder of sample S6	75
3.8(d)	SEM photograph of fracture and powder of sample S7	76
3.9	Plots of grain size vs processing temperature of samples processed under different oxygen partial pressures	77
3.10	Plots of Po_2 vs processing temperature for grain sizes 5, 15 and 33 μm	79
3.11	SEM photographs of the sample processed in air at 950 ⁰ C with soaking periods 12 hrs and 60 hrs	81
3.12	Plots of grain size vs soaking period of samples processed under different temperature and Po_2	82
4.1	Typical XRD patterns of pure and alkali metals substituted samples	90
4.2(a)	SEM fractographs of the $Li_{0.2}$, $Na_{0.2}$ and $K_{0.2}$ substituted YBCO samples	91
4.2(b)	SEM fractographs of the $Li_{0.1}$, $Na_{0.1}$ and $K_{0.1}$ substituted YBCO samples	92
4.2(c)	SEM fractograph of $Li_{0.05}$, $Na_{0.05}$ and $Ko_{0.05}$ substituted YBCO samples	93

<u>Figure No.</u>	<u>Title</u>	<u>Page No.</u>
4.2(d)	SEM fractograph of the pure YBCO	94
4.3	Plot of grain size v s substituent concentration	95
5.1	Typical structure of $\text{YBa}_2\text{Cu}_3\text{O}_7$	101
5.2	Typical TG-curves of two samples	107
5.3	Typical TG-curve and corresponding calculated curve	109
5.4	Plot of oxygen content at 920°C vs substituent stoichiometry of the samples	112
5.5	Plots of oxygen content at 920°C by calculation and observation vs substituent stoichiometry of different samples	113
5.6	Plots of number of oxygen absorbed/unit cell vs substituent stoichiometry of different samples	116
6.1	Typical SEM photograph of the platy grains	121
6.2	Typical SEM photograph of the pressed surface of the sample	123
6.3	Plots of orientation index of pressed surface vs applied pressure	124
6.4	Plot of orientation index vs different depth	125
6.5	Typical XRD patterns of the pressed surface of as-pressed, 6 hrs sintered and 36 hrs sintered sample	127
6.6	Plots of orientation index vs different depths of sintered sample	129
6.7	SEM photographs taken near the edge of the surface of the sintered samples prepared from the batches S2 and S4	131

<u>Figure No.</u>	<u>Title</u>	<u>Page No.</u>
7.1	Experimental set up for vacuum calcination	139
7.2	XRD patterns of YBCO powders synthesized by vacuum calcination and conventional method	141
7.3	DT-curves of vacuum calcined and conventionally synthesized powders	143
7.4	TG-curves of vacuum calcined and conventionally synthesized powders	144
7.5	$J_c(B)$ characteristics of samples prepared from vacuum calcined and conventionally synthesized powders	145
7.6	SEM photograph of the vacuum calcined powder	146
7.7	XRD patterns of vacuum calcined and conventionally processed powders kept in air for two years	148
8.1	Typical XRD pattern of BPSCCO	154
8.2	Plots of HTf, $T_c(O)$, ΔT_c vs x	156
8.3	Plots of J_c , If, T_{001} vs x	157
8.4	XRD patterns of different Ca-stoichiometric samples	160
8.5	SEM fractograph of the sample having Ca-stoichiometry 2.2	161
8.6	$J_c(B)$ characteristics of samples 1, 2 & 3	162
8.7	Plots of HTf vs x of different stoichiometric samples after 120 hrs and 120 + 80 hrs of heat treatment	164
8.8	Plots of T_{001} vs x of different stoichiometric samples after 120 hrs and 120 + 80 hrs of heat treatment	166

<u>Figure No.</u>	<u>Title</u>	<u>Page No.</u>
9.1	Typical XRD patterns of samples having different annealing period	171
9.2(a)	SEM fractograph of sample S1	173
9.2(b)	SEM fractograph of the sample S2	174
9.2(c)	SEM fractograph of the sample S3	175
9.2(d)	SEM fractograph of the sample S4	176
9.3	Experimental set up for suspension	178
9.4	SEM fractograph of the samples prepared conventionally and by suspension method	180
10.1	XRD patterns of samples having different wt. % Ag	186
10.2(a)	Optical micrograph of the polished surface of the sample containing 5 wt. % Ag (X 400)	188
10.2(b)	Optical micrograph of the polished surface of the sample containing 10 wt. % Ag (X 400)	189
10.2(c)	Optical micrograph of the polished surface of the sample containing 20 wt. % Ag (X 400)	190
10.2(d)	Optical micrograph of the polished surface of the sample containing 40 wt. % Ag (X 400)	191
10.3	Plots of flexural strength and % deflection at breakage vs wt. % Ag	193
10.4	Plots of hardness and porosity vs wt. % Ag	195

LIST OF TABLES

<u>Table No.</u>	<u>Title</u>	<u>Page No.</u>
1.1	List of major high temperature superconductors	4
1.2	X-ray powder data for $\text{YBa}_2\text{Cu}_3\text{O}_7$	7
1.3(a)	Final crystallographic data for $\text{YBa}_2\text{Cu}_3\text{O}_{6.85}$ at room temperature	8
1.3(b)	Selected bond distance, angle and strength data for $\text{YBa}_2\text{Cu}_3\text{O}_{6.85}$	9
3.1	Oxygen partial pressure, orientation index and grain size of the samples processed at a temperature 960°C	65
3.2	Temperature, orientation index and grain size of the samples processed at $\text{Po}_2 \ 34 \pm 1\%$	72
4.1	Co-ordination number and ionic radii of different alkali metals	88
4.2	Orientation index and $T_c(0)$ of the alkali metals substituted and pure YBCO samples processed at $920 \pm 5^\circ\text{C}$	96
5.1	Activation energies of oxygen absorption	110
5.2	Results of isothermal experiments done at 430°C	111
6.1	Orientation index of the cold pressed and sintered samples made from the batch S2 of powder	126
6.2	J_c of the sintered samples made from different batches of powder	128
6.3	J_c values of alkali metal substituted YBCO samples	132
7.1	2θ values corresponding to two major peaks of common impurity phases in YBCO compounds	140

<u>Table No.</u>	<u>Title</u>	<u>Page No.</u>
8.1	Different P.S. parameters, T_c , ΔT_c and J_c of the samples having different (Bi,Pb) stoichiometric ratio, after 120 + 80 hrs heat treatment	155
8.2	P.S. parameters, T_c , ΔT_c and J_c of the sample having initial stoichiometry $\text{Bi}_{1.6}\text{Pb}_{0.4}\text{Sr}_{1.8}\text{Ca}_{2.2}\text{Cu}_3\text{O}_y$	158
8.3	HTf and T_{001} corresponding to 120 hrs and 120 + 80 hrs heat treated cu-rich stoichiometric samples	165
9.1	Ratio of the intensities of (0012) and (119) and HTf of different samples	170
9.2	$T_c(0)$ and J_c of samples prepared conventionally and by suspension method	179
10.1	Room temperature resistivity, contact resistance, $T_c(0)$ and J_c of the composites	185
10.2	HTf, If and T_{001} of the composites	192

CHAPTER 1

GENERAL INTRODUCTION

CHAPTER 1

GENERAL INTRODUCTION

1.1 SUPERCONDUCTIVITY, THE PHENOMENON

The electrical resistance of many materials drops suddenly to zero when it is cooled to a sufficiently low temperature. This phenomenon is known as superconductivity. The temperature at which this change occurs, is the transition (critical) temperature (T_c). In 1911 Dutch Physist H. Kammerlingh Onnes observed this phenomenon for the first time [1]. He found that the electrical resistance of Hg below 4 K remained effectively zero. Thereafter over a thousand materials were found to exhibit superconductivity. Till 1986, the maximum value of T_c was 23.3 K for Nb_3Ge alloy [2, 3].

1.2 HIGH TEMPERATURE SUPERCONDUCTORS

The breakthrough in this field was made by George Bednorz and Alex Müller in 1986 [4]. They observed superconductivity in $Ba_x La_{5-x} CuO_5 (3-y)$ ($x = 1$ and 0.75 , $y > 0$) system, at an unprecedented high temperature of ~ 30 K. Later the superconducting phase was identified as $La_{2-x} Ba_x CuO_4$ ($x = 0.0 - 0.2$). The breakthrough by Bednorz and Müller was really two fold. One the demonstration of a new previously unrecognized class of ceramic superconducting materials. The other, a big advance in the superconducting transition temperature to a value believed by many theorists to be the limiting

temperature for the operation of the electron phonon interaction which is the basis of BCS theory [5].

1.2.1 Superconductivity in Y-Ba-Cu-O system

The next dramatic breakthrough came with the report in January 1987 that superconductivity had been observed in Y-Ba-Cu-O compound at a temperature above that of liquid nitrogen (77 K). Chus's group at the University of Houston had observed transition onset temperature in Y-Ba-Cu-O compound as high as 92 K [6]. Soon after it became evident that a number of groups around the world independently observed the same transition in similar material [7-9]. The superconducting phase was later identified as $\text{YBa}_2\text{Cu}_3\text{O}_{7-\delta}$ (YBCO) [10]. Further investigations showed that in YBCO, yttrium can be replaced by rare-earths except Pr, Tb and Ce without affecting the transition temperature. These inventions have generated great interest both scientifically and technologically all over the world because of its immense practical importance. In the past liquid helium (temp. 4 K) was used for the refrigeration of superconductors, which needed bulky cooling equipments making the process too expensive. But for the new materials liquid nitrogen can be used as the coolant. The refrigeration system thus required for this is much cheaper and simple compared to liquid helium system.

1.2.2 Superconducting bismuth cuprates

In early 1988 Michel et al [11] showed that an oxide superconductor with T_c in the range 7-22 K is present in Bi-Sr-Cu-O system.

Later Maeda et al [12] found that the introduction of additional element calcium in Bi-Sr-Cu-O leads to superconductivity above liquid nitrogen temperature. Later several compositions of the Bi-Sr-Ca-Cu-O have found to exhibit superconductivity [13-17]. Among these two important superconducting phases are $\text{Bi}_2\text{Sr}_2\text{CaCu}_2\text{O}_{8+\delta}$ (2212) with a transition temperature 85 K [18-20] and $\text{Bi}_2\text{Sr}_2\text{Ca}_2\text{Cu}_3\text{O}_{10}$ (2223) with a transition temperature 110 K [21, 22]. The synthesis of phase pure 2223 phase is more difficult than the synthesis of 2212 phase. It has been established that the partial substitution of Bi by Pb favours the formation of 2223 phase [23].

1.2.3 Thallium cuprate superconductors

Studying the substitution of yttrium by the trivalent cation thallium in YBCO, Sheng et al [24] at the end of 1988, found superconductivity at 85 K. The structure determination studies [25, 26] lead to the composition $\text{TL}_2\text{Ba}_2\text{CuO}_6$ for this compound. Shortly the same authors [27, 28] discovered $\text{TL}_2\text{Ba}_2\text{Ca}_2\text{Cu}_3\text{O}_{10}$ (2223) which has a T_c of 125 K and $\text{TL}_2\text{Ba}_2\text{CaCu}_2\text{O}_6$ (2212) which has a T_c of 108 K. Later many compositions of TL-Ba-Ca-Cu-O system was found to be superconducting [29-31].

1.2.4 Other high temperature superconducting phases

$\text{Y}_1\text{Ba}_2\text{Cu}_4\text{O}_8$ [124] is an important compound with $T_c \sim 80$ K [32]. The importance of this compound is that its oxygen content is constant. $\text{Ba}_{1-x}\text{K}_x\text{BiO}_3$ is a copper free superconductor $T_c \sim 30$ K [33].

A list of major high temperature superconductors are given in Table 1.1 [34].

Table 1.1: List of major high temperature superconductors

Compound	T_c (K)
$\text{La}_{2-x}\text{Ba}_x\text{CuO}_4$	35
$\text{YBa}_2\text{Cu}_3\text{O}_{7-\delta}$	92
$\text{NdBa}_2\text{Cu}_3\text{O}_{7-\delta}$	92
$\text{SmBa}_2\text{Cu}_3\text{O}_{7-\delta}$	88.3
$\text{EuBa}_2\text{Cu}_3\text{O}_{7-\delta}$	93.7
$\text{GdBa}_2\text{Cu}_3\text{O}_{7-\delta}$	92.2
$\text{DyBa}_2\text{Cu}_3\text{O}_{7-\delta}$	91.2
$\text{HoBa}_2\text{Cu}_3\text{O}_{7-\delta}$	92.2
$\text{ErBa}_2\text{Cu}_3\text{O}_{7-\delta}$	91.5
$\text{TmBa}_2\text{Cu}_3\text{O}_{7-\delta}$	91.2
$\text{YbBa}_2\text{Cu}_3\text{O}_{7-\delta}$	85.66
$\text{LuBa}_2\text{Cu}_3\text{O}_{7-\delta}$	88.2
$\text{Bi}_2\text{CaSrCuO}_{6+\delta}$	60 ± 20
$\text{Bi}_2\text{Sr}_2\text{CaCu}_2\text{O}_{8+\delta}$	84
$\text{Bi}_2\text{Sr}_2\text{Ca}_2\text{Cu}_3\text{O}_{10}$	110
$(\text{Bi}, \text{Pb})_2\text{Sr}_2\text{Ca}_2\text{Cu}_3\text{O}_{10}$	110
$\text{TL}_2\text{Ba}_2\text{CaCu}_2\text{O}_6$	108
$\text{TL}_2\text{Ba}_2\text{Ca}_2\text{Cu}_3\text{O}_{10}$	125
$\text{TLBa}_2\text{Ca}_2\text{CuO}_9$	120
$\text{TLBa}_2\text{CaCu}_2\text{O}_7$	65
$\text{TL}_2\text{Ba}_2\text{Ca}_3\text{Cu}_4\text{O}_{12}$	105
$\text{YBa}_2\text{Cu}_4\text{O}_8$	80
$\text{Ba}_{1-x}\text{K}_x\text{BiO}_3$	30

Among the various high temperature superconductors listed in Table 1.1 the present work undertaken is on $\text{YBa}_2\text{Cu}_3\text{O}_{7-\delta}$ (YBCO) and $(\text{Bi, Pb})_2\text{Sr}_2\text{Ca}_2\text{Cu}_3\text{O}_{10}$ (BPSCCO) compounds. Hence it will be appropriate to give more details about YBCO and BPSCCO compounds.

1.3 STRUCTURE OF $\text{YBa}_2\text{Cu}_3\text{O}_{7-\delta}$

The structure of YBCO was first deduced from x-ray powder diffraction experiments [35-37] and subsequent refinement was done by neutron diffraction studies [38-45]. From the studies it was found that YBCO has a layered oxygen deficient perovskite structure with orthorhombic symmetry ($a = 3.816 \text{ \AA}$, $b = 3.8883 \text{ \AA}$, and $c = 11.698 \text{ \AA}$). Figure 1.1 shows a typical structure of YBCO. The lattice spacings with corresponding indices of $\text{YBa}_2\text{Cu}_3\text{O}_7$ are given in Table 1.2.

Later more detailed studies on structure have been reported [46-49] using single crystals. The details of the structure are summarised in Table 1.3a&b [42].

Of the two sets of Cu atoms Cu(2) is surrounded by four oxygen atoms, two at 1.929 \AA and two at 1.96 \AA giving rise to a square pyramidal coordination for Cu forming CuO_2 layers. In the other set, the Cu(1) atoms are surrounded by four oxygen atoms two at 1.942 \AA and two at 1.845 \AA . Here the oxygen atoms form near rectangles connected by vertices, and resulting in the Cu-O chains along the b-axis.

1.4 ANISOTROPY IN YBCO

YBCO superconductor has a perovskite based layered structure

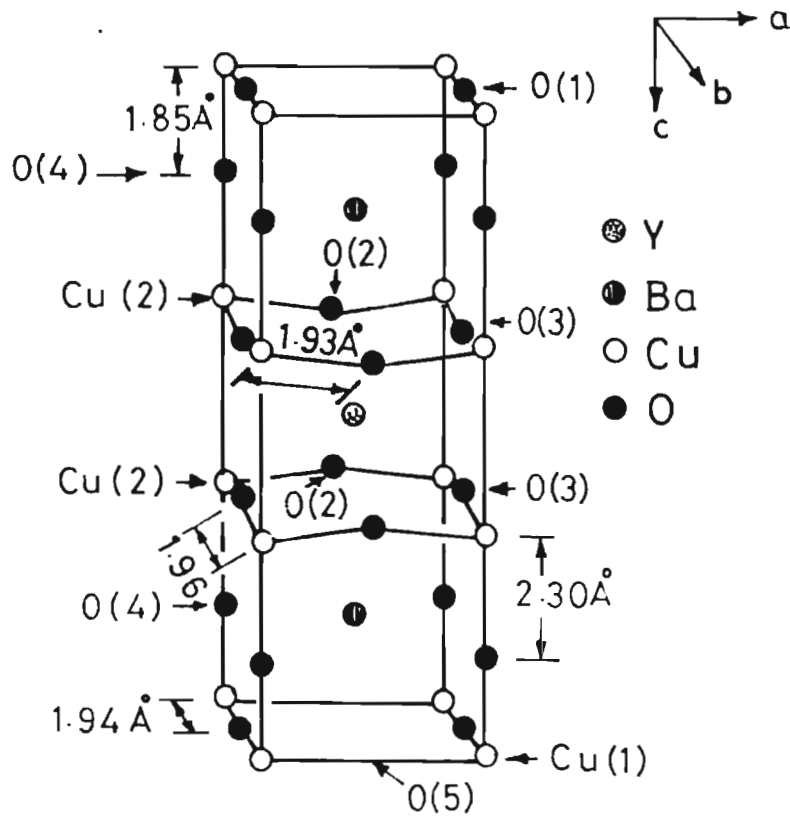


Fig. 1.1: Typical structure of $\text{YBa}_2\text{Cu}_3\text{O}_7$

Table 1.2: X-ray powder data for $\text{YBa}_2\text{Cu}_3\text{O}_7$

$\text{YBa}_2\text{Cu}_3\text{O}_7$						
$a = 3.816 \text{ \AA}$		$b = 8.883 \text{ \AA}$		$c = 11.698 \text{ \AA}$		
P_{mmm}						
Obs	2θ calc	d_{calc}	obs	I/I_0	calc	hkl
	7.56	11.70			2	0 0 1
	15.15	5.849			3	0 0 2
22.86	{ 22.81 22.90	{ 3.899 3.883	8		{ 10 8	{ 0 1 0 0 0 3
23.30	23.31	3.816	2		6	1 0 0
27.73	27.57	3.235	2		5	0 1 2
27.90	27.92	3.196	4		9	1 0 2
32.60	32.54	2.751	50		89	0 1 3
32.88	{ 32.84 32.91	{ 2.727 2.722	100		{ 96 100	{ 1 1 0 1 0 3
33.75	33.81	2.651	1		2	1 1 1
36.46	36.41	2.468	3		5	1 1 2
38.57	{ 38.48 38.54	{ 2.340 2.336	17		{ 6 11	{ 0 1 4 0 0 5
38.75	38.79	2.321	1		4	1 0 4
40.46	40.41	2.232	19		28	1 1 3
46.68	{ 46.58 46.79	{ 1.950 1.941	33		{ 17 31	{ 0 0 6 0 2 0
47.63	47.66	1.908	17		29	2 0 0
51.58	51.51	1.774	5		6	1 1 5
52.68	52.52	1.742	4		2	0 1 6
	52.66	1.738			2	0 2 3
52.87	52.91	1.730	3		2	1 2 0
53.43	{ 53.46 53.51	{ 1.714 1.712	6		{ 2 2	{ 2 0 3 0 0 7
55.00	54.94	1.671	3		2	0 0 7
55.37	55.37	1.659	2		3	1 2 2
55.88	55.95	1.643	1		2	2 1 2
58.26	{ 58.21 58.34	{ 1.585 1.582	49		{ 37 32	{ 1 1 6 1 2 3
58.87	58.90	1.568	25		32	2 1 3

Table 1.3(a): Final crystallographic data for $\text{YBa}_2\text{Cu}_3\text{O}_{6.85}$ at room temperature (After 42)

Atom	Wyckoff symbol	x/a	y/b	z/c	$B(\text{\AA}^2)$	Site
Y	1h	1/2	1/2	1/2	0.9(1)	
Ba	2t	1/2	1/2	0.1844(5)	0.8(1)	
Cu(1)	1a	0	0	0	0.9(1)	
Cu(2)	2q	0	0	0.3544(3)	0.6(1)	
O(1)	1e	0	1/2	0		
O(2)	2s	1/2	0	0.3788(5)	0.3(4)	0.92(3)
O(3)	2r	0	1/2	0.3771(5)	0.6(1)	
O(4)	2q	0	0	0.1579(3)	0.8(1)	

Table 1.3(b): Selected bond distance, angle and strength data for $\text{YBa}_2\text{Cu}_3\text{O}_{6.85}$

Bond	Distance (Å)	Number	Bond	Distance (Å)	Number
Y-O(3)	2.387	x4	Cu(1)-O(4)	1.843	x2
Y-O(2)	2.402	x4	Cu(1)-O(1)	1.942	x2
Ba-O(4)	2.741	x4	Cu(2)-O(2)	1.929	x2
Ba-O(1)	2.877	x2	Cu(2)-O(3)	1.958	x2
Ba-O(3)	2.949	x2	Cu(2)-O(4)	2.306	x1
Ba-O(2)	2.986	x2			

Bond	Angle (deg)
O(1)-Cu(1)-O(1)	180
O(1)-Cu(1)-O(4)	90
O(2)-Cu(2)-O(3)	88.96
O(2)-Cu(2)-O(4)	98.14
O(3)-Cu(2)-O(4)	97.42

Bond strength data:

Assuming	Cu^{2+}	Cu^{3+}	
Cu(1)-O(4)	2x0.33	2x0.38	
Cu(1)-O(1)	2x0.24	2x0.26	
Summed strengths	2.27	2.5 = calculated valence	Cu(1)
Cu(2)-O(2)x2	2x0.23	2x0.25	
Cu(2)-O(3)x2	2x0.23	2x0.25	
Cu(2)-O(4)x1	0.17	0.16	
Summed strengths	2.01	2.16 = calculated valence	Cu(2)

which causes a large anisotropy of the superconducting properties. Single crystal studies of YBCO showed marked anisotropic behaviour in resistivity [50] magnetic susceptibility [51] critical magnetic field [51,52] and critical current density [53,54].

1.5 PHASE TRANSFORMATION IN YBCO

Phase transition in YBCO is a direct result of the variation in oxygen stoichiometry which results in disorders as well as structural distortion. There are many reports which deal with structural transformation [55-59]. The oxygen content of YBCO can be varied from 6 to 7 by appropriate heat treatment in controlled oxygen atmosphere. Orthorhombic YBCO loses oxygen at a high temperature of above 700°C. The oxygen at O_1 sites are lost gradually and the compound becomes tetragonal and nonsuperconducting when the oxygen content is ≤ 6.5 .

This decomposition is reversible and while annealing in oxygen atmosphere at lower temperature of 400-500°C, the tetragonal YBCO absorbs oxygen and the stoichiometry become $YBa_2Cu_3O_{7-\delta}$ (δ close to zero). During this absorption O_1 sites are filled and the compound becomes orthorhombic and superconducting again. When the oxygen content is in the range 6-6.5, the compound is tetragonal and above 6.5 the compound is orthorhombic upto 7 [44]. The unit cell volume increases with δ from 173.7 \AA^3 ($\delta = 0.0$) to 176.2 \AA^3 ($\delta = 1$) [60].

Typical structure and XRD patterns of orthorhombic and tetragonal phases are given in Fig. 1.2a&b, 1.3 a&b respectively.

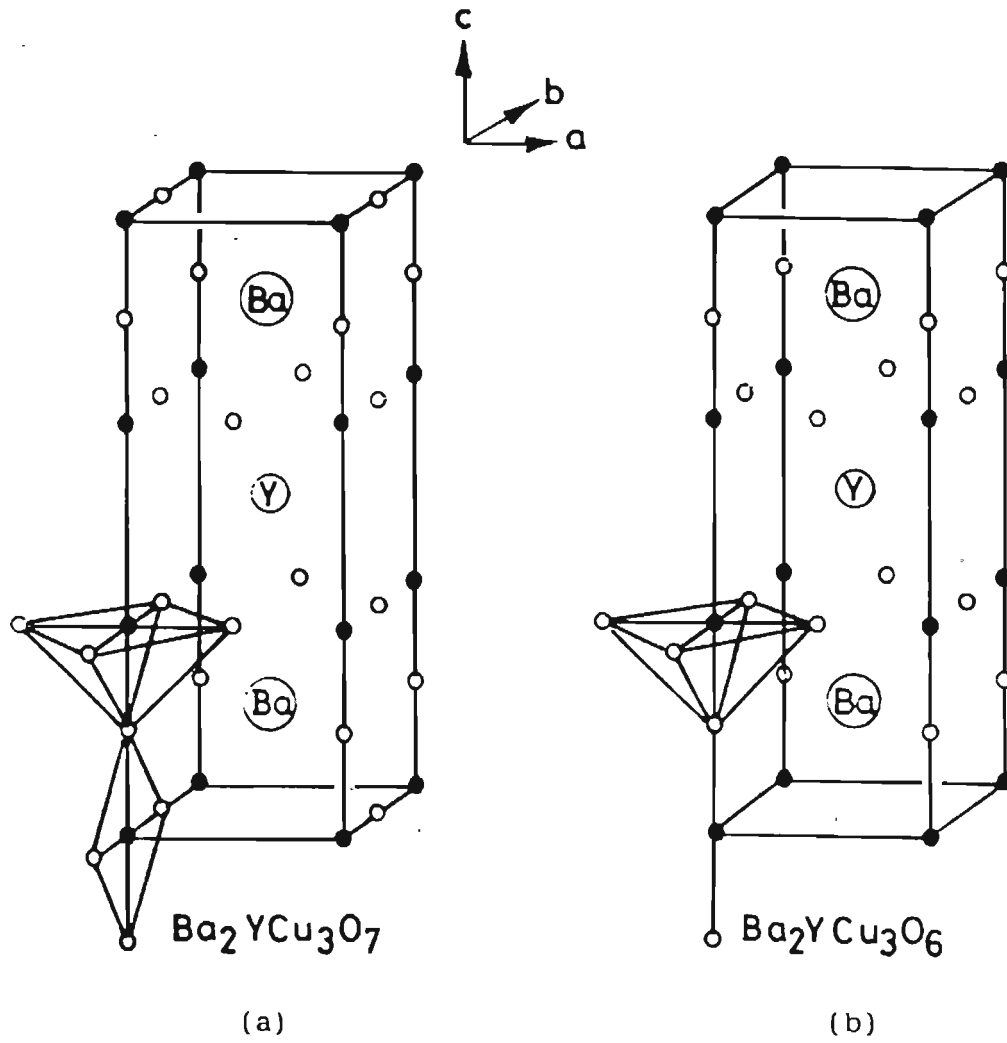


Fig. 1.2: Typical structure of orthorhombic and tetragonal phase

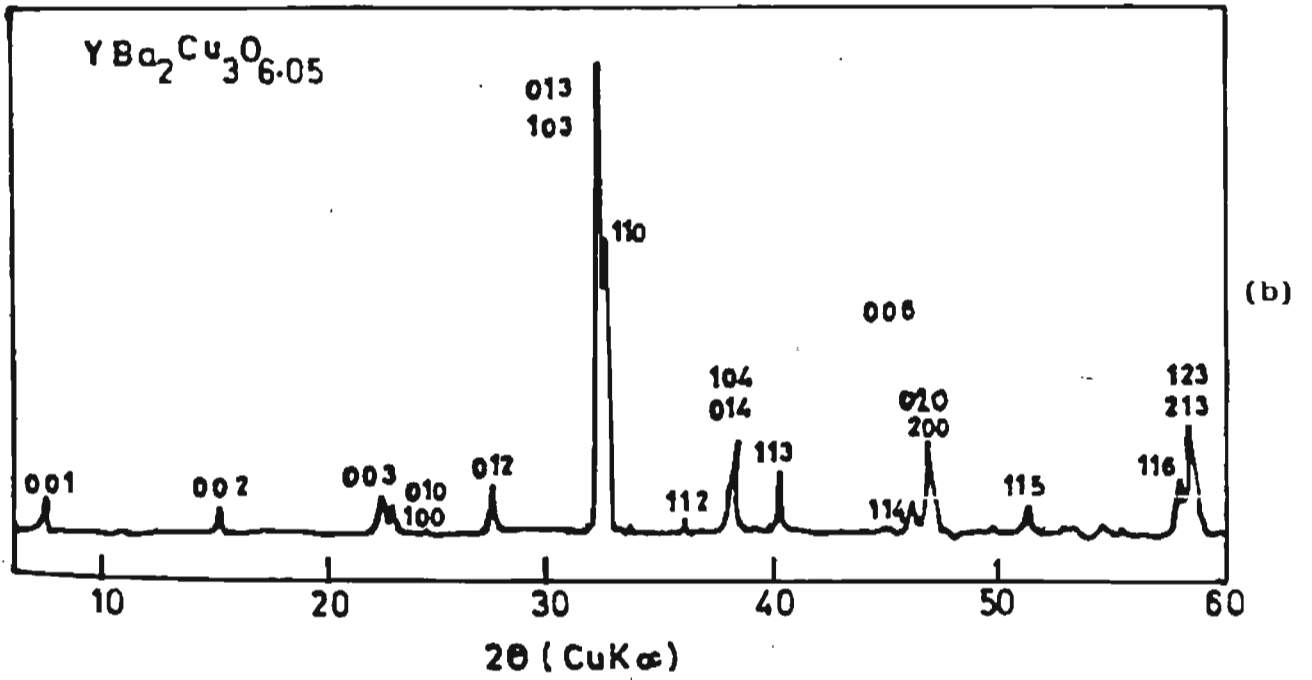
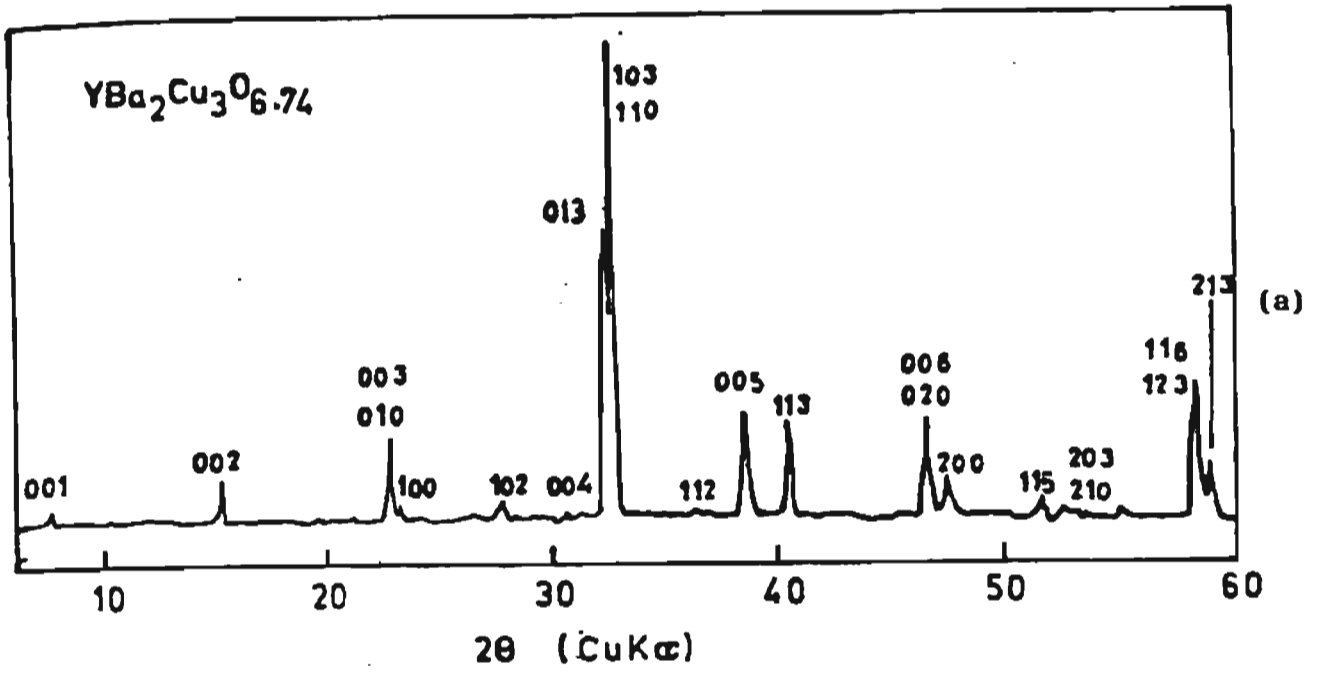


Fig. 1.3: Typical XRD patterns of (a) orthorhombic, and (b) tetragonal YBCO

Quenching YBCO from higher temperature (above 900°C) results in oxygen deficiency and the compound is tetragonal. If the compound is slowly cooled in oxygen atmosphere, from a higher temperature of above 900°C more oxygen is absorbed and the associated tetragonal to orthorhombic transition occurs in the $600\text{-}750^{\circ}\text{C}$ range depending on the oxygen partial pressure [61].

1.6 OXYGEN STOICHIOMETRY, OXYGEN ORDERING AND SUPERCONDUCTING PROPERTIES

Many researchers have looked into such structural transformation accompanying change in oxygen content and its dependence on superconducting properties of YBCO [62-66]. Chen et al [67] reported the existence of orthorhombic I and orthorhombic II forms. The oxygen content is different for orthorhombic I and II. For orthorhombic I, it is 6.7-7 and for orthorhombic II it is 6.5-6.7. The three forms, tetragonal, orthorhombic I and orthorhombic II differs in their cell parameters. For tetragonal symmetry $a = b < c/3$, for orthorhombic I, $a < b = c/3$ and for orthorhombic II, $a < b < c/3$ [68]. Gallagher et al [55] attributed the orthorhombic II regime to the coexistence of orthorhombic I and tetragonal forms. The orthorhombic I form exists in the temperature range $400\text{-}500^{\circ}\text{C}$ and orthorhombic II form in the range $500\text{-}600^{\circ}\text{C}$.

The effect of varying oxygen content on T_c of YBCO has been studied by many groups [56,57,69-71]. A typical curve for the variation of T_c with oxygen content is shown in Fig. 1.4.

For $x = 7\text{-}6.8$, T_c remains almost 90 K, leading to a plateau

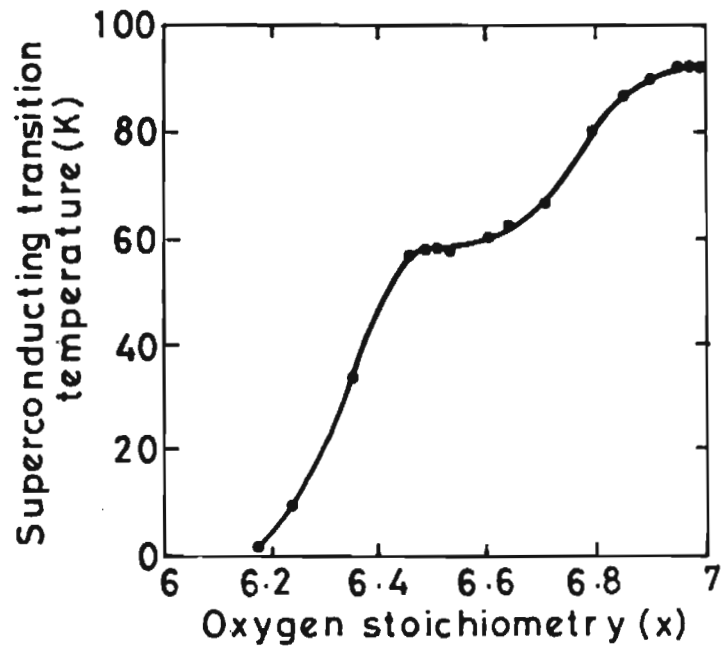


Fig. 1.4: Typical plot of T_c vs oxygen stoichiometry

in the curve, but falls suddenly to 60 K, for $x = 6.75-6.5$. At 60 K it exhibits a second plateau in the curve and then falls rapidly to 4 K for higher oxygen deficiency. The T_C change to 4 K is followed by a phase transition i.e. orthorhombic to tetragonal. Many groups have suggested an ordering of oxygen in YBCO [72-74]. For $\delta = 0$, all the O_1 sites are occupied. When $\delta = 0.5$ alternate unit cell have O_1 positions occupied. When $\delta = 1$, all the O_1 positions are empty.

The melting point of YBCO is dependent on the atmosphere because of the pronounced changes in the oxygen content at the melting temperature. The melting point varies from about 975°C in nitrogen to 1035°C in oxygen [75].

1.7 PHASE DIAGRAM OF Y_2O_3 -BaO-CuO system

Many researchers have carried out the phase diagram studies of Y_2O_3 -BaO-CuO system [76-79]. These preliminary studies established phase stability fields below solidus temperature (around 950°C). Compatibility regions in the pseudoternary Y_2O_3 -BaO-CuO system as determined at 950°C is shown in Fig. 1.5. The known copper compounds in this system are $BaCuO_2$, $Y_2Cu_2O_5$, Y_2BaCuO_5 , $YBa_3Cu_2O_7$ and $YBa_2Cu_3O_{7-\delta}$ [76]. In addition there are four possible barium yttrium oxides, $Y_2Ba_2O_5$, $Y_4Ba_3O_9$, $Y_2Ba_4O_7$ and YBa_4O_7 [76]. Karpanski et al [80] carried out investigations on the high pressure phase diagram (1-3000 bar oxygen) in Y-Ba-Cu-O system. They found the existence of a multiphase region consisting of $YBa_2Cu_4O_8$ [124], $Y_2Ba_4Cu_7O_{14}$ [247] and $YBa_2Cu_3O_{7-\delta}$ [123] in the pressure range 50-200 bar

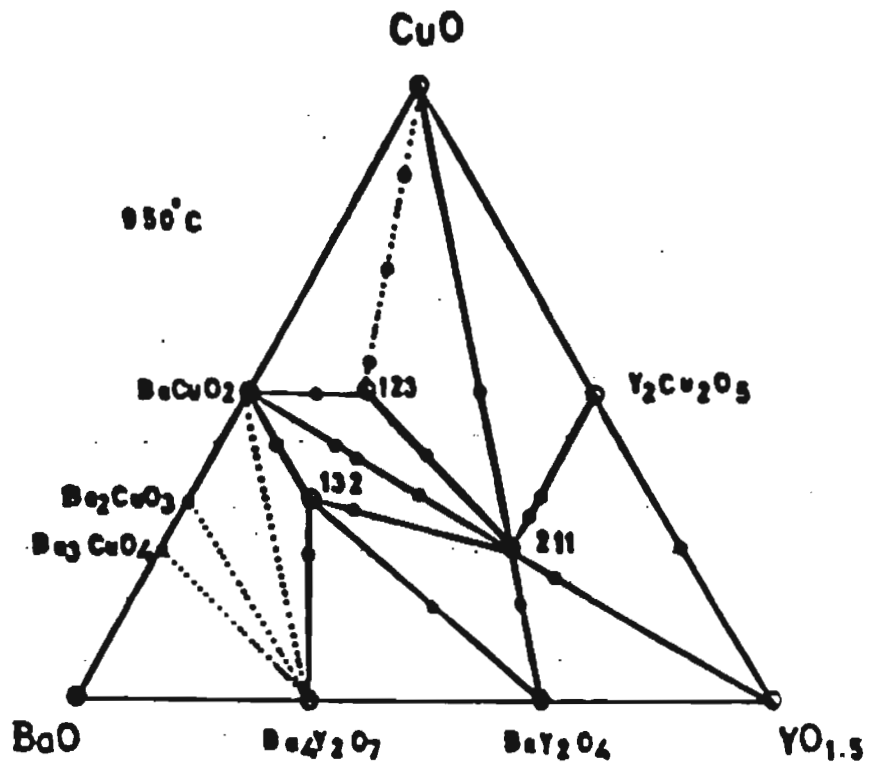


Fig. 1.5: Compatibility regions in the pseudoternary Y_2O_3 -BaO-CuO system as determined at $950^\circ C$

oxygen. Among these phases only $\text{YBa}_2\text{Cu}_3\text{O}_{7-\delta}$ [123] and $\text{YBa}_2\text{Cu}_4\text{O}_8$ [124] are found to be superconducting.

1.8 PREPARATIVE METHODS

Pure and homogeneous materials with uniform oxygen stoichiometry and good superconducting properties can be obtained by several methods. The more important among them are discussed below.

1.8.1 Ceramic route

This is the most commonly used method of preparation. Pure $\text{YBa}_2\text{Cu}_3\text{O}_{7-\delta}$ has been synthesised [81-86] by high temperature solid state reaction between constituent oxides/carbonates/nitrates. In this process, the powders of different components in the appropriate ratio are mixed well and heated for 12-48 hrs at 850-950^oC in air with intermittent grinding. $\text{YBa}_2\text{Cu}_3\text{O}_{7-\delta}$ obtained by this process is oxygen deficient and nonsuperconducting. This compound is annealed in an oxygen atmosphere at 400-500^oC. Then it absorbs more oxygen and acquires superconducting property. Platinum or alumina crucibles are widely used for the preparation. YBCO prepared by this way shows superconducting transition temperature of 92 K.

1.8.2 Chemical route

Many groups have reported the successful preparation of $\text{YBa}_2\text{Cu}_3\text{O}_{7-\delta}$ from precursor powders made by co-precipitation of hydroxides, carbonates or acetates [87-90]. The sol-gel method also has been used [91-93]. The advantage of the above methods are that they yield fine powders having particle sizes less than 1 μm and a better

homogeneity of phase. A major drawback of these processes are side reaction of the constituent metal ions. The co-precipitated precursor powders are generally calcined at 850°C in air and the product thus obtained is later annealed in oxygen at $400\text{-}500^{\circ}\text{C}$ to get the superconducting properties.

Experiments starting from metallic precursor are also reported [94,95] where Y, Ba and Cu metals are first alloyed and then oxidised.

1.9 FABRICATION OF YBCO FOR PRACTICAL APPLICATIONS

The major techniques involved in fabrication process are, (1) powder process, (2) melt process, (3) thin and thick film preparation.

1.9.1 Powder process

The bulk synthesised powder with suitable additives or binders are extruded in the form of wires or tapes. Ceramic metal composites as well as ceramic polymer composites have been fabricated for application purposes [96-98].

Silver is commonly used for fabrication of ceramic metal composites. Several techniques have been used for the fabrication of different shapes from powder. Expansion compaction or shock compaction [99] hot isostatic pressing [100] aluminium cladding by thermal compression bonding [101] and uniaxial pressure application are some of the methods used for this purpose.

Novel methods such as electron discharge compaction or high energy high rate process [102] and sinter forge techniques [103] have also been reported.

1.9.2 Melt process

In several laboratories YBCO has been processed from a melt of the same material. The techniques used are melt drawing, melt spinning or wire melting. In melt drawing a bar shaped pressed YBCO compact is heated at 1200-1300⁰ C and the melted portion is drawn in the form of a wire by pulling apart the unmelted ends [94]. The product obtained by this way is usually nonsuperconducting but has higher density and texturing. Annealing these wires in oxygen restores the superconducting property. The critical current density (J_c) of the material is relatively higher [104]. Melt spinning [104] involves the ejection of the molten YBCO on a ring of rotating metal wheel. In the wire melting method the experiment is conducted using a ceramic/metal-core composite, superconducting wire as a preform. The metal core is melt processed [104] by rapidly moving the torch flame and melting the outer portion of the YBCO shell.

Coating a metal ribbon or wire with YBCO has also been tried [96] with encouraging results.

1.9.3 Thin films and thick films

Thick and thin films of YBCO have technological applications. Thick films can be used for magnetic shielding devices, electrical interconnects etc. and thin films for computer applications, SQUIDs, etc.

Thick films can be prepared by screen printing [105,106] plasma spraying [107], laser ablation technique, dipping metal or substrates in a melt of YBCO. SrTiO_3 and MgO are used as substrates for these purposes.

Various methods are used in thin film deposition. The common methods are evaporation techniques like electron beam evaporation [108], molecular beam epitaxy [108] as well as the sputtering techniques like DC, AC and RF magnetron [108].

1.10 SINGLE CRYSTAL GROWTH

To study the intrinsic properties of YBCO one should use single crystals. Many groups have tried to grow single crystals of YBCO [109-111]. YBCO melts incongruently above 970°C . So single crystal cannot be obtained by a solidification of the melt. Only the flux method can be used to grow single crystals. The fluxes used are $\text{BaCuO}_2/\text{CuO}$ mixtures. Phase diagram studies [76,78,112] gave an idea about the temperature at which YBCO is formed. 40 mole % BaO and 60 mole % CuO mixtures at 935°C [113], 28 mole % BaO, 72 mole % CuO at 870°C are found to be useful as fluxes for the growth of single crystals of YBCO. Usually flaky crystals of a few mm size are obtained by the flux method.

1.11 SOME BASIC PROPERTIES OF $\text{YBa}_2\text{Cu}_3\text{O}_{7-\delta}$

Some of the important properties of YBCO have been summarised by Malozemoff et al [114] and are as follows:

1. It is a type II superconductor
2. Hall carrier density: $4 \times 10^{21} \text{ cm}^{-3}$ (for a material of resistivity = $400 \mu\Omega\text{-cm}$, just above T_c)
3. $dH_{C_2}/dT = 2 \text{ T/K}$
 BCS coherence length (ξ) = 1.4 nm
 London penetration depth = 200 nm
 Main free path = 1.2 nm.
4. $H_{C_1}(0) = 1 \text{ T}$
5. $H_{C_2}(0) = 120 \text{ T}$
6. Critical current density:
 In bulk sample at 77 K = $10^2 - 10^3 \text{ A/cm}^2$
 Thin films on SrTiO_3 = 10^7 A/cm^2 at 77 K
 Depairing current density = $10^7 - 10^8 \text{ A/cm}^2$.

1.12 DIFFICULTIES FOR PRACTICAL APPLICATIONS AND SOLUTIONS

1.12.1 Low critical current density (J_c)

The potential of a superconducting material for practical applications depends mainly on their critical current characteristics. A high critical current density of the order $10^4 - 10^5 \text{ A/cm}^2$ in 2-5 T fields is required for the major electrical applications. But bulk samples of YBCO have shown poor values of transport critical current density or intergrain critical current density of the order of $10^2 - 10^3 \text{ A/cm}^2$ at 77 K in zero applied field [115-118]. Even this modest current density is substantially reduced in magnetic fields of only 1 mT.

But the interest in this material is related to the properties within the grains. It was found that the critical current density of the single grain or single crystal (intra-grain critical current density) is very large of the order of 10^7 - 10^8 A/cm² at 77 K in zero field [119-121]. Even at liquid nitrogen temperature they can carry a commercially usable current. Critical current density in polycrystalline YBCO is thus a complex quantity whose values depend on many factors.

1.12.1.1 Causes for low J_c values in bulk YBCO

All the aspects for low J_c values in bulk have not yet been clearly understood. Some of the factors for low transport critical current density in bulk YBCO are (i) anisotropy, (ii) weak nature of grain connectivity, (iii) oxygen instabilities.

i. Anisotropy

As we have already seen, the YBCO superconductor has a perovskite based layered structure which causes a large anisotropy of the superconducting properties. Measurements on single crystals of YBCO have shown that J_c along a-b plane is one order of magnitude higher than along c-axis [122]. Therefore the misorientation of grains in the bulk causes reduction of J_c .

ii. Weak nature of grain connectivity

A number of possibilities exist for the source of weak nature of grain connectivity. The major one is the presence of impurity layers such as carbonates, or other non-superconducting phases at the

grain boundary. It was found that traces of silicon impurities can dramatically decrease J_c [123]. When the thickness or length of the interlayers between the grains is greater than coherence length (ξ) of YBCO, it can catastrophically limit the critical current density. It was found that the intergrain boundary layers have thickness ranging from 10-50 Å. But coherence length of YBCO is only 7 to 34 Å. At the same time, it is well established that the distribution of minor amounts of certain impurities in the superconducting matrix can enhance the J_c value significantly by acting as flux pinning centres.

The presence of micro-cracks or stress concentrations resulting from the severely anisotropic thermal expansion in different crystallographic directions can limit J_c .

iii. Oxygen instabilities

The YBCO material is highly characterized with oxygen instabilities. As we have already seen in $YBa_2Cu_3O_{7-\delta}$ if $\delta \geq 0.5$, the material is non-superconducting. It has also been found that J_c decreases almost linearly with decrease in oxygen content from 7 onwards [124].

1.12.2 Reaction with water

YBCO material is highly reactive with water and moisture. The superconducting properties get destroyed if it is kept in contact with water/moisture.

1.12.3 Brittleness

The high T_c superconductors are highly brittle. It is very sensitive to hammering or shocks etc.

1.12.4 Possible solutions

The possible solutions for the above problems are:

- i. The control of the formation and thickness of the impurity layers between the grains. It should be less than 10 \AA . By the preparation of phase pure material, this can be achieved.
- ii. Relative orientation of the grains can be improved by following appropriate texturing technique.
- iii. By identifying and incorporating suitable flux pinners J_c and $J_c(B)$ characteristics can be improved.
- iv. The critical current density is found to be maximum when the oxygen content of the sample is between 6.82-6.95 [124]. This can be achieved by proper oxygen treatment.
- v. The material which is having density around 90% of the theoretical value shows maximum current density [124]. By following proper processing technique, this can be achieved.
- vi. Following a very slow cooling rate the formation of cracks can be avoided.
- vii. The contact with water/moisture can be avoided by giving polymer like coating to the material.

viii. Ductility can be imparted by adding silver in the superconducting material.

1.13 STRUCTURE OF BISMUTH CUPRATES

The superconducting bismuth cuprates are orthorhombic and have structures similar to those of YBCO. The structure of the $\text{Bi}_2\text{Sr}_2\text{CaCu}_2\text{O}_{8+\delta}$ (84 K phase) has been analyzed by many groups [125- 128]. A typical structure of $\text{Bi}_2\text{Sr}_2\text{CaCu}_2\text{O}_{8+\delta}$ is shown in Fig. 1.6. The unit cell of the single crystal of composition $\text{Bi}_2\text{Sr}_2\text{Ca}_{0.8}\text{Cu}_2\text{O}_{8+\delta}$ was determined [128] and it was found to be orthorhombic with lattice parameters $a = 5.414 \text{ \AA}$, $b = 5.418 \text{ \AA}$, and $c = 30.89 \text{ \AA}$ and pseudo symmetry Fmmm. This result is in substantial agreement with Hazen et al [12] who worked on polycrystalline samples. In this structure the infinite number of CuO_2 planes separated by Ca in the same way that the planes of $\text{YBa}_2\text{Cu}_3\text{O}_{7-\delta}$ are separated by Y. The copper oxygen coordination polyhedron is a square pyramid of similar geometry to that found in $\text{YBa}_2\text{Cu}_3\text{O}_{7-\delta}$, but with an important difference in the bond length of the Cu to the apical oxygen. The inplane Cu-O distances in $\text{Bi}_2\text{Sr}_2\text{CaCu}_2\text{O}_{8+\delta}$ are 1.875 \AA , and the apical oxygen is at 2.05 \AA , considerably shorter than for the Cu-apical oxygen distance in $\text{YBa}_2\text{Cu}_3\text{O}_{7-\delta}$ (2.3 \AA). The bismuth coordination is basically octahedral. The difference between the structures of the different superconducting phases in the Bi-Sr-ca-Cu-O system is only in the number of CuO_2 layers between Bi-O layers. The 2212 compound has two CuO_2 layers and 2223

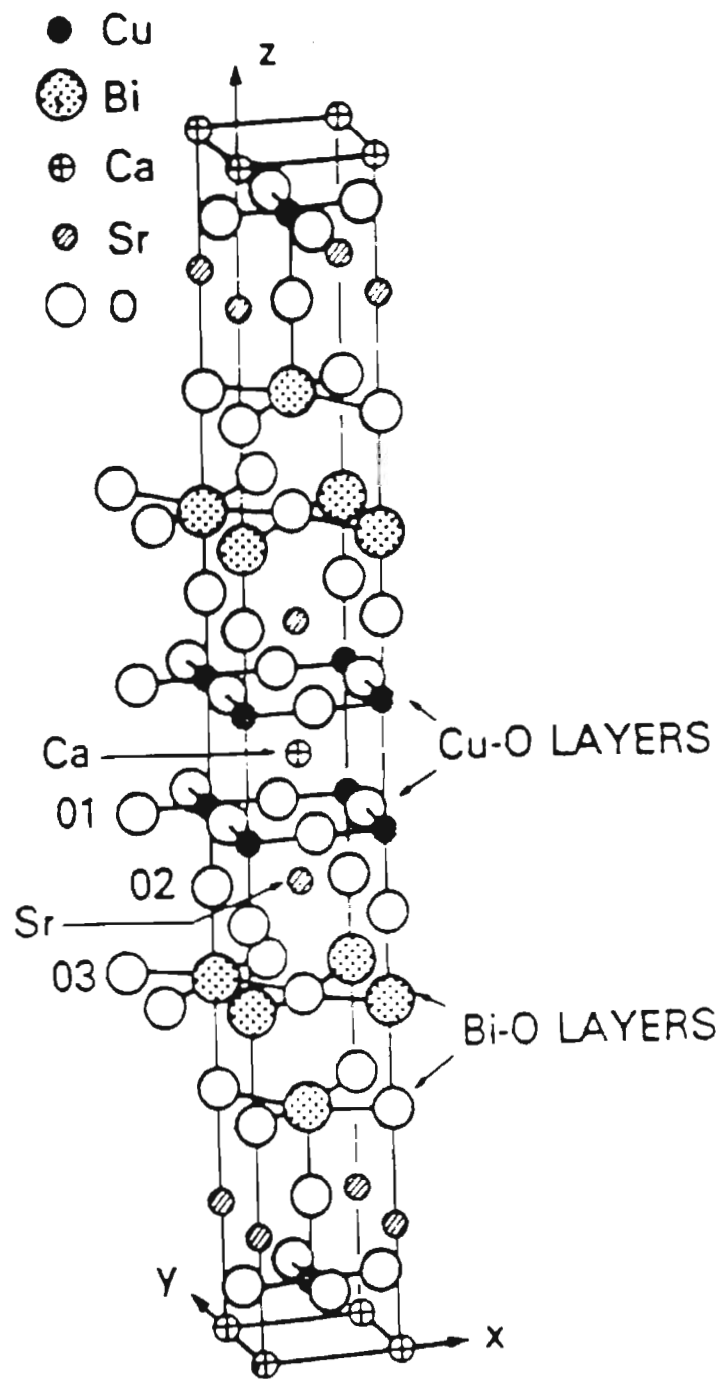


Fig. 1.6: Typical structure of $\text{Bi}_2\text{Sr}_2\text{CaCu}_2\text{O}_{8+\delta}$

compound has three CuO_2 layers. With the variation in number of CuO_2 layers, the orthorhombic c-parameter also varies. The orthorhombic c-parameters corresponding to the number of CuO_2 layers in 1,2,3 members are 25, 31 and 37 \AA respectively.

Almost all the problems faced by YBCO are encountered with bismuth based superconductors also except for oxygen content and weatherability which are not sensitive as observed in the case of YBCO.

1.14 AIM, SCOPE AND OBJECTIVE OF THE PRESENT WORK

Between the new breed of high temperature superconducting materials and its vast potential for practical applications lies a few hurdles which are neither easy nor seems impossible to overcome. One of the main hurdles as discussed earlier is its low critical current density in bulk. The problem identified for the present investigation, about five years back, was on this line to find ways and means to achieve higher critical current density for practical applications. The fact that ab-plane can carry one order of magnitude higher current compared to ac- or bc- planes prompted to study textured grain growth in YBCO material.

Since in ceramic materials, texturing can be imparted by suitable processing techniques, the main aim of the present work was

- I. TO STUDY THE EFFECT OF PROCESSING CONDITIONS AND SUBSTITUENTS ON TEXTURED GRAIN GROWTH OF YBCO.

With this in mind, experiments were carried out

- II. TO FIND FOR THE FIRST TIME THE EFFECT OF Po_2 AND TEMPERATURE DURING CALCINATION ON TEXTURED GRAIN GROWTH OF YBCO.

Having investigated the above effect, it was thought that if vacancy is the driving force for such textured grain growth, selective substitution should also lead to similar effect and thus the next aim was

- III. TO FIND THE EFFECT OF ALKALI METALS SUBSTITUTION ON TEXTURED GRAIN GROWTH.

Alkali metals with '+1' valency, viz, Na, K and Li was used to replace Y/Ba/Cu which are all either double or triple valent. Hence these substitutions should in principle, be able to generate oxygen vacancies which will aid textured grain growth.

It is now imperative to find a suitable explanation and a model to explain the observed textured grain growth by changing either the processing conditions or by substitutions. Hence next aim was

- IV. TO SUGGEST A POSSIBLE MECHANISM FOR THE FIRST TIME FOR ENHANCED TEXTURED GRAIN GROWTH ON THE BASIS OF OXYGEN VACANCY CREATION IN YBCO.

An interesting observation made in the above work was that decreasing Po_2 reduced the processing temperature. This led to develop a process of

V. DYNAMIC VACUUM CALCINATION TO PREPARE PHASE PURE YBCO IN A SHORT TIME AND AT A LOW TEMPERATURE.

The application of vacuum (\sim 2-10 mm of Hg) reduces the time and temperature of processing whereas dynamic process takes care of gases evolved during the reaction and thereby restricting any back reaction to be operative which results in impurities.

Inherent properties of BPSCCO has put itself ahead of YBCO due to high T_c , better weatherability and better texture. But literature showed considerable ambiguity in the initial stoichiometry to be chosen for the synthesis of phase pure BPSCCO material having higher J_c . Thus our next aim was

VI. TO STUDY THE EFFECT OF INITIAL STOICHIOMETRY VARIATIONS ON THE FORMATION OF HIGH T_c , LOW T_c , IMPURITY PHASES, TEXTURING AND POSSIBLE PINNING CENTRES.

After achieving certain experimental procedures and better understanding in synthesizing platy grains of YBCO and BPSCCO the next aim was

VII. TO FIND OUT SUITABLE ALIGNMENT TECHNIQUE AND SINTERING SCHEDULE TO MAKE SINTERED BULK WITH HIGHER J_c .

It is well known that addition of Ag has no poisoning effect in YBCO whereas it improves mechanical properties. But a few initial reports showed addition of Ag has a poisoning effect on BPSCCO when processed in air. Thus a study was undertaken

VIII. TO FIND SUITABLE METHOD OF Ag-BPSCCO PROCESSING TO INCREASE J_c AND ITS MECHANICAL PROPERTIES.

The present study is described in three sections. Part A, consists of study of textured grain growth in YBCO under different P_{O_2} , temperature and by substitution. Mechanism for enhanced textured grain growth and preparation and characterization of textured sintered bulk YBCO by cold pressing and heat treatment are also included in this part.

Part B gives details of the preparation of phase pure YBCO by dynamic vacuum calcination and its characterization.

In Part C, studies on the effect of initial compositional variation on the structural and superconducting properties of (Bi,Pb)-Sr-Ca-Cu-O system, textured grain growth of BPSCCO, preparation and characterization of sintered textured bulk BPSCCO by suspension method, superconductivity in Ag added BPSCCO system and the mechanical properties of BPSCCO/Ag composite are included.

REFERENCES

1. H. Kammerligh Onnes, Akad. Van Wetenschappen, 14, 818 (1911).
2. M.R. Beasley, T.H. Geballe, Phys. Today, 36, 60 (1984).
3. J. Muller, Rep. Prog. Phys., 43, 663 (1980).
4. J.G. Bednorz and K.A. Muller, Z. Phys. B 64, 189-193 (1986).
5. J. Bardeen, L.N. Cooper and Schrieffer, Phy. Rev., 108, 1175 (1957).
6. C.W. Chu, P.H. Hor, R.L. Meng, L. Gao, Z.J. Huang and Y.Q. Wang, Phys. Rev. Lett., 58, 405 (1987).
7. M.K. Wu, J.R. Ashburn, C.J. Torng, P.H. Hor, R.L. Meng, L. Gao, Z.J. Huang, Q. Wang and C.W. Chu, Phys. Rev. Lett., 58, 908 (1987).
8. Z. Zhao, C. Liquein, Y. Qiansheng, H. Yuzhen, C. Genghua, T. Ruming, L. Guirong, C. Changgeng, C. Lie, W. Lianzhong, G. Shuquan, L. Shanlin and B. Jianqing, "Superconductivity Above Liquid Nitrogen Temperature In Ba-Y-Cu Oxides", Kexue Tongbao, No.6, 1987.
9. P. Ganguly, A.K. Raychaudhuri, K. Sreedhar and C.N.R. Rao, Pramana J. Phys., 27, L 229 (1987).
10. C.N.R. Rao, P. Ganguly, A.K. Raychadhuri, R.A. Mohan Ram and K. Sreedhar, Nature,, 326, 856 (1987).
11. C. Michel, M. Hervieu, M.M. Borel, A. Grandin, F. Deslandes, J. Provost and B. Revean, Z. Physik. B., 68, 421 (1987).
12. H. Maeda, Y. Tahatea, M. Fukutomi and T. Asano, Jap. J. Appl. Phys., 27, L 209 and L 548 (1988).

13. ✓ R.M. Hazen, C.T. Prewitt, R.J. Angel, N.L. Ross, L.W. Finger, C.G. Hadidiacos, D.R. Velden, P.J. Heaney, P.H. Hor, R.L. Meng, Y.Y. Sun, Y.Q. Wang, Y.Y. Xue, Z.J. Huang, L. Gao, J. Bechtold and C.W. Chu, *Rev. Lett.*, 60, 1174 (1988).
14. ✓ H. Maeda, T. Tanaka, M. Fukutomi, T. Asano, K. Togano, H. Kumakura, M. Hehara, S. Ikeda, K. Ogawa, S. Horiuchi and Y. Matsui, *Physica C*, 153, 602 (1988).
15. ✓ Seiji Adachi, Osamu Inone and Syunichiro Kawashima, *Jap. J. Appl. Phys.*, 27, L 344 (1988).
16. ✓ Eiji Takayama-Muromachi, Yoshishige Uchida, Akira Oho, Fujio Izumi, Mitsko Onoda, Yoshio Matsui, Kosuke Kosuda, Shunji Takekawa and Katsuo Kato, *Jap. J. Appl. Phys.*, 27, L 365 (1988).
17. ✓ J.M. Tarascon, W.R. Mchinnon, P. Barboux, D.M. Hwang, B.G. Bagley, L.H. Green, G. Hull, Y. Le Page, N. Stoffel and M. Giroud, *Phys. Rev. B.*, 38, 2504 (1988).
18. ✓ M. Onada, A. Yamamoto, E. Takayama-Muromachi, S. Takekawa, *Jap. J. Appl. Phys. Pt. 2*, 27, L 833 (1988).
19. ✓ T.M. Shaw, S.A. Shiva Shankar, S.J. La Placa, J.J. Cuomo, T.R. McGuire, R.A. Roy, K.H. Kellecher and D.S. Yee, *Phys. Rev. B.*, 37, 9856 (1988).
20. ✓ M. Hervieu, C. Michel, B. Domenges, Y. Laligant, A. Lebail, G. Fery and B. Ravean, *Modern Phys. Lett.*, B2, 491 (1988).
21. ✓ C.C. Torardi, M.A. Subramanian, J.C. Calabrese, J. Gopalakrishnan, K.J. Morissey, T.R. Askew, R.B. Flippen, U. Chowdhry and A.W. Sleight, *Science*, 240, 631 (1988).
22. ✓ H.W. Zandbergen, Y.K. Huang, M.J. Menken, J.N. Li, K. Kadonak, A.A. Menovsky, G. Vanm Tendeloo and S. Amelinckx, *Nature*, 332, 620 (1988).

23. ✓ P. Bordet, C. Chaillouut, J. Chenavas, J.L. Hodean, M. Marezio, J. Karpinski and E. Kaldis, *Nature*, 334, 596 (1988).
24. ✓ Z.Z. Zheng, A.M. Hermann, A. El Ali, C. Almasan, J. Estrada, T. Datta and R.J. Matson, *Phys. rev. Lett.*, 60, 937 (1988).
25. ✓ Z.Z. Sheng and A.M. Hermann, *Nature*, 332, 55 (1988).
26. ✓ C.C. Torardi, M.A. Subramanian, J.C. Calabrese, J. Gopalakrishnan, E.M. McCarron, K.J. Morissey, T.R. Askew, R.B. Flippen, U. Chowdhry and A.W. Sleight, *Phys. Rev. B.*, 38, 2285 (1988).
27. ✓ Z.Z. Sheng and A.M. Hermann, *Nature*, 332, 138 (1988).
28. ✓ Z.Z. Sheng, W.K. Kiehl, J. Bennet, A. Elali, D. Marsh, G.D. Mooney, F. Armamash, J. Smith, D. Viar and A.M. Hermann, *Appl. Phys. Lett.*, 52, 1738 (1988).
29. ✓ C. Martin, C. Michel, A. Maignan, M. Hervieu and B. Reveau, *C.R. Acad. Sci.*, 307, Ser.II, 27 (1988).
30. ✓ M. Hervieu, A. Maignan, C. Martin, C. Michel, J. Provost and B. Raveau, *J. Solid State Chem.*, 75, 212 (1988).
31. ✓ M. Hervieu, A. Maignan, C. Martin, C. Michel, J. Provost and B. Raveau, *Modern Phys. Lett. B.*, 2, 1103 (1988).
32. H.W. Zandbergen, R. Gronsky, K. Wang and G. Thomas, *Nature*, 331, 596 (1988).
33. L.F. Matheiss, E.M. Gyorgy and D.W. Johnson, Jr., 1988, *Phys. Rev. B.*, 37, 3745 (1988).
34. A.V. Narlikar, C.V. Narasimha Rao and S.K. Agarwal, "Studies of High Temperature Superconductors", Edited by A.V. Narlikar, Vol. 1, 341 (1989).
35. ✓ R.J. Cava, B. Batlogg, R.B. Van Dover, D.W. Murphy, S. Sunshine, T. Siegrist, J.P. Rameika, E.A. Rietman, S. Zahurak and G.P. Espinosa, *Phys. Rev. Lett.*, 58, 1676 (1987).

36. ✓ Y. Lepage, W.R. Mckinnon, J.M. Tarascon, L.H. Greene, G.W. Hull and D.M. Hwang, Phys. Rev. B., 35, 7245 (1987).
37. / G. Roth, D. Ewert, G. Heger, C. Michel, M. Hervieu, B. Raveau, F.D. Yvoire and A. Revcderschi, Z. Phys. B., 69, 21 (1987).
38. ✓ M.A. Beno, L. Soderholm, R.W. Capone, d.G. Hinks, J.D. Jorgensen, I.K. Schuller, C.U. Segre, K. Zhang and J.D. Grace, Appl. Phys. Lett., 51, 57 (1987).
39. ^ J. Capponi, C. Chaillout, A.W. Hewat, P. Lejay, M. Marezio, N. Ngayen, B. Raveau, J.L. Soubeyroux, J.L. Tholence and R. Tournier, Europhys. Lett., 12, 1301 (1987).
40. ~ J.E. Greedan, A.H. O'Reilly and C.V. Stager, Phys. Rev. B., 35, 8778 (1987).
41. ' F. Beech, S. Miraglia, A. Santoro and R.S. Roth, Phys. Rev. B., 35, 8778. (1987).
42. \ W.I.F. David, W.T.A. Harrison, J.M.F. Gum, O. Moze, A.K. Soipper, P. Day, J.D. Jorgensen, D.G. Hinks, M.A. Beno, L. Soderholm, D.W. Capone, I.K. Schuller, Q.C.U. Segre, K. Zhang and J.D. Grace, Nature, 327, 310 (1987).
43. } W. Schafer, E. Jansen, G. Will, J. Faber Jr. and B. Veal, Mat. Res. Bull., 23(10), 1439 (1988).
44.) J.D. Jorgensen, D.G. Hinks, H. Shaked, B. Dabrowski, B.W. Veal, A.P. Paulikas, L.J. Nowicki, G.W. Crabtree, W.K. Kwok, A. Umezawa, L.H. Nunez and B.D. Dunlap, Physica B., 156-157, 877 (1989).
45. ✓ M. Kikuchi, Y. Syono, A. Tokiwa, K. Oh-ishi, H. Arai, K. Hiraga, N. Kobayashi, T. Sasaoka and Y. Muto, Jap.- J. Appl. Phys., 26, L 1066 (1987).
46. ~ Y. Le Page, T. Siegrist, S.A. Sunshine, LK.F. Schneemeyer, D.W. Murphy, S.M. Zahurak, J..V. Waszczak, W.R. Mckinnon, J.M. Tarascon, G.K. Hull and L. H. Greene, Phys. Rev. B., 36, 3617(1987).

47. ✓ T. Siegrist, S.A. Sunshine, D.W. Murphy, R.J. Cava and S.M. Zahurak, *Phys. Rev. B.*, 35, 7137 (1987) .
48. ✓ F.P. Okamura, S. Sueno, I. Nakai and A. Ono, *Mat. Res. Bull.*, 22(8), 1081 (1987).
49. ✓ M. Hazen, L.W. Finger, R.J. Angel, C.T. Prewitt, N.L. Ross, H.K. Mao, C.G. Hadjidakos, P.H. Hor, R.L. Meng and C.W. Chu, *Phys. Rev. B.*, 36, 3966 (1987).
50. ✓ S.W. Tozer, A.W. Kleinsasser, T. Penney, D. Kaiser, F. Holtzberg, *Phys. Rev. Lett.*, 59, 1768 (1987).
51. ✓ T.R. McGuirie, T.R. Dinger, P.J.P. Freitas, W.J. Gallagher, T.S. Plaskett, R.L. Sandstrom and J.M. Shaw, *Phys. Rev. B.*, 36, 4032 (1987).
52. ✓ J.S. Moodera, R. Merservey, J.E. Tkaczyk, C.X. Hao, G.A. Gibs and P.M. Tedrow, *Phys. Rev. B.*, 37, 619 (1987).
53. ✓ T.R. Dinger, T.K. Worthington, W.J. Gallagher, R.L. Sandstrom, *Phys. Rev. Lett.*, 58, 2687 (1987).
54. ✓ G.W. Crabtree, J.Z. Liu, A. Umezawa, W.K. Kwok, C.H. Sowers, S.K. Malik, *Phys. Rev. B.*, 36, 4021 (1987).
55. ✓ P.K. Gallagher, H.M. O'Bryan, S.A. Sunshine and D.W. Murphy, *Mat. Res. Bull.*, 22, 995 (1987).
56. ✓ Kohji Kishio, Jun-ichi Shimoyama, Tetsunya Hasegawa, Koichi Kitazawa and Kazho Fueki, *Jap. J. Appl. Phys.*, 26(7), L 1228 (1987);.
57. ✓ Y. Ueda and K. Kosuge, *Physica C*, 156, 281 (1988).
58. ✓ R.J. Cava, B. Batlogg, C.H. Chen, E.A. Rietman, S.M. Zahurak and D. Werder, *Phys. Rev. B.*, 36, 5719 (1987)
Nature, 329, 423 (1987).

59. R.J. Cava, B. Batlogg, K.M. Rube, E.A. Rietman, P.K. Gallagher and L.W. Rupp Jr., *Physica C*, 156, 523 (1988).
60. C.N.R. Rao, *J. Solid State Chem.*, 74, 147 (1988).
61. H.M. O'Bryan and P.K. Gallagher, *Adv. Ceram. Mater.*, 2(38), 640 (1987).
62. P. Gourieux, G. Krill, M. Maurer, M.F. Ravet, A. Menny, H. Tolentino and A. Fontaine, *Phys. Rev. B.*, 37, 7516 (1988).
63. D.C. Johnston, A.J. Jacobson, J.M. Newsam, J.J. Lewandowski, D.P. Gosborn, D. Xie and W.B. Yelon in "Chemistry of High Temperature Superconductors", ACS Symposium Series 35, edited by D.L. Nelson, M.S. Whittingham and T.F. George (American Chemical Society, Washington, DC 1987).
64. P. Meuffels, B. Rupp and E. Porschke, *Physica C*, 156, 441 (1988).
65. B.G. Bagley, L.H. Greene, J.M. Tarascon and G.W. Hull, *Appl. Phys. Lett.*, 51, 622 (1987).
66. Douglu Shi and D.W. Capone II, *Appl. Phys. Lett.*, 53, 159 (1988).
67. I. Wei Chen, S.J. Keating, C.Y. Keating, X. Wu, J. Xu, P.E. Reyes-Morel and T.Y. Tien, *Solid State Commun.*, 63(11), 997 (1987).
68. P.K. Gallagher, H.M. O'Bryan, S.A. Sunshine and D.W. Murphy, *Mat. Res. Bull.*, 22, 995 (1987).
69. J.D. Jorgensen, H. Shaked, D.G. Hinks, B. Dabrowski, B.W. Veal, A.P. Paulikas, L.J. Nowicki, G.W. Crabtree, W.K. Kwok, L.H. Nunez and H. Claus, *Physica C*, 153-155, 578 (1988).
70. Y. Hariharan, M.P. Janawadkar, V. Sankara Sastry and T.S. Radhakrishnan, *Pramana J. Phys.*, 31, L 59 (1988).

71. W.E. Farneth, R.K. Bordia, E.M. McCarron III, M.K. Crawford and R.B. Flippen, *Solid State Commun.*, 66, 953 (1988).
72. B.W. Veal et al, *Phys. Rev. B.*, 42, 4770 (1990).
73. J.D. Jorgensen et al, *Physica C*, 167, 571 (1990).
74. D. de Fontaine, LT. Wille and S.C. Moss, *Phys. Rev. B.*, 36, 5709 (1987).
75. P.K. Gallagher, *Adv. Ceram. Mater.*, 2(3B), 632 (1987).
76. K.G. Frase and D.R. Clarke, *Adv. Ceram. Mater.*, 2(3B), 295 (1987).
77. R.S. Roth, K.L. davis and J.R. Dennis, *Adv. Ceram. Mater.*, 2(3B), 303 (1987).
78. G. Wang, s.J. Hwu, S.N. Song, J.B. Ketterson, L.D. Marks, K.R. Poeppelmeier and T.D. Mason, *Adv. Ceram. Mater.*, 2(3B), 313 (1987).
79. D.G. Hinks, L. soderholm, D.W. Capone II, J.D. Jorgensen, Ivan K. Schuller, C.U. Segre, K. Zhug and J.D. Grace, *Appl. Phys. Lett.*, 50(23), 1688 (1987).
80. J. Karpinski, C. Beeli, E. Kaldis, E. Wisard and E. Jilek, *Physica C*, 153, 830 (1988).
81. Akira Ono and Yoshio Ishizawa, *Jap. J. Appl. Phys.*, 26(6), L 1043 (1987).
82. V. Bhat, A.K. Ganguli, K.S. Nanjunda Swamy, R.A. Mohan Ram, G.J. Gopalakrishnan and C.N.R. Rao, *Phase Transitions*, 10, 87 (1987).
83. R.M. Hazen, L.W. Finger, R.J. Angel, C.T. Prewitt, N.L. Ross, M.K. Mao, C.G. Hadidiacos, P.H. Hor, R.L. Meng and C.W. Chu, *Phys. Rev. B.*, 35, 7238 (1987).

84. J.M. Williams, B.K. Flandermeyer and R.B. Popel, *Inorg. Chem.*, 26, 1474 (1987).
85. G.F. Holland and A.M. Stacy, *Acc. Chem. Res.*, 21, 8 (1988).
86. T.W. Huang, N..C. Wu, Y.H. Chou, W.J. Lin, T.C. Wu, T.S. Chin, P.T. Wu, H.H. Yen and Y.S. Chen, *J. Cryst. Growth*, 91, 402 (1988).
87. D.H.A. Blank, J. Flokstra, G.J. Gerritsma, L.J.M. Van de Klundert and G.J.M. Velders, *Physica (B+C)*, 145(2), 222 (1987).
88. W. Desisto, N. Kamegashira, W.Y. Chung, M. Hart, J. Baglio, K. Dwight and A. Wold, *Prog. High temp. Supercond.*, 7, 32 (1988) (World Sci. Publ., Singapore).
89. A. Manthiram and J.B. Goodenough, *Nature*, 329, 701 (1987).
90. J.D. Jorgensen, H.B. Schuttler, D.G. Hinks, D.W. Capone, K. Zhang, M.B. Brodsky and D. Schalapino, *Phys. Rev. Lett.*, 58, 1024 (1987).
91. J.M. tarascon, P. Barbonx, B.G. Bagley, L.H. Greene, W.R. Mckinnon and G.W. Hull, *ACS Symp. Ser.*, 351, Chap. 20 (1987).
92. J.M. Tarascon, P. Barboux, P.F. Miceli, B.G. Bagley, L.H. Greene, G.W. Hull and M. Giroud, *J. Phys. Colloq.*, C 8, 2081 (1988).
93. E.C. Behrman, *Adv. Ceram. Mater.*, 2(3B), 539 (1987).
94. S. Jin, R.C. Sherwood, R.B. Van Dover, T.H. Tiefel and D.W. Johnson Jr., *Appl. Phys. Lett.*, 51, 203 (1987).
95. H. Hsu, L. Masur, C. Joshi, K. Sandhage, W. Carter and G.J. Yurek, *Proc. of Appl. Superconductivity Conf. San Francisco, CA Aug. 1988.*

96. U.V. Varadaraju and G.V. Subba Rao, "Studies of High Temperature Superconductors", 3, 229 (1989). Ed. A.V. Narlikar, Nova Science Publishers.
97. F.H. Streitz, M.Z. Cieplak, Gang Xiao, A. Gavrin, A. Bakhshai and C.L. Chien, Appl. Phys. Lett., 52(11), 927 (1988).
98. D.W. Johnson Jr., E.M. Gyorgy, W.W. Rhodes, R.J. Cava, L.C. Feldman and R.B. Van Dover, Adv. Ceram. Mater., 2(3B), 364 (1987).
99. L.E. Murr, A.W. Hare and N.G. Eror, Nature, 329, 6134 (1987).
100. B.C. Hendrix, J.C. Borofka, T. Abe, J.K. Tien, T. Caulfield and S.M. Reichman, Proc. of the North East Regional Meet, Processing and Application of High Tc Supercond. Status and Prospects, May 9-11, Pitscaway, USA, 1988.
101. T.J. Richardson and L.C. Dejonghe, Appl. Phys. Lett., 53, 2342 (1988).
102. G. Arcangel, R. Fava, A. Masci, A. Nardi, R. Vattaroui and C. Zondini, World Congress on Superconductivity, Prog. in High Temp. Superconductivity, Series, 8, 433 (1988).
103. Quentin Robinson, P. Georgopoulos, D. Lynn Johnson, Henry O. Marcy, Carl. R. Kannewurf, S.J. Hwu, Tobin J. Marks, K.R. Poeppelmeier, S.N. Song and J.B. Ketterson, Adv. Ceram. Mater., 2(3B), 380 (1987).
104. S. Jin, T.H. Tiefel, R.C. Sherwood, G.W. Kammlott and S.M. Sahurak, Appl. Phys. Lett., 51, 943 (1987).
105. E. Beyne, C. Deneffe, J. roggen, J. Fransaer, O. Arkens and O. Vanderbiest, Physica C, 153-155, 808 (1988).
106. N.P. Bansal, R.N. Simon and D.E. Farrell, Proc. 90th Annual Meeting of the Am. ceram. Soc., cincinnati, May 1988.

- U.V. Varadaraju, G.V. Subba Rao, K.D. Chandrasekaran and B. B. Baradarajan, *Thin Solid Films*, 164, 119 (1988).
107. J.J. Cuomo, C. Richard Guarnieri, S.A. Shivashankar, R.A. Roy, D.S. Yee and r. Rosenberg, *Adv. Ceram. Mater.*, 2, 422 (1987).
108. S. Mohan, "High Temperature Superconductor", Edited by S.V. Subramanyam and E.S. Raja Gopal, Wiley Eastern Ltd., 234 (1989).
109. A.B. Bykov, L.N. Demyanets and I.P. Zibrov, *J. Cryst. Growth*, 91, 302 (1988).
110. Y. Hidaka, Y. Enomot, M. Suzuki, M. Oda and T., Murakami, *J. Cryst. Growth*, 85, 581 (1987).
111. Z. Chen, Y. Quian, D. Sun, M. Fang, J. Xia, Z. Zhao, Y. Zhao, and W.Y. Kuan, *Physica C*, 153-155, 409 (1988).
112. H.J. Scheel and F. Licci, *J. Cryst. Growth*, 85, 607 (1987).
113. F. Licci, H.J. Scheel and T. Besagni, *Physica C*, 153-155, 431 (1988).
114. A.P. Malozemoff, W.J. Gallagher and R. Schwall, *ACS Symp. Series*, 351, Chap. 27 (1987).
115. V.G. Baryakhtar, V.M. Pan, V.G. Prokhorov et al, *Pisma Zh Eksp Teor Fiz (Sov)*, 46, 168 (1987).
116. V.M. Pan, V.G. Prkhorov, C.G. Kaminsky et al, *Fiz. Nizk Temp. (Sov)*, 13, 861 (1987).
117. R. Watanabe, Y. Kasai, T. Machiku et al, *Jap. J. Appl. Phys.*, 26, L 657 (1987).
118. U. Dai, G. Deutscher and R. rosenbaum, *Appl. Phys. Lett.*, 51, 460 (1987).

119. P. Chaudhary, R.H. Koch, R.B. Laibowitz, T.R. McGuire and R.J. Gambino, *Phys. Rev. Lett.*, 58, 2684 (1987).
120. Y. Enomoto, T. Murakami, M. Suzuki and K. Moriwaki, *Jap. J. Appl. Phys.*, 26, L 1248 (1987).
121. T.R. Dinger, T.K. Worthington, W.J. Gallagher and R.L. Sandstrom, *Phys. Rev. Lett.*, 58, 2687 (1987).
122. S. Jin, *Science*, 238, 1655 (1987).
123. B.A. Camps, J.E. Evetts, B.A. Glowacki, S.B. Newcomb, R.E. Somekh and W.H. Stoobs, *Nature*, 329, 229 (1987).
124. N. McN Alford, W.J. Clegg, M.A. Harmer, J.D. Bircha, K. Kendall and D.H. Jones, *Nature*, 332, 58 (1988).
125. P. Borrdet, J.J. Capponi, G. Chaillout, J. Chenavas, A.W. Hewat, E.A. Hewat, J.L. Hodeau, M. Marezio, J.L. Tholence and D. Tranqui, *Physica C*, 153-155, 623 (1988).
126. I. Kajitani, K. Kusaba, M. Kikuchi, N. Kobayashi, Y. Syono, T.B. Williams and M. Hirabayashi, *Jap. J. Appl. Phys. Pt. 2*, 27, L 587 (1988).
127. H.G. Von Schnering, L. Walz, M. Schwarz, W. Becker, T. Hatweg, B. Popp, B. Hettich, P. Muller and G. Kampf, *Angew. Chem. Intl. Ed. (Engl.)*, 27, 574 (1988).
128. S.A. Sunshine, T. Siegrist, L.F. Schneemeyer, D.W. Murphy, R.J. Cava, B. Batlogg, R.B. Van Dover, R.M. Fleming, S.H. Glarum, S. Nakahara, R. Farrow, J.J. Krajewski, S.M. Zahurak, J.V. Wuszcak, J.H. Marshall, P. Marsh, L. W. Rupp Jr. and W.F. Peck, *Phys. Rev. B.*, 38, 893 (1988).

CHAPTER 2

EXPERIMENTAL METHODS AND INSTRUMENTAL TECHNIQUES

CHAPTER 2

EXPERIMENTAL METHODS AND INSTRUMENTAL TECHNIQUES

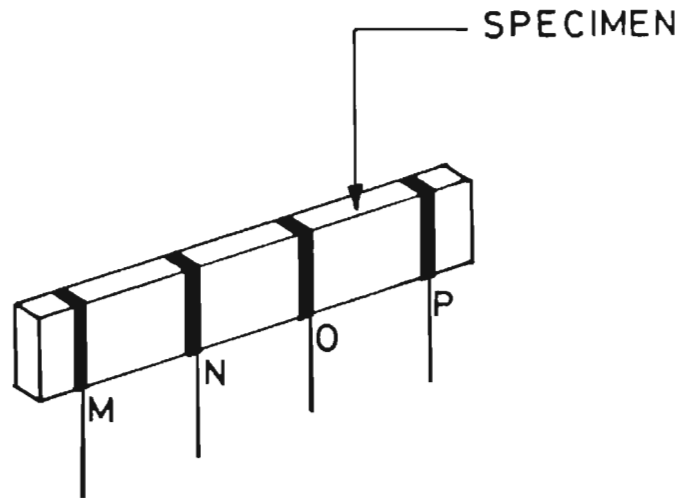
2.1 INTRODUCTION

In this chapter a brief description of the major experimental techniques and methods used for the characterization of high temperature superconductors are given. A description of the instruments used for the characterization of the materials are also included here. Further experimental details are given in the appropriate chapters.

2.2 TRANSITION TEMPERATURE (T_c) MEASUREMENT

T_c of the samples was measured by standard four probe method [1] using an APD cryostat. Bar shaped specimens of dimensions 20 mm x 4 mm x 2 mm were prepared and point contacts were given at the points M,N,O,P as shown in Fig. 2.1 using silver paste 309 (Demetron) and curing was done at 100^oC. Copper wire was soldered at these points.

To measure the resistance, a constant d.c. current (in the range 1-10 mA from Keithley constant current source model 220) was sent through the sample between contacts M & P. The voltage drop was measured between the contacts N and O with a Keithley 181 nanovoltmeter. The sample was initially cooled to around 20 K and then slowly heated at the rate of 1 K/min while the measurements were reading done. At the superconducting transition temperature, the voltmeter suddenly raised from zero while a current is passing through the sample.



M,P - Current leads
N,O - Voltage leads

Fig. 2.1: Four-probe contacts

2.3 CRITICAL CURRENT DENSITY (J_c) MEASUREMENTS

Sample holder as shown in the figure 2.2 for the measurements of J_c was fabricated. Bar shaped specimens were used for the measurements. For making the current leads end of the sample was first coated with silver paste and then pressure contact was given by using the sample holder. For the voltage leads copper wire was soldered on the coating of silver paste at an interval of 1 cm. A powerful battery was used as the current source. Critical current at 77 K was determined by the resistive transition with 1 μ V/cm criterion.

2.4 XRD ANALYSIS

In the present study, X-ray powder diffraction was used as the main tool for the identification of phases, for the determination of lattice parameters and for the identification of crystallographic plane of grain growth and its quantification in both YBCO and BPSCCO.

The basic principle of X-ray powder diffraction is Bragg's law. Since the atoms or molecules in a crystal are arranged with a definite spatial symmetry, Bragg assumed that a set of equidistant parallel planes can be drawn through any crystal. A very large number of such families of planes may be drawn. The planes of each family are separated from each other by a characteristic distance. These planes are known as Bragg's planes and their separations as Bragg's spacing 'd'.

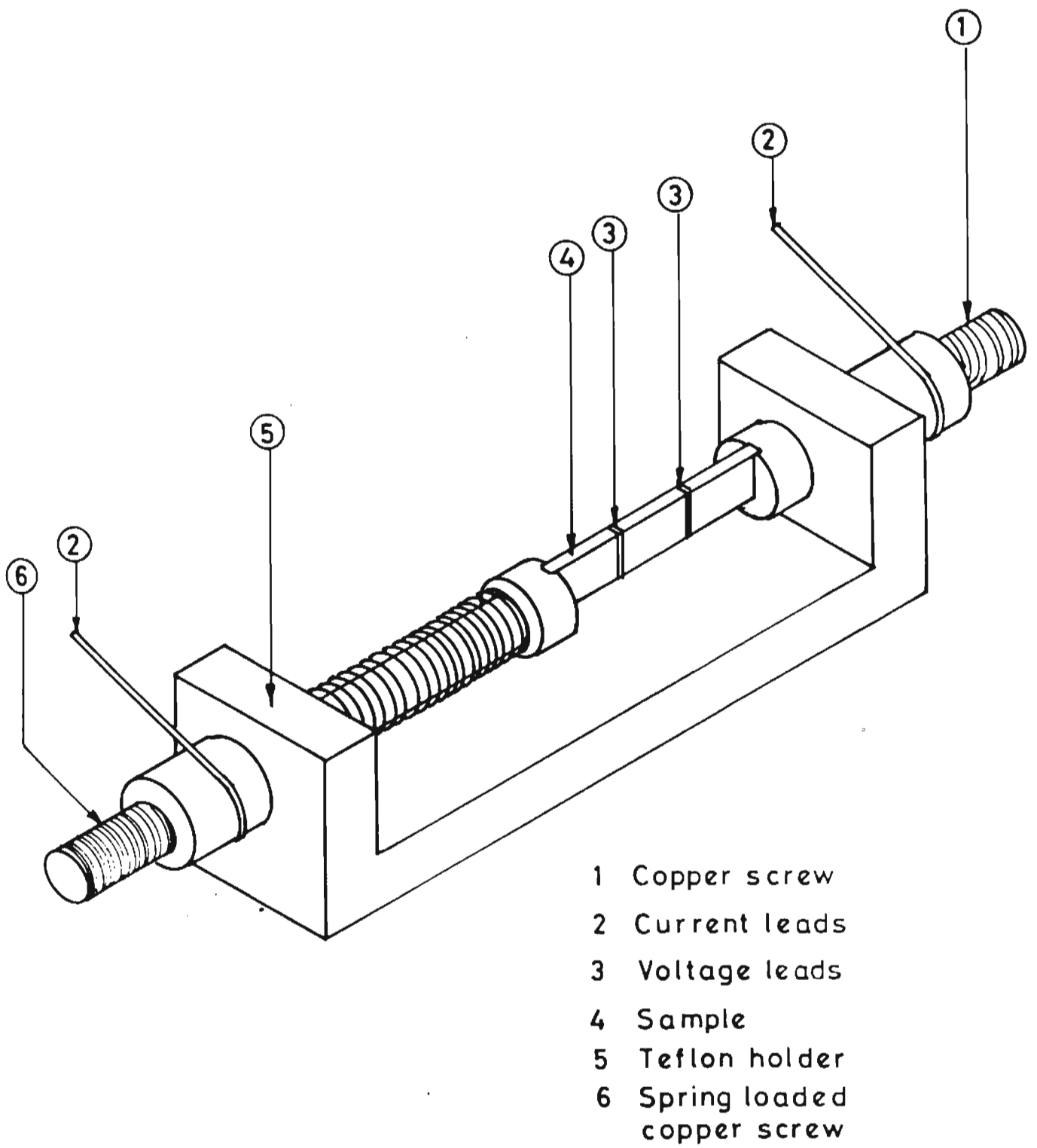


Fig. 2.2: Sample holder for the measurement of J_c

Let us consider several parallel planes in the crystal. Let X-ray wave front enter from the left making an angle θ with the crystal plane, 'pp'. It can be reflected only if after scattering, it proceeds in a direction making again an angle θ with the plane considered. It is represented by Fig. 2.3. From the Fig. 2.3, it can be easily seen that the rays reflected from the second plane 'p₁p₁' travel a greater distance than those from the plane 'pp'. In order that reflection from the second and successive planes should reinforce we must have these additional distances as some integral multiples of the X-ray wave length.

$$\text{ie, } 2d\sin\theta = n\lambda$$

where n - is the order of reflection.

The above equation is known as the Bragg equation.

The X-ray powder diffractometer is an out growth of the Bragg ionization spectrometer [2] which was applied as early as 1913 to the measurement of reflections from single crystals. Unlike the ionization spectrometer which disperse a spectrum of X-ray wavelengths, by means of a crystal gratings of some fixed spacing d_{hkl} , the diffractometer is designed to disperse X-rays of a single wave length by diffracting them from planes of different spacing. Furthermore, an X-ray powder diffractometer is characterized by the use of a local intensity receiver (quantum counter) rather than a photographic film and a parafocussing arrangement is usually employed to increase the intensity and the resolution.

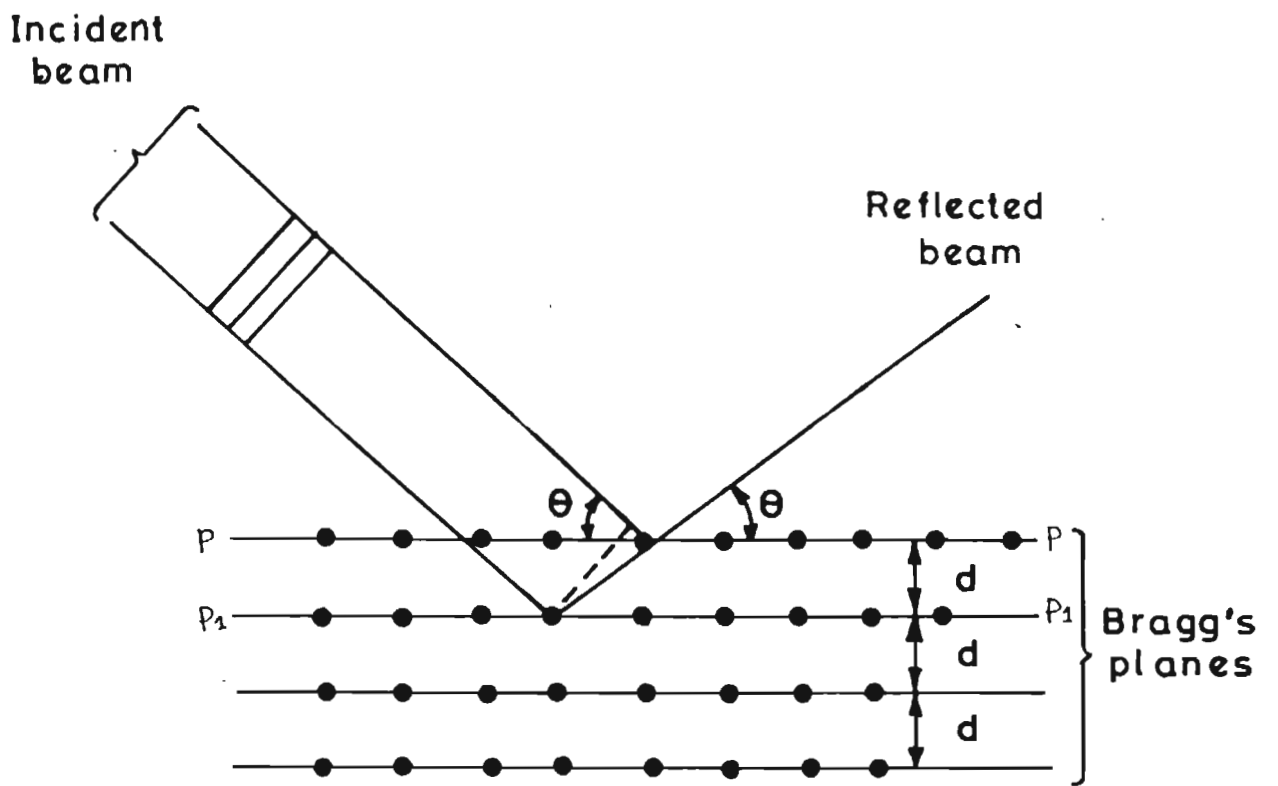


Fig. 2.3: X-ray diffraction in crystals

For the present studies, the X-ray diffractograms were recorded with Philips PW 1710 powder diffractometer. The X-ray generator is operated at 35 kV and 20 mA. Cu K α radiation is used with a Ni filter. The scanning range employed is 4-100^o. The normal scanning speed is 2^o/min with chart speed being 1 cm/min. When precise lattice parameter measurements are to be made the reflection peaks are recorded with slow scanning speed (0.3^o/min with chart speed 1.5 cm/min). When comparative studies are to be made on various test samples, the instrumental parameters are kept constant. Silicon is used as the internal standard for precise measurements. The lattice parameters were determined using the least square method [3].

2.5 MICROSCOPIC TECHNIQUES

Microscopic techniques are very good tools for the accurate observation of morphology, size of grains and surface properties of materials. For the micrographs, desirable magnification is required in order to get the details one is looking for. Optical microscopy is usually adequate for characterisation of particles greater than 0.5 to 1 μm in size. Electron microscopes (both transmission and scanning) can measure particles sizes as less as 0.001 μm .

In scanning electron microscopy a focussed electron beam is impinged on the sample. The reflected beam is analysed by suitable devices to get well defined pictures of sample surface. In the course of present investigation, scanning electron microscope (SEM), JEOL-

JSM35C was used. The electron gun was operated at an electron energy of 15-25 KeV with a beam diameter of 20-25 nm. The unit is operated at 1 KV and 10 mA current. Polished as well as fracture surfaces have been examined by the SEM. Before loading the sample in the chamber, conductive gold coating was given using a sputtering unit (JEOL, Fine Coat, JFC 1100, Japan). The thickness of coating was $>100 \text{ \AA}$. This helps to remove the charging effect which is produced on the sample surface due to high energetic beam. For taking the photographs of these gold coated samples, it was mounted in the chamber and the system as evacuated to 10^{-6} torr pressure. The electron beam was directed on the selected areas according to the requirement. In the present study, most of the photographs were taken at a magnification of 1000-2000.

Optical photographs of the polished surface of the superconductor/Ag composites were taken using a Leitz Metalloplan optical microscope with different magnification under bright field illumination.

2.6 THERMAL METHODS OF ANALYSIS

Thermal analysis is a general term which covers a group of related techniques in which the temperature dependence of the parameters of any physical property of a substance is measured [4,5]. The physical property is determined as a function of temperature. The more important thermal analysis are thermogravimetry (TG), Differential thermal analysis (DTA) and Differential scanning calorimetry (DSC). In the present study, TG and DTA are used for the characterization of high temperature superconductors.

Thermogravimetry is defined as the technique whereby the mass of a substance in an environment heated or cooled at a controlled rate is recorded as a function of time or temperature.

Differential thermal analysis is a thermal technique in which a record is made of the temperature difference between the sample and an inert reference material against time or temperature while the two specimens are subjected to identical temperature regimes in an environment heated or cooled at a controlled rate. The graphical records of DTA curves shows sharp increase or decrease in the temperature difference depending on whether a change in the sample causes liberation or absorption of heat. The reference substance should not undergo decomposition or phase transition in the temperature range of interest. α -Alumina is often used as the reference material which behaves satisfactorily upto 1950^oC.

The basic components of a TGA apparatus is thermobalance. The main part of a thermobalance are (a) recording balance, (b) furnace, (c) furnace temperature programmer and controller, and (d) recorder.

The basic components of a DTA equipment are (a) furnace, (b) sample holder, (c) temperature sensor, (d) property (ΔT or dA/dt) sensor, (e) recorder, and (f) furnace temperature programmer.

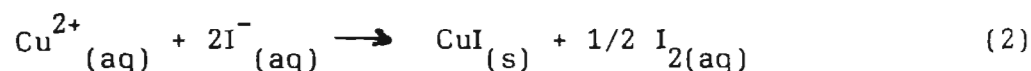
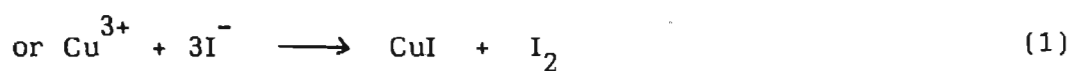
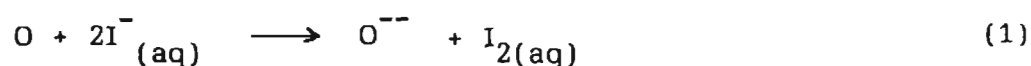
Du Pont 2000 thermal analysis system in conjunction with 951 TGA and 1200 DTA were used for the present study.



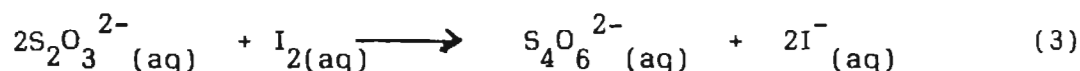
2.7 DETERMINATION OF OXYGEN STOICHIOMETRY BY IODOMETRIC TITRATION

An iodometric titration was developed by Harris et al [6] for the determination of oxygen content in YBCO superconductor [6-8]. This method is widely employed for the determination of oxygen content in YBCO superconductor [7,8].

The Cu^{2+} and excess oxygen content (Cu^{3+}) of $\text{YBa}_2\text{Cu}_3\text{O}_{7-\delta}$ was measured by two iodometric titrations. In experiment A, approximately 25 mg of YBCO powder was dissolved under Ar in 7 ml of 1 MKI + 0.7 M HCl solution. Cu^{3+} or excess oxygen behaves as a two electron oxidant and Cu^{2+} as a one electron oxidant.



The solution was diluted with 8 ml water and the liberated iodine was titrated with sodium thiosulphate. One mole of thiosulphate corresponds to one equivalent of oxidant (I or O) in the original sample.



In experiment B approximately 25 mg of powder was dissolved

in 5 ml of 1 M HCl in air and boiled gently for 10 minutes. As stated earlier Cu^{3+} or excess oxygen in YBCO reacts with the hydrochloric acid to liberate oxygen and is reduced to Cu^{2+} or O^{2-} . Then 10 ml of 0.7 M KI was added under argon and the liberated iodine (I_2) was titrated with thiosulphate. In this case all the copper is in the form of Cu^{2+} . It follows that the fraction of Cu in the trivalent state is $(A-B)/B$ where A and B represent the moles of titrant required per gram of samples in experiments A and B respectively. Then the oxygen content of the material is

$$6.5 + \left(\frac{A-B}{B} \right) \frac{3}{2}$$

Iodometric titrations were carried out under Ar to prevent air-oxidation of iodide ion. Sodium thiosulphate titrant was standardised against standard $\text{K}_2\text{Cr}_2\text{O}_7$ solution. Starch indicator was added just before the end point in the titrations.

REFERENCES

1. L.J. van der Pauw,, Philips Res. Rep., 13, 1 (1958).
2. W. Perrish, advances in x-ray diffractometry and x-ray spectrography, Centrex Publishing Company, Eindhoven, The Netherlands, 1962.
3. H.P. Klung and L.E. Alexander, X-ray diffraction procedures, 2nd edition, Wiley-Interscience Publications, 597, 1974.
4. J.N. Kapur and H.C. Saxena, Mathematical statistics, 88th edn., Chand & Co., New Delhi (1976) p.280.
5. C. Mack, Essentials of statistics for scientists and technologists , Plenum Press, New York (1967) p.106.
6. D.C. Harris and T.A. Hewston, J. solid State Chem., 69, 182 (1987).
7. A. Manthiram, J. Swinnea, Z.T. Sui, H. Steinfink and J.B. Goodenough, J. Amer. Chem. Soc., 109, 6667 (1987) .
8. J.D. Jorgensen, B.W. Veal, A.P. Paulikas, L.J. Nowicki, G.W. Crabtree, H. Claus and W.K. Kwok, Phys. Rev. B., 41, 1863 (1990).

P a r t A

CHAPTER 3

STUDIES ON TEXTURED GRAIN GROWTH IN YBCO UNDER DIFFERENT OXYGEN PARTIAL PRESSURES AND TEMPERATURES

CHAPTER 3

STUDIES ON TEXTURED GRAIN GROWTH IN YBCO UNDER DIFFERENT OXYGEN PARTIAL PRESSURES AND TEMPERATURES *

3.1 INTRODUCTION

As mentioned in the general introduction part, the major hurdle in the practical applications of YBCO is its poor value of transport critical current density (J_c). For major high current electrical applications it should be at least of the order of 10^5 A/cm² whereas it is frequently reported to be of the order of 10^2 - 10^3 A/cm² in bulk at 77K in zero applied field [1-4]. In spite of low J_c observed in bulk, the interest in this material is related to the fact that J_c of single crystal or single grain is as high as 10^7 - 10^8 A/cm² [5-7]. One of the major reasons for the large difference between inter-grain and intra-grain J_c is the anisotropic nature of J_c [7,8]. From the single crystal studies it was found that J_c is about an order of magnitude higher along ab-plane than along c-axis [9]. Therefore for getting higher critical current density in bulk, the individual grains should be aligned or textured so that their ab-planes lie in the direction of current.

Single crystals of YBCO are difficult to grow in large sizes. Conventional methods of fabrication of bulk material, though easy, result in random orientation of the particles and shows average isotropic properties only [10]. Therefore fabrication processes which yield textured microstructure are needed.

*This work has been partly published in:

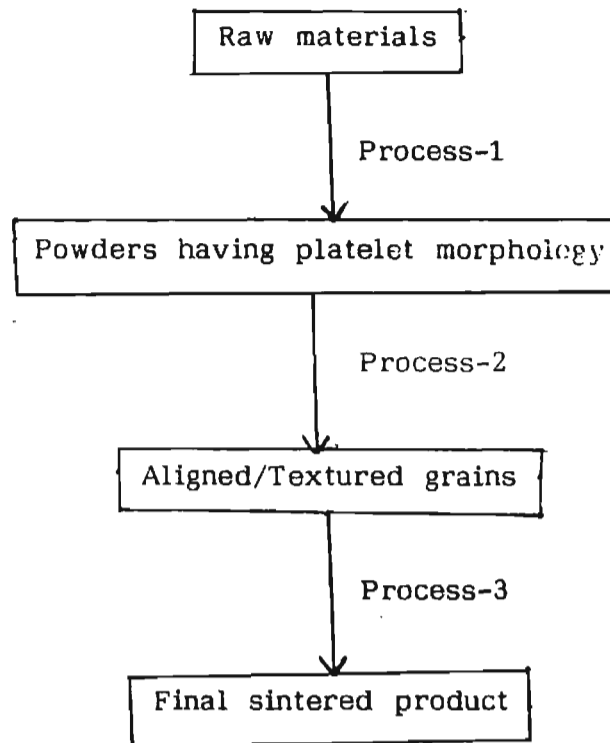
a. Solid State Commun., 72, 93 (1989)

b. Superconductor Science & technology, 5, 54 (1992)

Grain-oriented fabrication in ceramics requires the presence of some form of anisotropy in the particles of the starting material or a driving force which is utilized during processing to encourage anisotropy in grain growth [10]. The grain-oriented fabrication method thus be tailored for the material depending on whether the anisotropy in the particle morphology is utilized or the anisotropy in some specific property of the particle is utilized. Both methods can be used separately or in conjunction with each other wherever possible to obtain enhanced orientation. The ordering force that can be used for orienting the grains are mechanical (including gravity), electrical, magnetic etc.

There are several different ways of introducing texture in bulk polycrystalline YBCO superconductors. The most important work in this direction has been the fairly recent achievement of J_c of the order of 10^4 - 10^5 A/cm² in melt textured YBCO [11,12] in which both peritectic reaction and directional solidification is induced by partial melting and temperature gradient.

An equally important technique is to grow preferentially the ab-planes in grains and aligning the resulting platelet shaped grains by mechanically or magnetically and finally sintering it so that the alignment is retained. The flow chart of this technique is as follows.



Raw materials are usually nitrates, carbonates or oxides of Y, Ba and Cu. In process-1, raw materials are well mixed and subjected to appropriate heat treatment so that it should give phase pure platelet grains having grain growth along ab-plane. In the process-2 these grains are aligned or textured, mechanically or magnetically so that their ab-plane lie in the same direction.

Mechanical alignment methods include (a) plastic extrusion, (b) tape casting, (c) hot pressing, (d) vibrational alignment, (e) cold pressing, and (f) suspension through a dense liquid.

In the magnetic alignment method slurry of the platelets prepared in an epoxy resin or other volatile solvent like heptane is dried in the presence of magnetic field of the order of 9-10T [13,14].

The grains get aligned because of its anisotropic paramagnetic susceptibility.

The aligned grains are then subjected to process-3 in which by proper heat treatment a sintered and oxygenated final product is obtained.

Many researchers have followed mechanical as well as magnetic alignment methods and they have obtained J_c about 5 to 10 times of magnitude higher than that of conventionally fabricated samples [15-23]. Among these, the report of X.G. Zheng et al [15] is a remarkable one which gives a J_c of $4200A/cm^2$ at 77K in YBCO by vibrational alignment method.

The key to the mechanical/magnetic alignment and sintering process is the powder with anisotropic morphology. Thus it is imperative to study the conditions under which such platy grain formation occurs in YBCO and to optimize the experimental conditions so as to yield the grain size within the range required for the successive processing steps as described above.

It is well known that in an oxidic ceramic system having a layered crystalline structure if the duration, temperature and oxygen partial pressure of calcination are optimized, the inherent growth anisotropy of the materials allow to develop platy particles.

In the present study the growth of platelet shaped YBCO grains under different oxygen partial pressures and temperatures during the calcination stage has been investigated.

3.2 EXPERIMENTAL

Powders weighing about 5-6 gm of Y_2O_3 , $BaCO_3$, and CuO (Aldrich, 99.9% pure) were well mixed in the molar ratio of 0.5:2:3 in an agate mortar in acetone medium. The mixed powder was loosely pressed into pellets (weighing about 3 gm) and put inside the furnace. The experimental set up is shown in Fig. 3.1.

Soaking was done at temperatures in the range $850^{\circ}C - 1050^{\circ}C$ for 12 hrs in different oxygen partial pressures (P_{O_2}) ranging from 4-60% in ambient pressure. The P_{O_2} inside the furnace was controlled by passing oxygen or nitrogen or a mixture of both and was measured by a stabilized zirconia type sensor (Raskin).

3.2.1 Measurement of textured grain growth

The textured grain growth in the calcined pellet was studied mainly by X-ray powder diffraction as well as scanning electron microscopy. Shape and size of the grains were determined from the SEM fractographs of the pellets. For example the SEM fractograph of samples S1 and S2 with grain size $5 \mu m$ and $15 \mu m$ given in Fig.3.2a&b respectively show that grains are of platelet shape in $15 \mu m$ sample whereas the grains are more or less spherical in the $5 \mu m$ sample. But from the SEM photograph it is impossible to identify the crystallographic direction of grain growth. X-ray diffraction can be successfully employed for this purpose.

For this the pellet was gently crushed and the grains were separated. A comparison of SEM photograph of the fracture (Fig.3.2b)

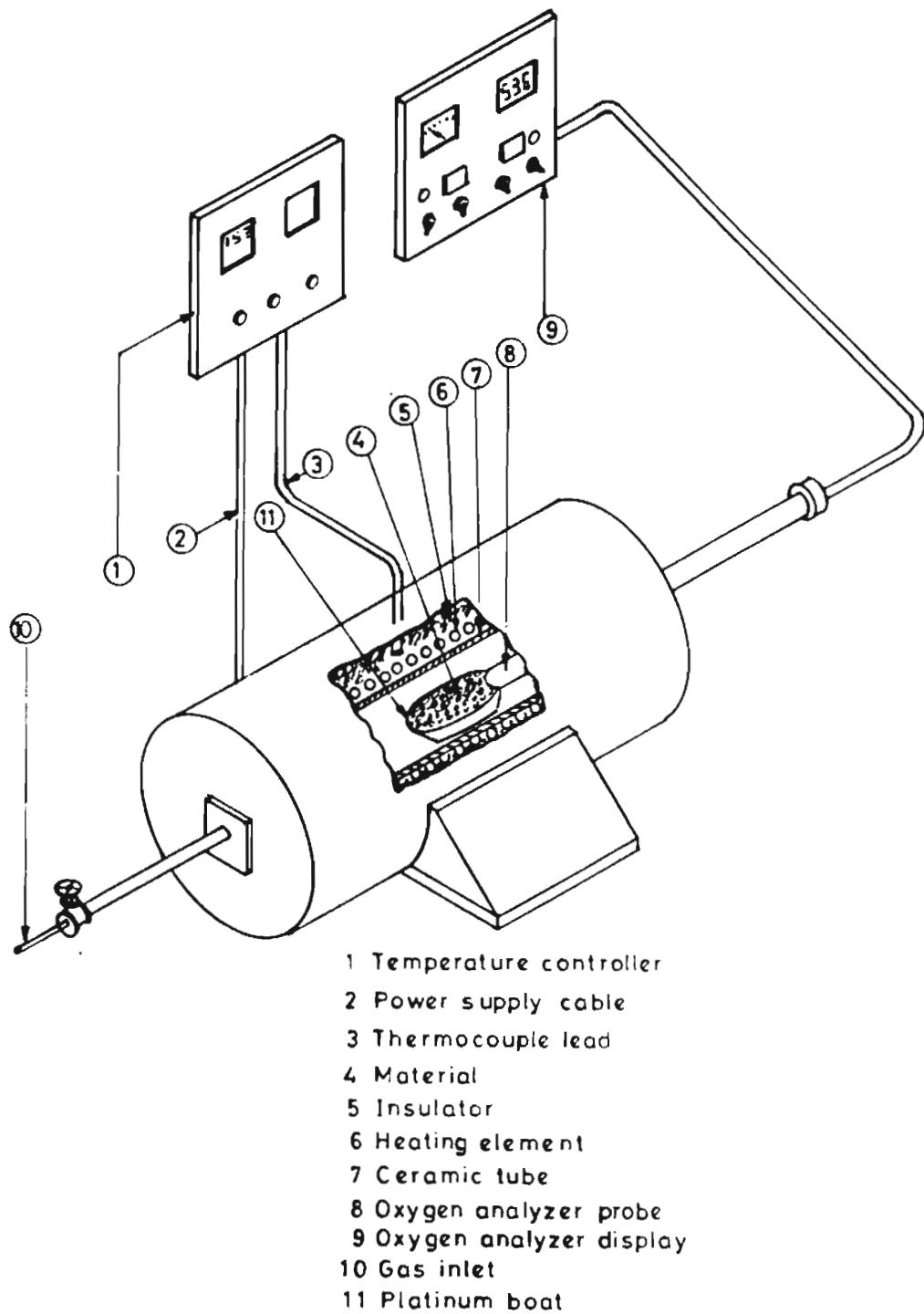
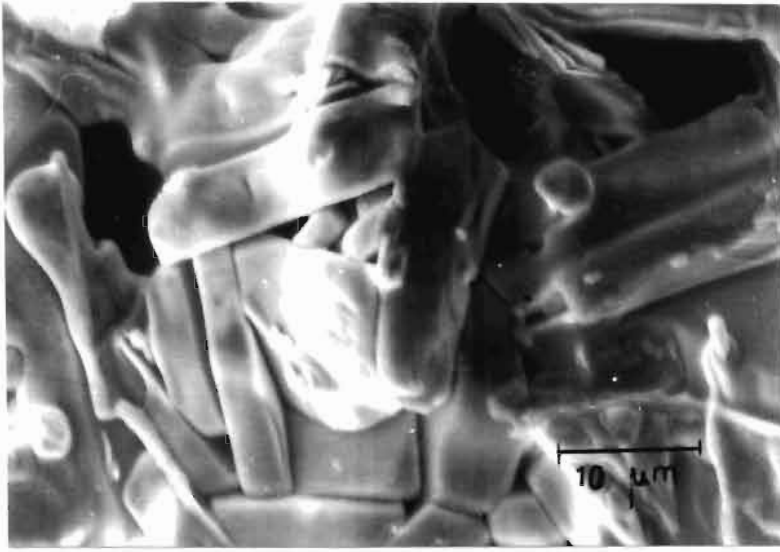
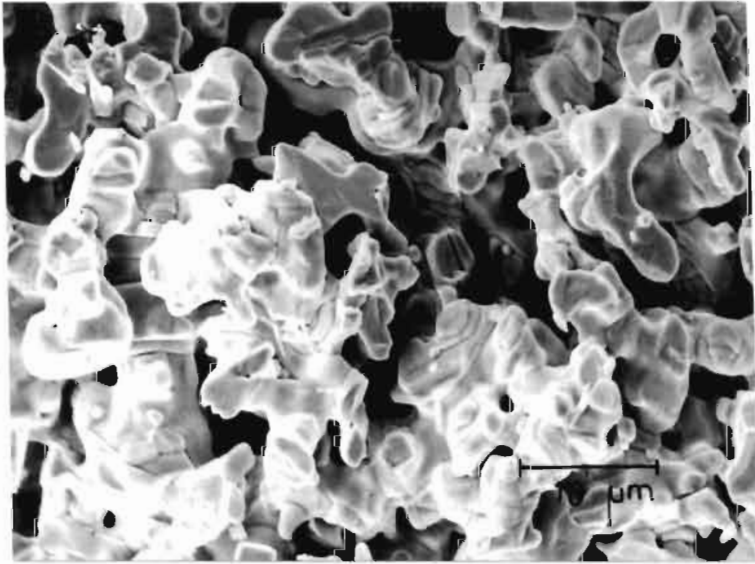


Fig. 3.1: Experimental set up for the processing of YBCO under different oxygen partial pressures and temperatures



(b)



(a)

Fig. 3.2: Typical SEM fractograph of samples having grain sizes 5 μm and 15 μm

with that of separated grains (Fig. 3.3) of sample S2 shows that the grains are still retaining the platyness to a large extent even after crushing.

The separated grains weighing about 4 gms were filled in a rectangular die having dimensions 20 mm x 15 mm x 5 mm and pressed under a pressure of about 75 MPa for 5 minutes which was found to give significant alignment even in samples with aspect ratio of grains just above unity.

X-ray diffraction was performed on the pressed surface of the sample which is perpendicular to the axis of compression. In the case of samples having grain size more than 5 μm , the intensities of (001) reflections were found to be enhanced significantly compared to other reflections. Typical XRD patterns of samples S1 and S2 are shown in Fig. 3.4a&b.

The increase in the intensities of (001) reflections in the XRD pattern of sample S2 indicate that the crystallites near the surface of the sample tend to be oriented so that their ab-plane lie in the same direction. This can happen only when the grain growth is along ab-plane.

The ratio of the intensities of (005) and (113) reflections which appear at $2\theta = 38.57^\circ$ and 40.46° respectively was taken as the orientation index (O.I.) not only for identifying the crystallographic direction of grain growth but also for measuring the extent of grain growth in different samples. These reflections were chosen because the intensity

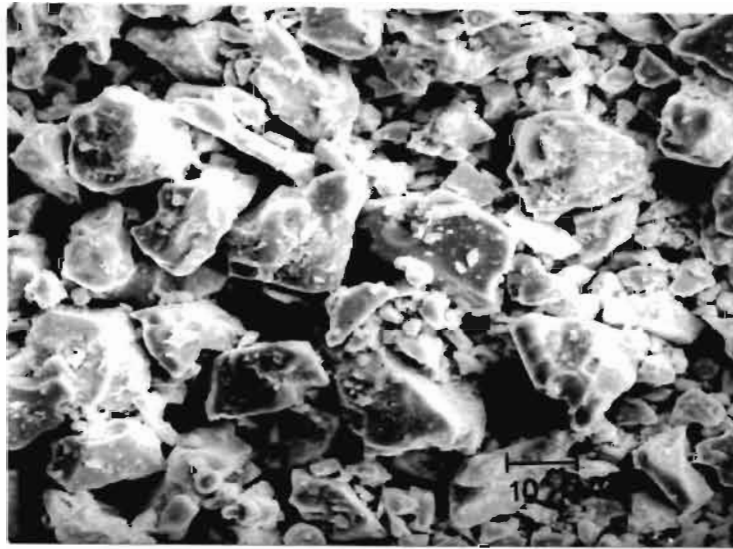


Fig. 3.3: SEM photograph of the separated grains of sample S2

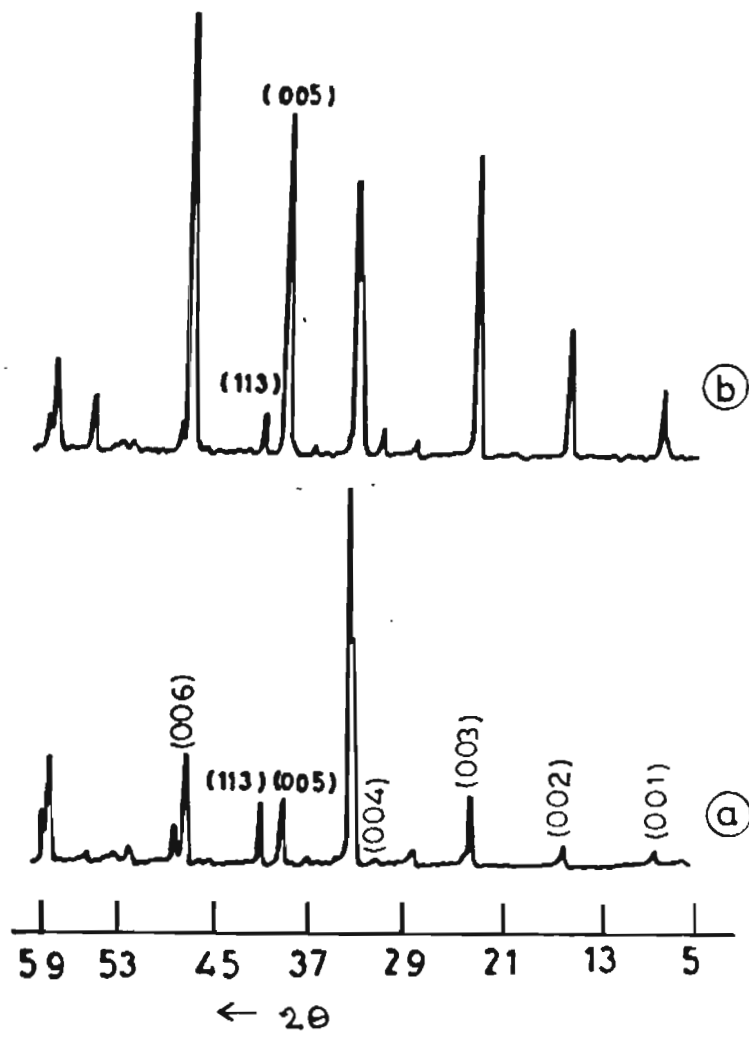


Fig. 3.4: XRD patterns of (a) sample S1 and (b) sample S2

of (113) reflection is found to be almost same even as the intensities of (001) seem to increase by tens of orders and that of (hk0) increases to a lesser extent as the textured grain growth increases.

Since the same pressing parameters are used during the preparation of samples for XRD, the alignment of grains will increase as the size of platy grains increase. Thus by defining O.I. as explained above we get a simple tool for the measure of grain growth along the ab-plane in addition to SEM photographs. Lotgering index [24] which is used by many researchers as a measure of texture is not employed in our analysis since there is substantial overlap among various reflections in YBCO, which makes its calculation tedious and erroneous when dealing with a large number of samples. In addition to the simplicity of the procedure, the O.I. as defined above has the following advantages.

- a. (005) and (113) are comparatively pure reflections
- b. Both reflections come nearby so that the instrumental errors will affect both intensities to the same extent

From the calculation of O.I. and the comparison with the SEM microstructure of the samples we find that the lower limit of O.I. is unity and it represents nearly spherical particle morphology.

3.3 RESULTS AND DISCUSSION

3.3.1 Effect of oxygen partial pressure

Experiment was done by keeping the temperature constant and varying the P_{O_2} , within a suitable range which gives single phase YBCO and the corresponding textured grain growth was studied. Table 3.1

gives the oxygen partial pressure, orientation index and grain size of the samples processed at a temperature 960°C .

Table 3.1: Oxygen partial pressure, orientation index and grain size of the samples processed at a temperature 960°C

Samples	P_{O_2} (%)	O.I.	Grain size (μm)
S1	34 ± 1	1	5
S2	23 ± 1	23	15
S3	18 ± 1	210	33

The XRD patterns of powdered samples and SEM photograph of both the fractures and the powders of S1, S2 and S3 are shown in Figs.3.5 and 3.6 respectively.

From the Table 3.1 and Figs.3.5 & 3.6(a,b,c) it is clear that at a processing temperature 960°C and the P_{O_2} in the range 17-35% the textured grain growth is more at $18 \pm 1\%$ P_{O_2} . Below 17% P_{O_2} at 960°C the sample was found to undergo incongruent melting resulting in multi-phase.

Similar experiment was done by fixing the temperatures to $920 \pm 2^{\circ}\text{C}$, $940 \pm 2^{\circ}\text{C}$, $960 \pm 2^{\circ}\text{C}$, $980 \pm 2^{\circ}\text{C}$, $1000 \pm 2^{\circ}\text{C}$, $1020 \pm 2^{\circ}\text{C}$ and choosing the range of oxygen partial pressure which gave single phase material. Fig. 3.7 shows the plot of grain size vs P_{O_2} of the samples processed at different temperatures.

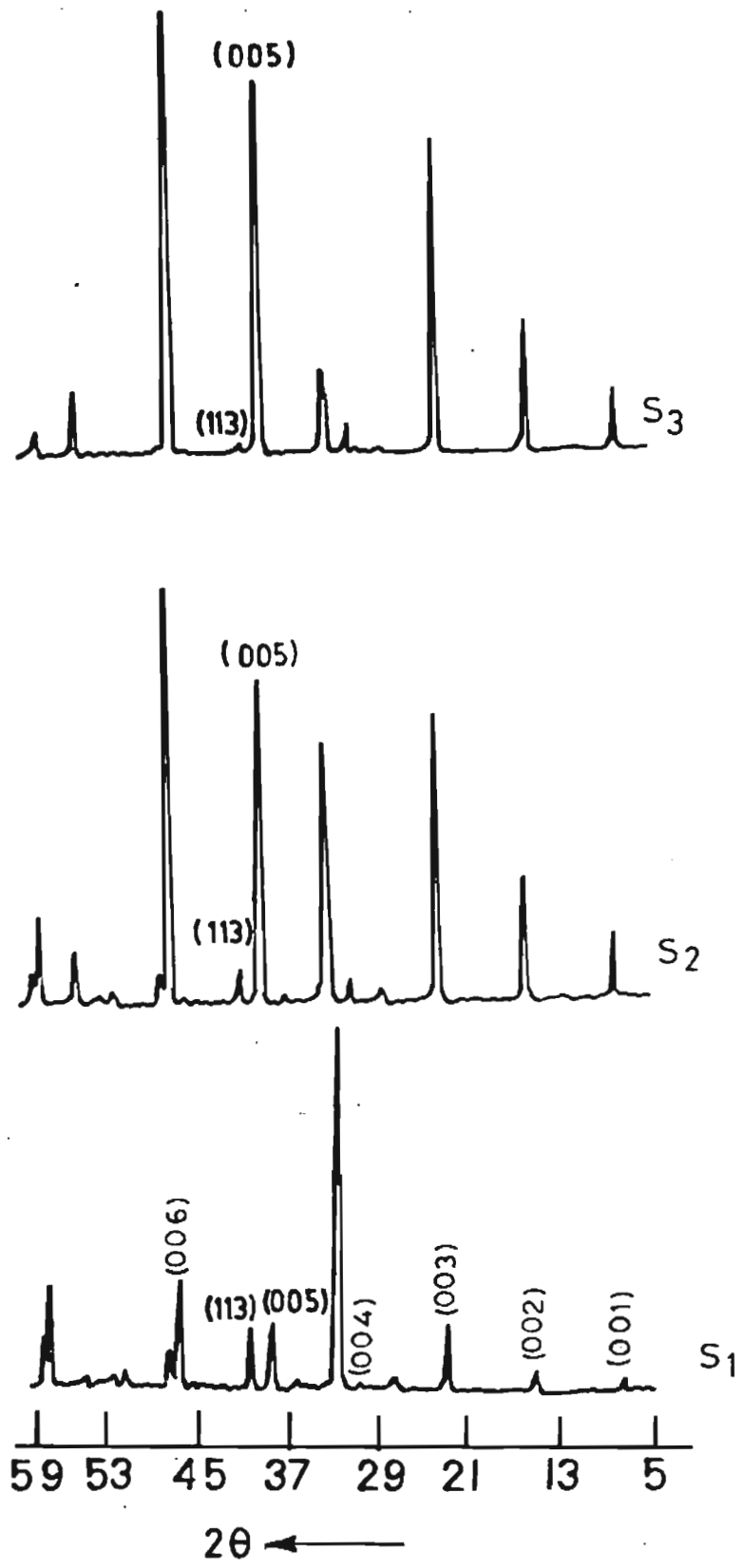
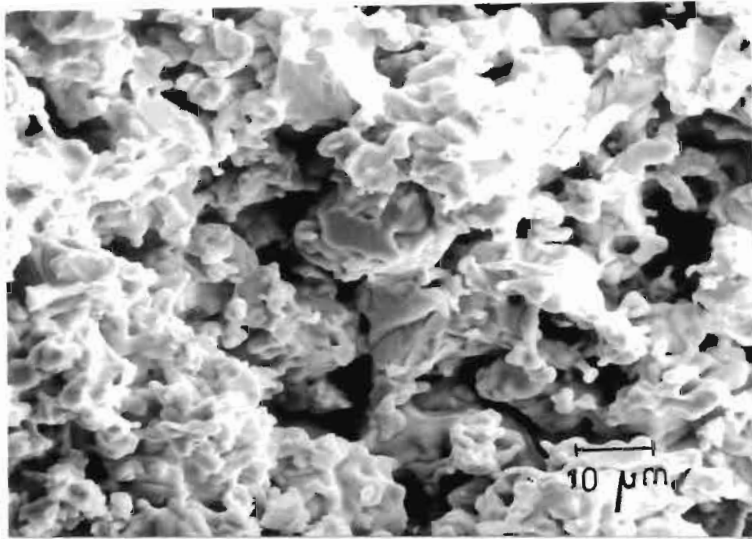
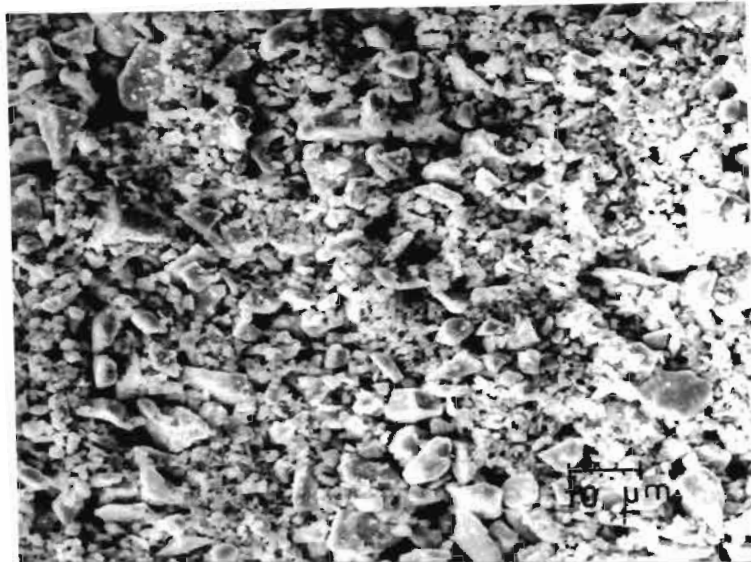


Fig. 3.5: XRD patterns of samples S1, S2 & S3

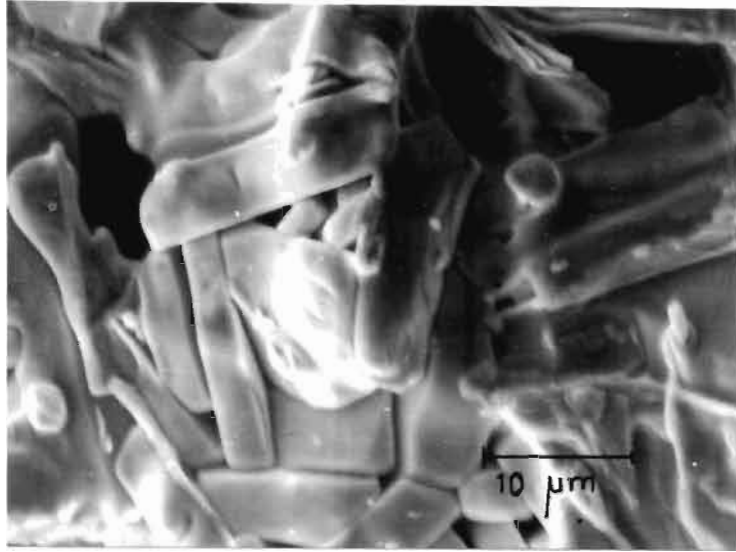


Fracture

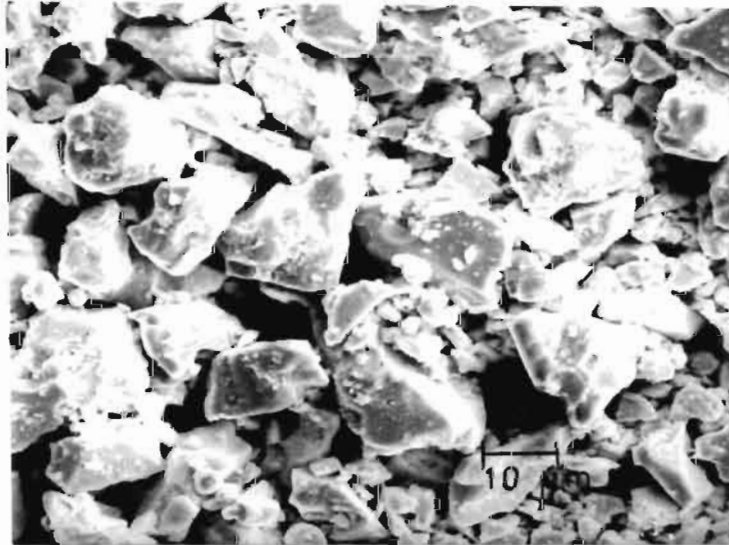


Powder

Fig. 3.6: (a) SEM photograph of fracture and powder of sample S1

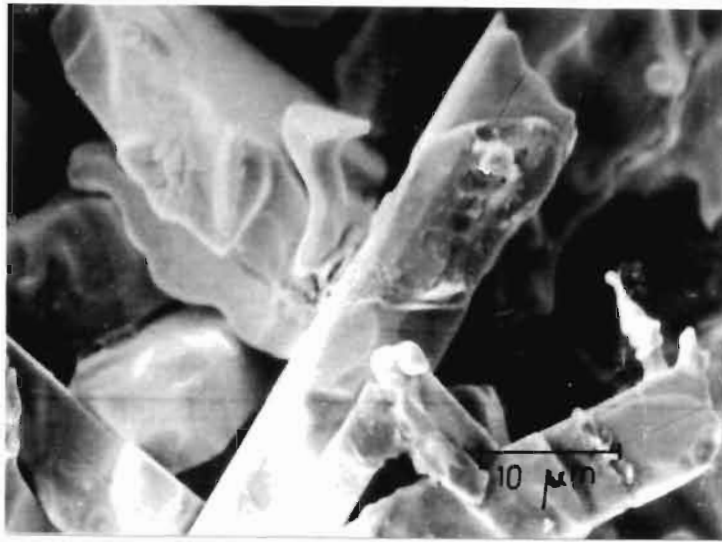


Fracture

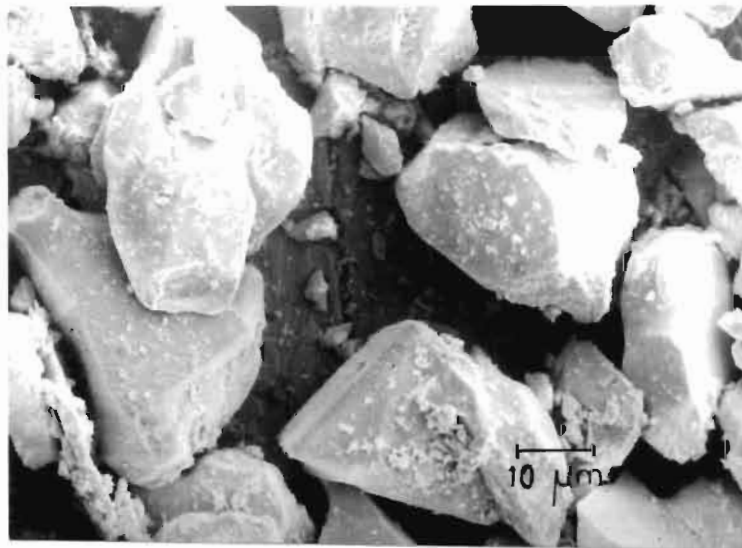


Powder

Fig. 3.6: (b) SEM photograph of fracture and powder of sample S2



Fracture



Powder

Fig. 3.6: (c) SEM photograph of fracture and powder of sample S3

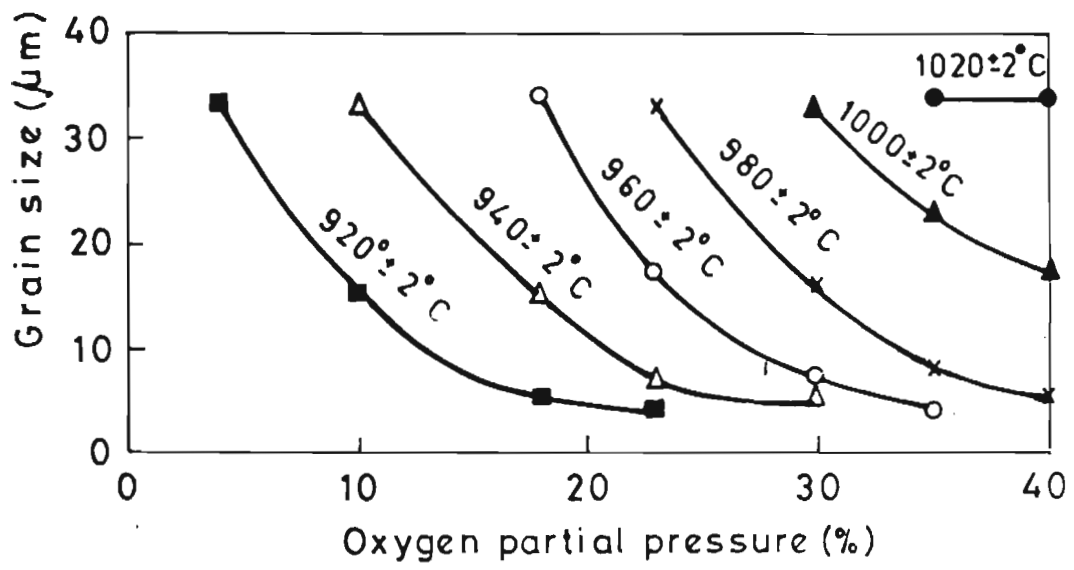


Fig. 3.7: Plots of grain size vs P_{O_2} of the samples processed at different temperatures

In all these cases the grain growth was found to be along ab-plane as observed from the strong reflections of (00l) from the XRD patterns.

From the studies it can be seen that at a fixed processing temperature and a range of Po_2 which gives single phase material, textured grain growth is more at lower Po_2 compared to that at higher Po_2 . Also it was found that the maximum grain size observed was around $33 \mu\text{m}$ in all cases and this maximum size occurred just below the beginning of incongruent melting as determined by the processing Po_2 . Another observation is that at lower processing temperatures the change in textured grain growth is more sensitive to the Po_2 than that at the higher processing temperatures. For example at $1020 \pm 2^\circ\text{C}$, an increase in Po_2 from $34 \pm 1\%$ to $50 \pm 1\%$ does not change the grain size much.

3.3.2 Effect of temperature

Experiment was done by keeping the Po_2 constant and varying the temperatures within a suitable range which gives single phase YBCO and the corresponding textured grain growth was studied.

Table 3.2 gives the temperature, orientation index and grain size of the samples processed at a Po_2 of $34 \pm 1\%$.

SEM photograph of the fracture and the powders of samples S4, S5, S6 and S7 are shown in Fig. 3.8.

Table 3.2: Temperature, orientation index and grain size of the samples processed at Po_2 $34 \pm 1\%$

Samples	Temperature ($^{\circ}C$)	O.I.	Grain size (μm)
S4	960 ± 2	1	5
S5	980 ± 2	25	15
S6	1000 ± 2	85	22
S7	1020 ± 2	215	34

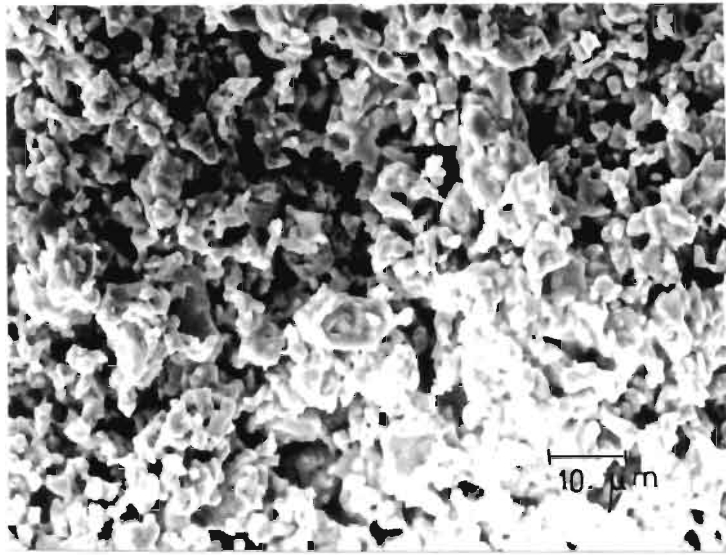
From the Table 3.2 and Fig. 3.8 it is clear that at a processing Po_2 of $34 \pm 1\%$ and the temperature in the range $960-1020^{\circ}C$ the textured grain growth is maximum at $1020^{\circ}C$. Above $1020^{\circ}C$ at a Po_2 of $34 \pm 1\%$ the sample was found to undergo incongruent melting resulting in multiphase.

Similar experiment was done at fixed Po_2 s, $4 \pm 1\%$, $10 \pm 1\%$, $18 \pm 1\%$, $23 \pm 1\%$, $30 \pm 1\%$, $34 \pm 1\%$ and choosing a range of temperature which gave single phase YBCO.

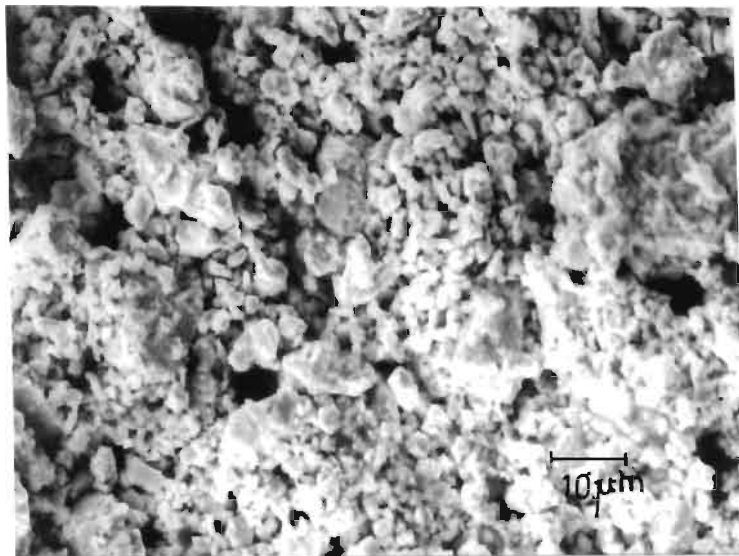
Fig. 3.9 shows the plot of grain size vs processing temperature of samples processed under different oxygen partial pressures.

In all these cases also the grain growth was found to be along ab-plane as observed from the XRD patterns of the samples.

From the studies it can be seen that at a fixed processing Po_2 and a range of temperature which gives single phase material, textured grain growth is more at higher temperature compared to that

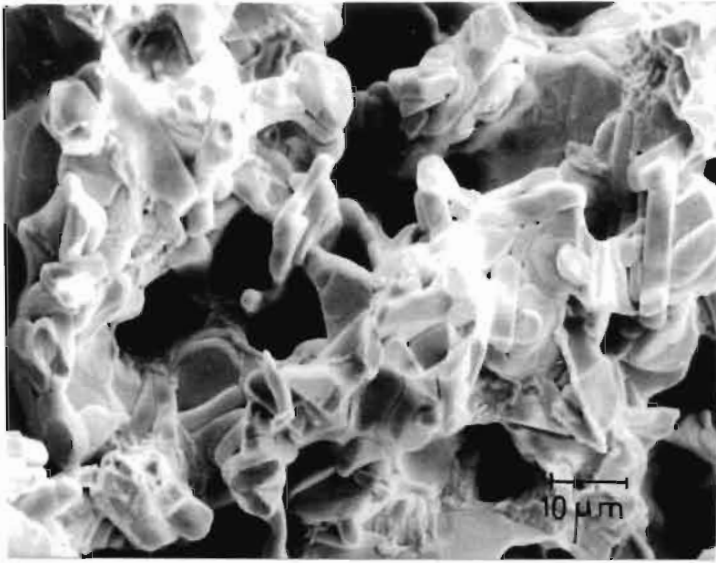


Fracture

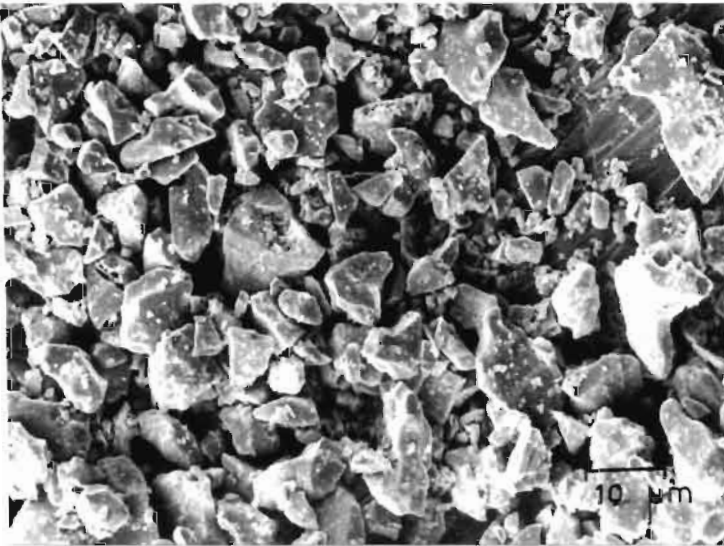


Powder

Fig. 3.8: (a) SEM photograph of fracture and powder of sample S4

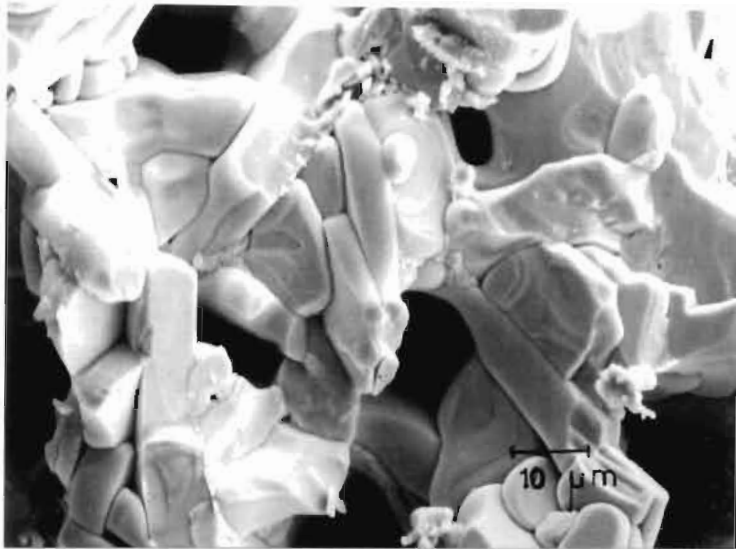


Fracture



Powder

Fig. 3.8: (b) SEM photograph of fracture and powder of sample S5

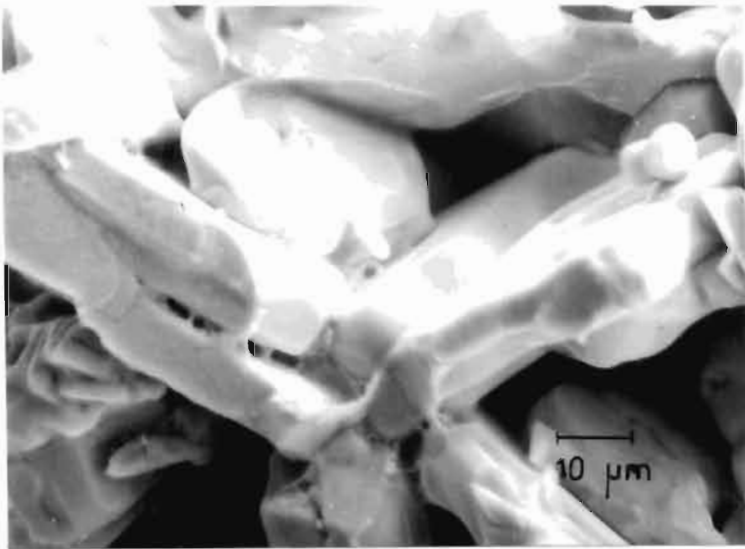


Fracture

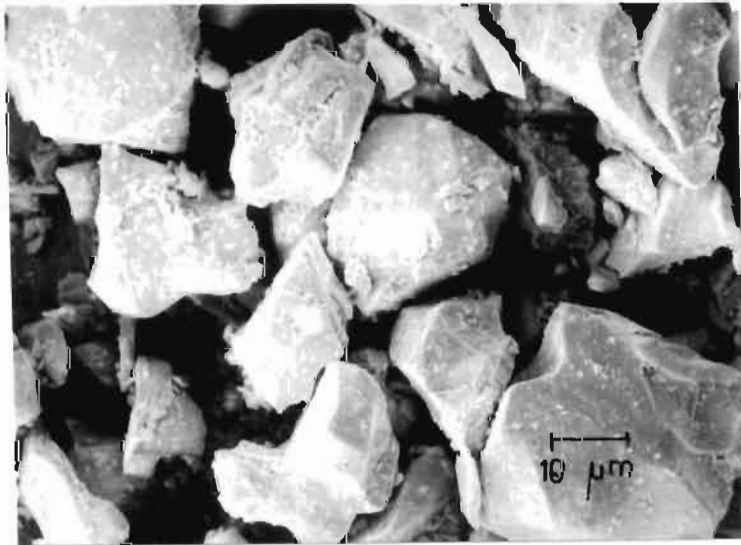


Powder

Fig. 3.8: (c) SEM photograph of fracture and powder of sample S6



Fracture



Powder

Fig. 3.8: (d) SEM photograph of fracture and powder of sample S7

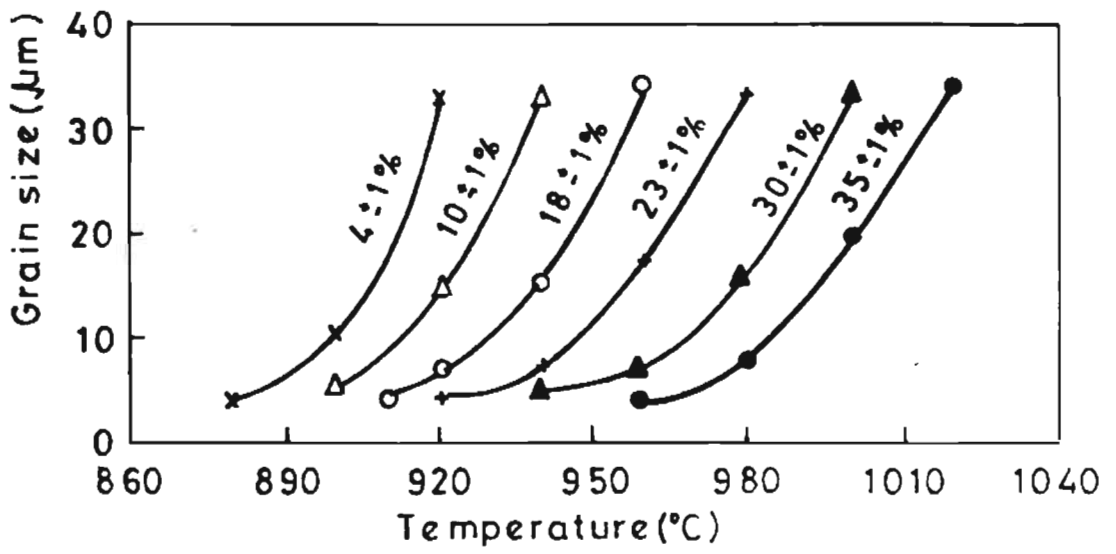


Fig. 3.9: Plots of grain size vs processing temperature of samples processed under different oxygen partial pressures

at lower temperature. Also it was found that the maximum grain size observed was around 33 μm in all cases and this maximum size occurred just below the beginning of incongruent melting as determined by the processing temperature.

3.3.3 Effect of oxygen partial pressure and temperature

From the above studies we have seen two things:

- a. At any temperature the textured grain growth is a maximum at the lowest P_{O_2} provided both the temperature and P_{O_2} are within their admissible range of values guaranteeing single phase YBCO.
- b. At any fixed P_{O_2} the higher the processing temperature the higher is the textured grain growth.

Fig. 3.10 shows the plot of P_{O_2} vs temperature for fixed grain sizes 5, 15 and 33 μm . Similar curves can be drawn for any average grain size lying between 5 and 33 μm under the present experimental conditions.

From the Fig. 3.10 it is clear that textured grain growth in YBCO is mainly dependent on the oxygen partial pressure and temperature and the grain growth can be controlled by adjusting them suitably.

From the figure it is also evident that the temperature for the formation of a fixed grain size reduces significantly as the processing P_{O_2} decreases. The plot corresponding to 5 μm has an added significance because the steady decrease in processing temperature

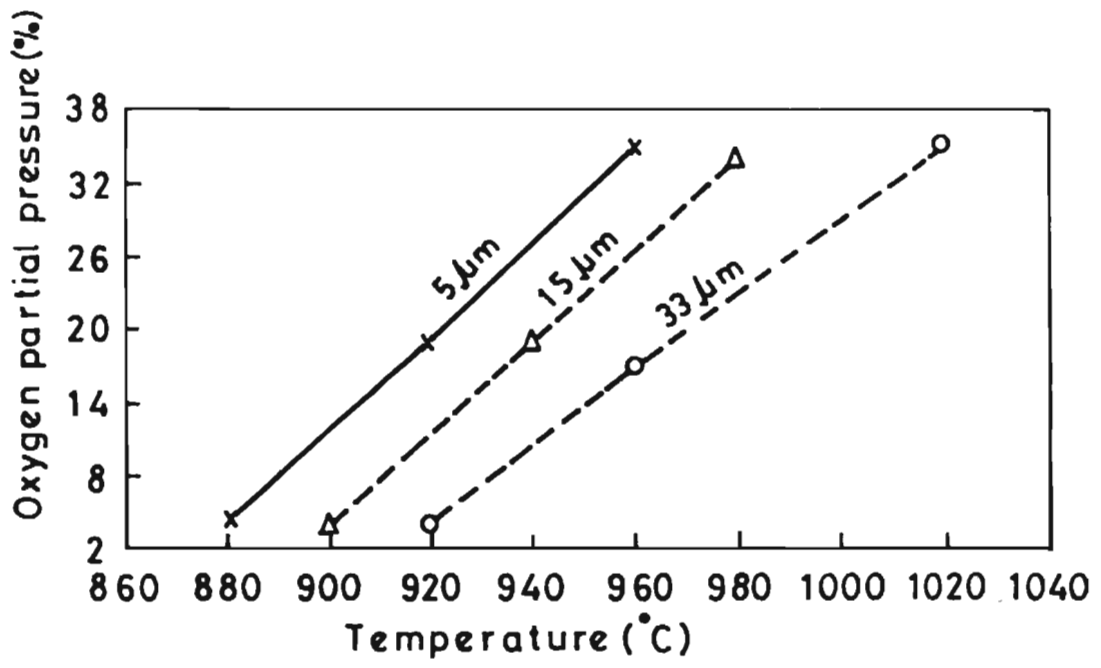


Fig. 3.10: Plots of P_{O_2} vs processing temperature for grain sizes 5, 15 and 33 μm

in it by the lowering of P_{O_2} is a clear indication for the decrease in the temperature of YBCO phase formation itself. These results led to the development of vacuum calcination process which has been dealt in part B of this thesis.

3.3.4 Effect of soaking period

By keeping P_{O_2} and temperature constant, textured grain growth of the samples in various soaking periods was studied. Fig. 3.11 shows the SEM photographs of the sample processed in air at 950°C with a soaking period of 12 hrs and 60 hrs respectively.

Fig. 3.12 gives the plot of grain size vs soaking period of samples prepared at temperatures $960 \pm 2^{\circ}\text{C}$, $1020 \pm 2^{\circ}\text{C}$ and P_{O_2} , $18 \pm 1\%$, $33 \pm 1\%$ respectively. Similar curves can be drawn for other temperatures and oxygen partial pressures also. From the figure it is clear that textured grain growth increases with the increase in soaking period. Also, by increasing the soaking period and choosing the appropriate oxygen partial pressure and temperature YBCO having grain size greater than $60 \mu\text{m}$ can be synthesized.

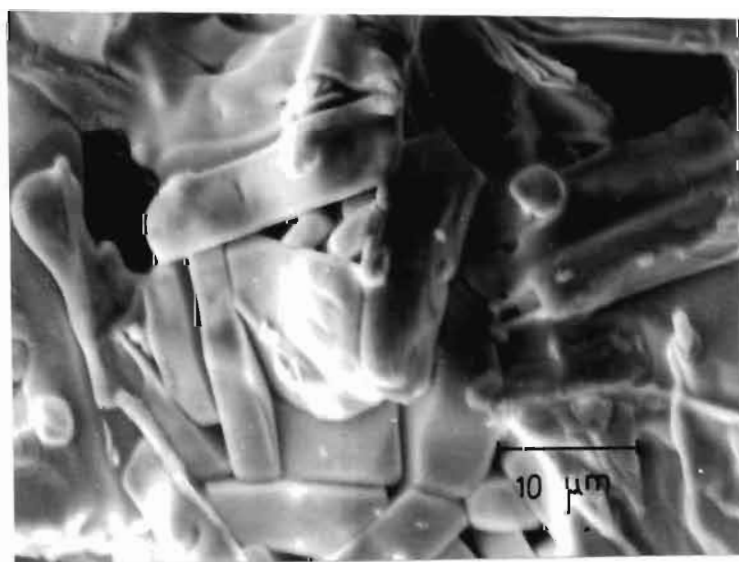
3.4 CONCLUSION

Studies were conducted on the growth of platelet shaped grains of YBCO under different processing parameters like P_{O_2} , temperature and soaking period during the calcination stage. The results clearly show that

- a. The grain growth along ab-plane is accelerated by the decrease of P_{O_2} , if the processing temperature is kept constant.



60 hrs



12 hrs

Fig. 3.11: SEM photographs of the sample processed in air at 950°C with soaking periods 12 and 60 hrs

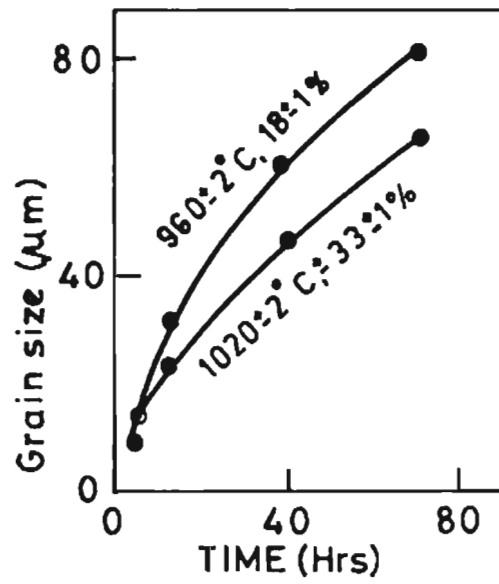


Fig. 3.12: Plot of grain size vs soaking period of samples processed under different temperature and P_{O_2}

- b. If the P_{O_2} is kept constant, the grain growth along ab-plane is accelerated as the processing temperature increases.
- c. If P_{O_2} , processing temperature and soaking period are suitably selected, platelet grains of desired size (within a range of 5-100 μm) can be synthesized.

Apart from establishing the dependence of growth of platy grains of YBCO on the processing parameters, this study has also indicated that $Y_1Ba_2Cu_3O_{7-\delta}$ phase formation in the conventional ceramic route commences at lower temperatures if the oxygen partial pressure is reduced.

REFERENCES

1. V.G. Baryakhtar, V.M. Pan, V.G. Prokhorov et al, Pisma Zh Eksp Teor Fiz (Sov), 46, 168 (1987).
2. V.M. Pan, V.G. Prokhorov, C.G. Kaminsky et al, Fiz. Nizk Temp. (Sov), 13, 861 (1987).
3. R. Watanabe, Y. Kasai, T. Machiku et al, Jap. J. Appl. Phys., 26, L657 (1987).
4. U. Dai, G. Deutscher and R. Rosenbaum, Appl. Phys. Lett., 51, 460 (1987).
5. P. Chaudhary, R.H. Koch, R.B. Laibowitz, T.R. McGuire and R.J. Gambino, Phys. Rev. Lett., 58, 2684 (1987).
6. Y. Enomoto, T. Murakami, M. Suzuki and K. Moriwaki, Jap. J. Appl. Phys., 26, L1248 (1987).
7. T.R. Dinger, T.K. Worthington, W.J. Gallagher and R.L. Sandstorm, Phys. Rev. Lett., 58, 2687 (1987).
8. G.W. Crabtree, J.Z. Liu, A. Umezawa, W.K. Kwok, C.H. Sowers and S.K. Malik, Phys. Rev. B., 36, 4021 (1987).
9. S. Jin, Science, 238, 1655 (1987).
10. C.T. decker, V.K. Seth and W.A. Schulze, Research update, 1988, "Ceramic Superconductors II" Edited by Man F. Yan, 169 (The American Ceramic Society, Inc., Westerville, Ohio, 1988) p.169.
11. S. Jin, R.C. Sherwood, T.H. Tiefel, R.B. van Dover, S. Nakahara and R.A. Fastnacht, Research update, 1988, "Ceramic Superconductors II" Edited by Man F. Yan (The American Ceramic Society, Inc., Westerville, Ohio, 1988) p.272.
12. K. Salama, V. Selvamanickam, L. Gao and K. Sun, Appl. Phys. Lett., 54, 2352 (1989).

13. D.E. Farrell, B.S. Chandrasekhar, M.R. DeGuire, M.M. Fang, V.G. Kogan, J.R. Clem and D.K. Finnemore, Phys. Rev. B 36, 4025 (1987).
14. R.H. Arendt, A.R. Gaddipati, M.R. Garbaskas, E.L. Hall, H.R. Hart, Jr., K.W. Lay, J.D. Livingston, F.E. Luborsky and L.L. Schilling, "High Temperature Superconductors" Edited by M. Brodsky H. Tuller, R. Dynes and K. Kitazawa (MRS Proceedings 99, Materials Research Society, Pittsburgh, PA, 1988) p.203.
15. X.G. ZHENG, H. Kuriyaki and K. HIRAKAWA, Jap. J. Appl. Phys., 28(1), L52 (1989).
16. M.R. De Guire, C.J. Kim, W.H. Lu, D.E. Farrel and D. Boyne, Research update, 1988, "Ceramic Superconductors II", Edited by Man F. Yan (The American Ceramic Society, Inc., Westerville, Ohio, 1988) p.343.
17. L.C. Stearns, M.D. Vaudin, c.P. Ostertag, J.E. Blendell and E.R. Fuller, Jr., Research update, 1988, "Ceramic superconductors II", Edited by Man F. Yan (The American Ceramic Society, Inc., Westerville, Ohio, 1988) p.315.
18. J.J. Balducci, V.K. Seth and W.A. Schulze, research update, 1988, "Ceramic Superconductors II" Edited by Man F. Yan (The American Ceramic Society, Inc., Westerville, Ohio, 1988) p.367.
19. C.P. Ostertag, R.D. Shull, M.D. Vaudin, J.E. Blendell, L.C. Stearns and E.R. Fuller, Jr., Research update, 1988, "Ceramic Superconductors II", Edited by Man F. Yan (The American Ceramic Society, Inc., Westerville, Ohio, 1988) p.332.
20. K.C. Goretta, A.J. Schultz, D.W. Capone II, T.L. Tolt, U. Balachandran, J.T. Dusek, M.T. Lanagan, R.B. Poeppel, J.P. Singh, D. Shi, R.L. McDaniel, D.S. Applegate, J.K. Degenerand and J.S. Kallend, research update, 1988, "Ceramic Superconductors II" Edited by Man F. Yan (The American Ceramic Society, Inc., Westerville, Ohio, 1988) p.323.

21. S.S. Kim, T.T. Srinivasan, T.R. ShROUT and R.E. Newnham, Research update, 1988, "Ceramic Superconductors II" Edited by by Man F. Yan (The American Ceramic Society, Inc., Westerville, Ohio, 1988) p.381.
22. L. Lynds, F. Galasso, E. Otterr, B.R. Weinberger, J.I. Budnick, D.P. Yang and M. Filipkowski, J. Am. Ceram. Soc., 571(3), C-130 (1988).
23. T. Takenaka, H. Noda, A. Yoneda and K. Sakata, Jap. J. Appl. Phys., 27, L1209 (1988).
24. F.K. Lotgering, J. Inorg. Nucl. Chem., 9, 113 (1959).

CHAPTER 4

**STUDIES ON TEXTURED GRAIN GROWTH IN $\text{YBa}_2\text{Cu}_3\text{O}_{7-\delta}$
BY ALKALI METALS SUBSTITUTION**

CHAPTER 4

STUDIES ON TEXTURED GRAIN GROWTH IN $\text{YBa}_2\text{Cu}_3\text{O}_{7-\delta}$
BY ALKALI METALS SUBSTITUTION*

4.1 INTRODUCTION

There have been numerous studies on substitution of Y, Ba and Cu by elements like alkali and alkaline earth metals, rare earths, transition metals (Ag, Au, Ni, Fe, Co) and Al, Pb, Ge, Zr, Bi, Tl, etc. in YBCO [1]. The vast literature does not allow to refer explicitly to each relevant paper. But almost all of them investigate the effect of substitution on transition temperature. Eventhough the substitution is likely to affect the grain size, grain morphology etc., not much attention has been paid to these aspects in most of the reports. Murugaraj et al [2] has found that addition of K_2CO_3 in a Ba deficient composition enhances textured grain growth in YBCO. At the same time addition of K in a stoichiometric composition did not result in such a pronounced texture effect [2]. There are also reports in which K^+ is suggested to substitute for Ba^{2+} in the YBCO lattice [3,4]. These results led to think about the possibility of textured grain growth associated with the other alkali metals substitutions as well.

The reports on alkali metals substitution in YBCO compound suggest that Li^+ occupies Cu^{2+} site [5], whereas Na^+ favours partially both Y^{3+} site and Ba^{2+} site [6-8]. As mentioned earlier, K^+ is suitable for Ba^{2+} site. These preferences of substitution of various

* This work has been partly published in:
Solid State Commun., 81, 253 (1992)

ions can also be seen from an inspection of the ionic radii and co-ordination numbers of various cations given in Table 4.1. [9].

Table 4.1: Co-ordination number and ionic radii of different alkali metals

Co-ordination number	Ionic radius (\AA)					
	Cu^{2+}	Y^{3+}	Ba^{2+}	Li^+	Na^+	K^+
4	0.57			0.59		
8		1.019			1.15	1.51
10			1.52		1.29	1.59

From the above discussion it is clear that alkali metals, Li, Na and K can be substituted for various cations in YBCO and K substitution enhances the grain growth along ab-plane. Therefore it is of interest to study the effect of alkali metal substitution on the textured grain growth of YBCO.

In the previous chapter it has been found that the processing temperature and Po_2 have a significant role in controlling the textured grain growth in YBCO at the calcination stage. In this chapter a similar study on the textured grain growth in YBCO by alkali metal substitution is described.

4.2 EXPERIMENTAL

Considering the substitutional site preferences of Li, Na and K in YBCO, samples having compositions $Y_1Ba_2Cu_{3-x}Li_xO_{7-\delta}$, $Y_{1-a}Ba_{2-b}Na_{x=a+b}Cu_3O_{7-\delta}$ (where a is 35% and b is 65% of x) and $Y_1Ba_{2-x}K_xCu_3O_{7-\delta}$ (where x = 0-0.2) were prepared as follows. Stoichiometric amounts of Y_2O_3 , $BaCO_3$, CuO and the carbonates or nitrates of alkali metals were well mixed in an agate mortar in acetone medium. The mixed powder was loosely pressed into pellets and heated in a closed platinum crucible so that the loss of volatile alkali metals is a minimum. The soaking was done at $920 \pm 5^\circ C$ for 12 hrs and after that the samples were furnace cooled. Textured grain growth of these samples were studied by x-ray and SEM. T_c of the sintered samples were measured by standard four probe method using an APD cryostat.

4.3 RESULTS AND DISCUSSION

Fig. 4.1 shows the typical XRD patterns of the pure and substituted samples. Fig. 4.2 shows SEM photographs of the different samples. Fig. 4.3 shows the plot of grain size vs substituent concentration. Table 4.2 gives the orientation index and $T_{c(0)}$ of the samples.

From the figures and table 4.2 it is clear that the grain growth along a-b plane enhanced significantly by the substitution of Li, Na and K. Textured grain growth is maximum for Li substitution followed by Na and K for the same substituent concentration. In all cases, with the increase in substituent concentration, textured grain

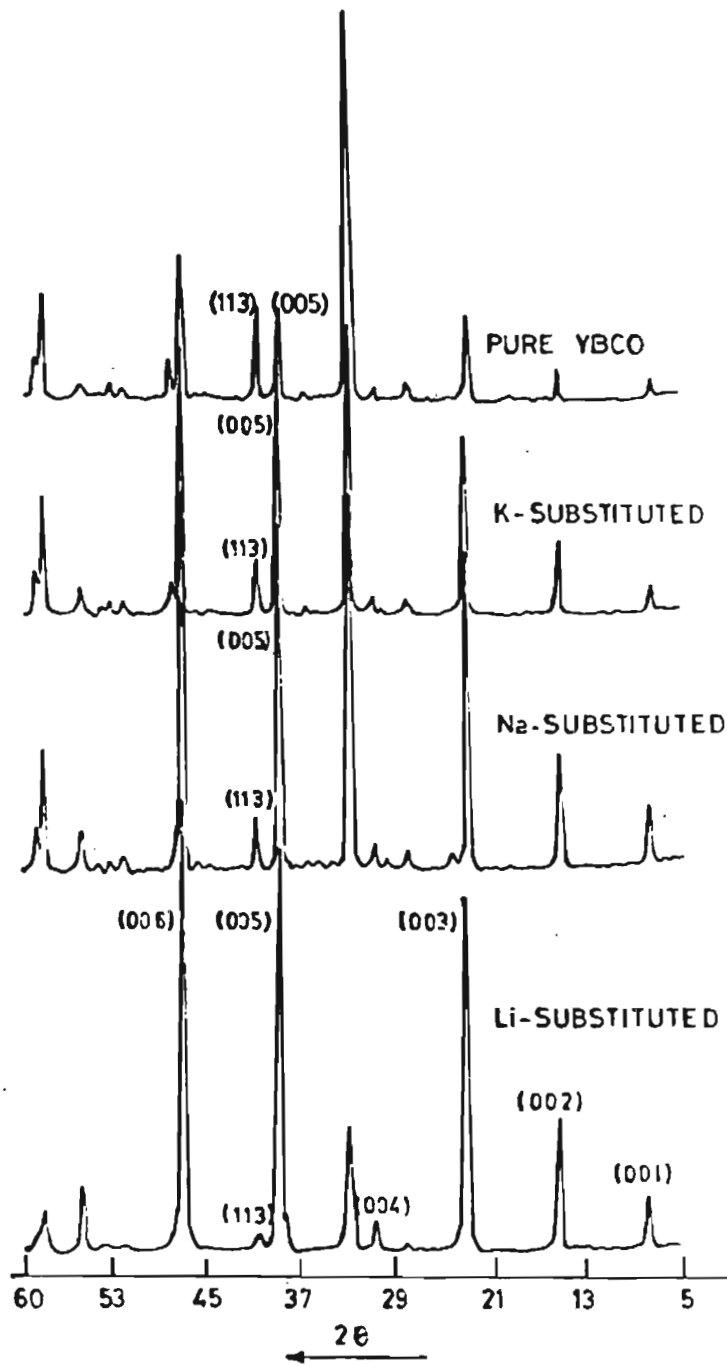
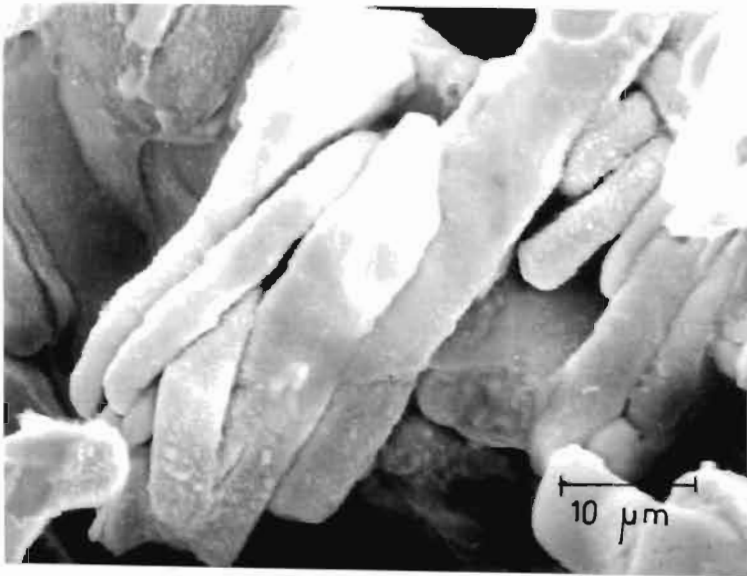
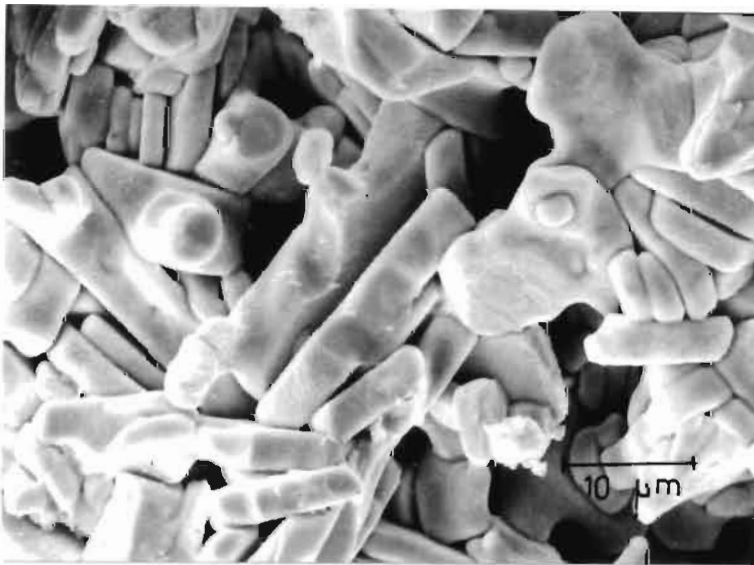


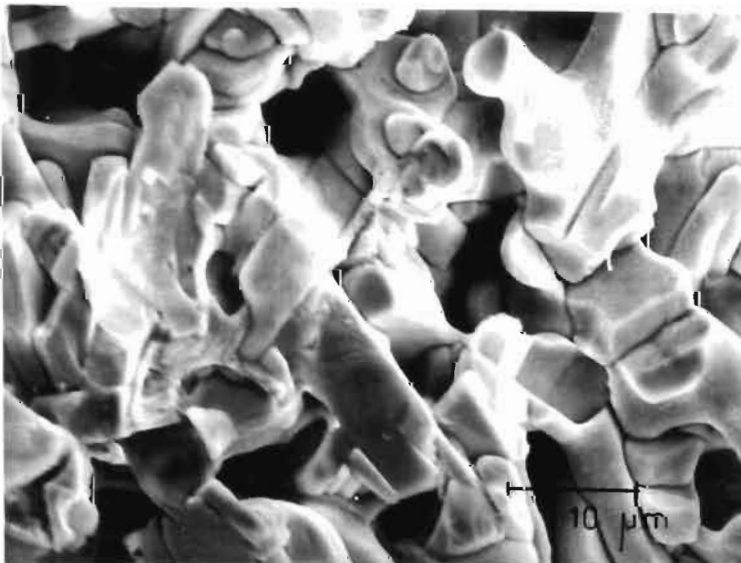
Fig. 4.1: Typical XRD patterns of pure and alkali metals substituted samples



Li_{0.2} - YBCO

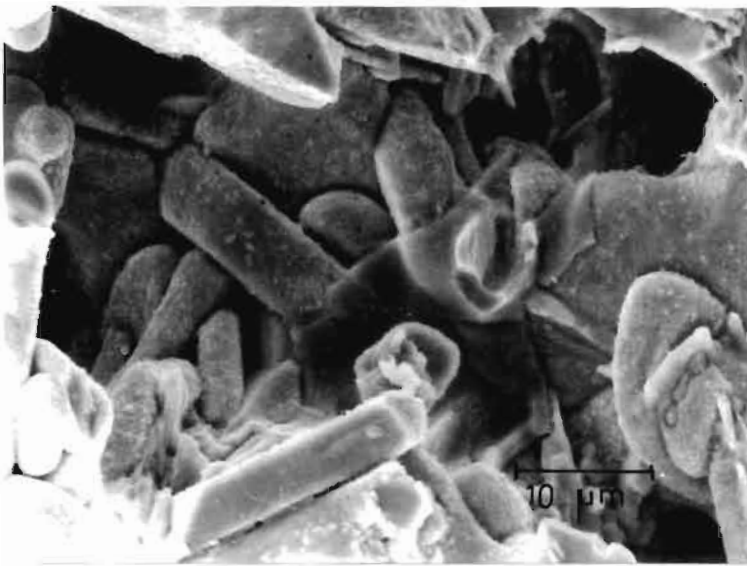


Na_{0.2} - YBCO

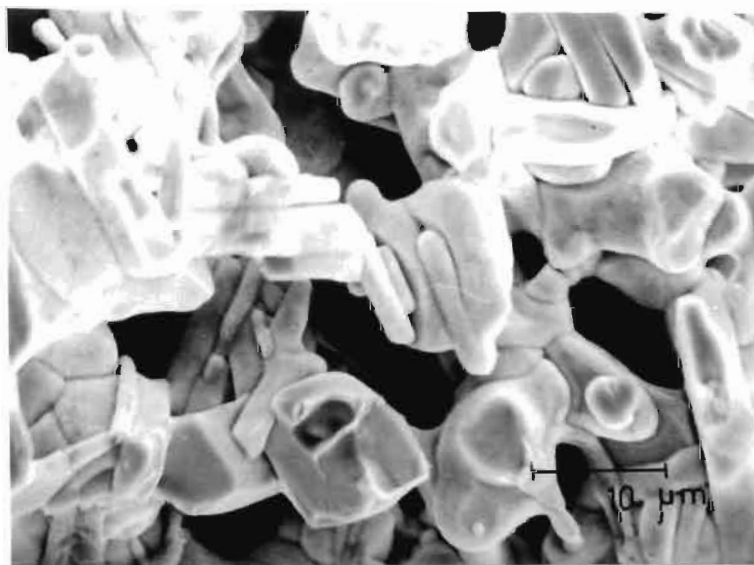


K_{0.2} - YBCO

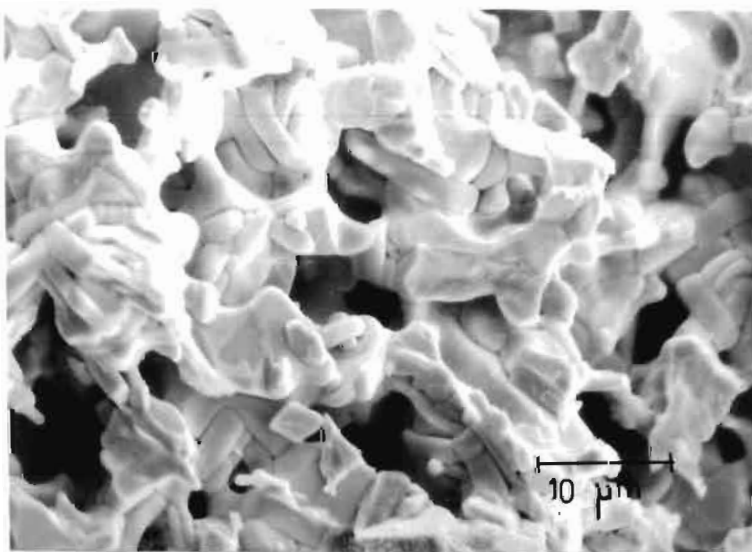
Fig. 4.2(a): SEM fractographs of the Li_{0.2}, Na_{0.2} & K_{0.2} substituted YBCO samples



Li_{0.1} - YBCO

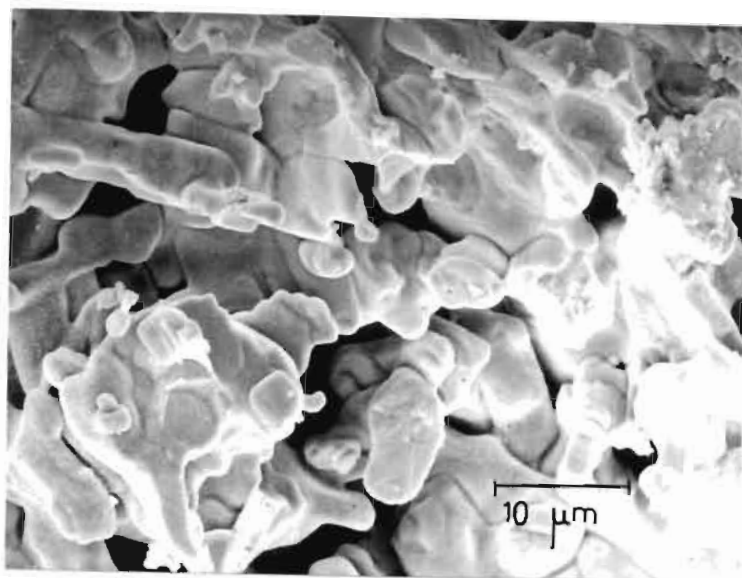


Na_{0.1} - YBCO

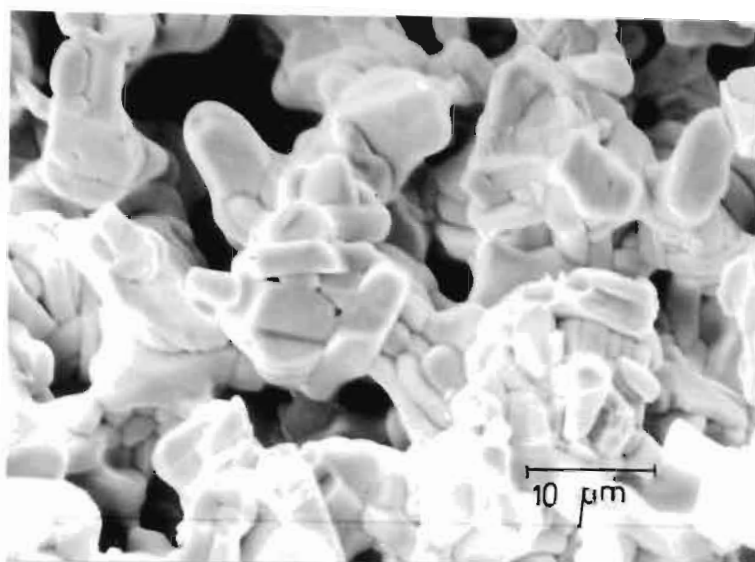


K_{0.1} - YBCO

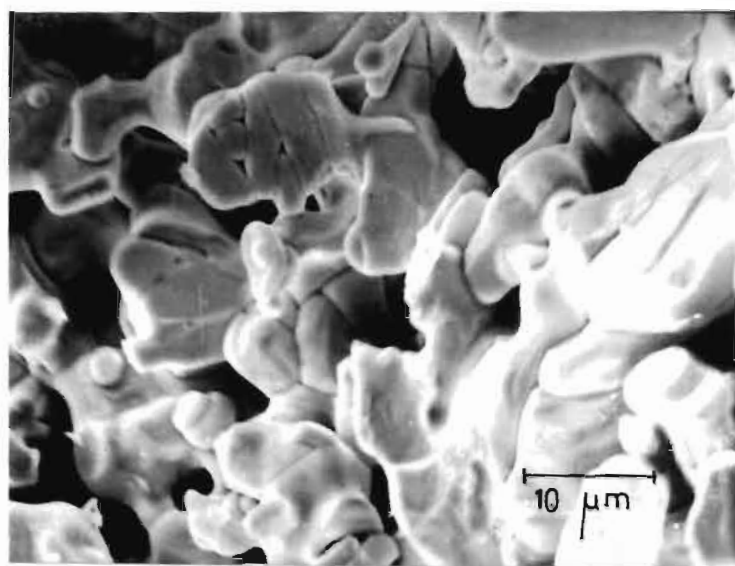
Fig. 4.2(b): SEM fractographs of the Li_{0.1}, Na_{0.1}, & K_{0.1} substituted YBCO samples



Li_{0.05} - YBCO

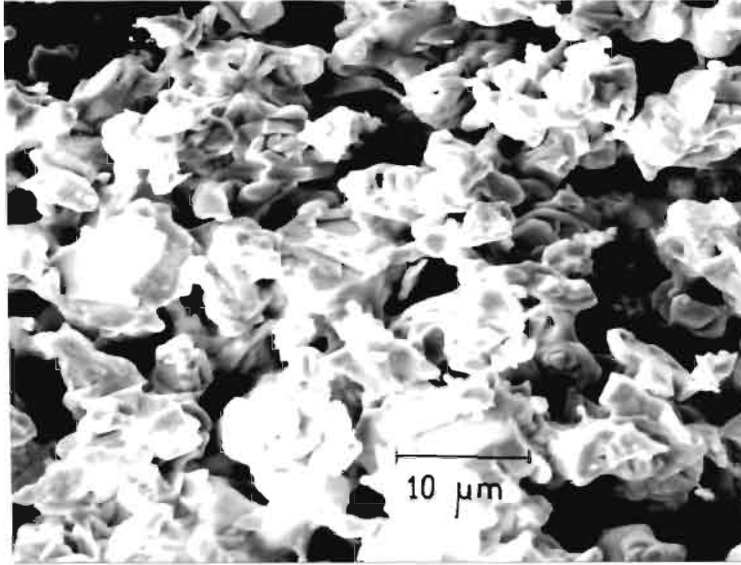


Na_{0.05} - YBCO



K_{0.05} - YBCO

Fig. 4.2(c): SEM fractograph of Li_{0.05}, Na_{0.05}, & K_{0.05} substituted YBCO samples



Pure YBCO

Fig. 4.2(d): SEM fractograph of the pure YBCO

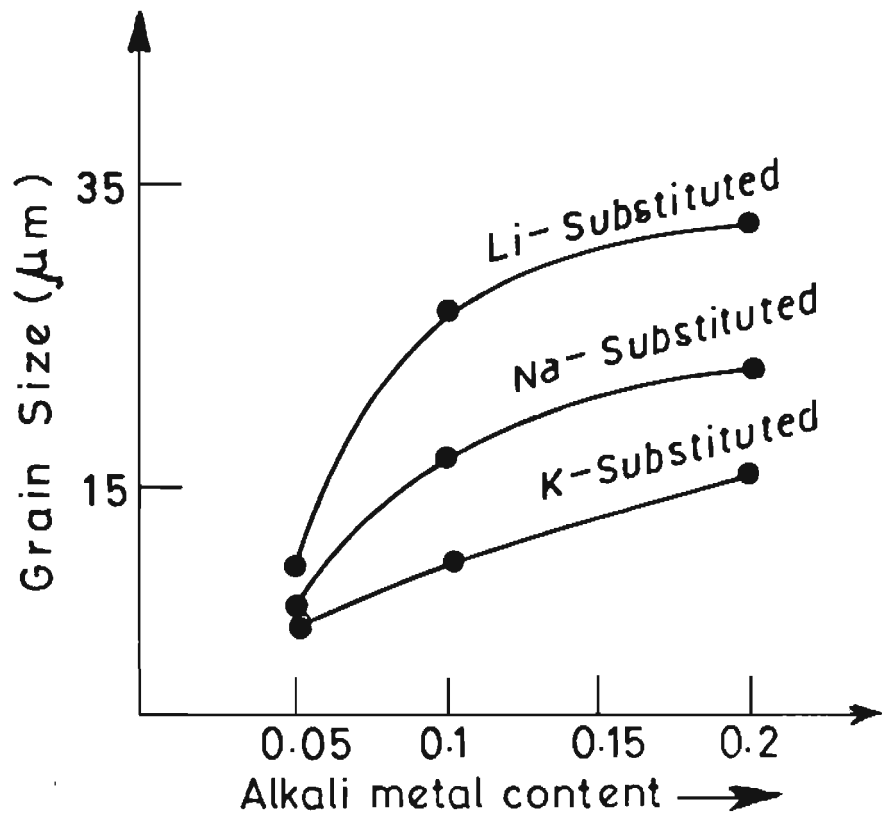


Fig. 4.3: Plot of grain size vs substituent concentration

Table 4.2: Orientation index and $T_{c(0)}$ of the alkali substituted and pure YBCO samples processed at $920 \pm 5^\circ\text{C}$

Stoichiometry of the substituent	Orientation index (I_{005}/I_{113})	$T_{c(0)}$ (K)
$\text{Li}_{0.2}$	201	77.1
$\text{Na}_{0.2}$	67	84
$\text{K}_{0.2}$	7	86
$\text{Li}_{0.1}$	27	78.05
$\text{Na}_{0.1}$	7	84
$\text{K}_{0.1}$	4.5	86
$\text{Li}_{0.05}$	2.3	82
$\text{Na}_{0.05}$	1.25	84
$\text{K}_{0.05}$	1.1	86
Pure YBCO processed at $915 \pm 5^\circ\text{C}$	1	92

growth is also found to be increased within the range of substituent concentration studied. When substituent concentration was raised beyond $x=0.2$, it was difficult to get single phase material.

Li-substitution severely affects $T_{c(O)}$ whereas the effect of Na and K are less pronounced. Except in Li-substituted samples, there is no change in $T_{c(O)}$ when the dopant concentration varies from 0.05 to 0.2.

Eventhough Rb and Cs were also tried as substituents for Ba, no significant textured grain growth was observed under the experimental conditions described above.

4.4 CONCLUSION

Textured grain growth of Li, Na and K substituted YBCO samples processed at $920 \pm 5^{\circ}\text{C}$ in air has been studied. Textured grain growth is maximum for Li substitution followed by Na and K for the same substituent concentration. In all the cases, with the increase in substituent concentration, textured grain growth is also found to be increased. Li substitution severely affects $T_{c(O)}$ whereas the effect of Na and K are less pronounced.

REFERENCES

1. A.V. Narlikar, C.V. Narasimha Rao and S.K. Agarwal, "Studies of High Temperature Superconductors", Edited by A. V. Narlikar, 1, 341 (1989), Nova Science Publisher.
2. P. Murugaraj, J. Maier and A. Rabenau, Solid State Commun., 66, 735 (1988).
3. I. Felner, M. Kowitt, Y. Lehavi, D. Edery, L. Ben-dor, Y. Wolfus and I. Nowik, Mod. Phys. Lett., B 2, 713 (1988).
4. Y. Saito, T. Noji, A. Edno, N. Higuchi, K. Fujimoto, T. Oikawa, A. Hattori and K. Furuse, Physica, B 148, 336 (1987).
5. M. Ausloos, Ch. Laurent, H.W. Vanderschueren, A. Rulmont and P. Tarte, Solid State Commun., 68, 539 (1988).
6. Y. Dalichaouch, M.S. Torikachvili, E.A. Early, B.W. Lee, C.L. Seaman, K.N. Yang, H. Zhou and M.B. Maple, Solid State Commun., 65, 1001 (1988).
7. A. Fartash and H. Oesterreicher, Solid State Commun., 66, 39 (1988).
8. J.L. Tallon, D.M. Pooke, M.P. Staines, M.B. Bowden, N.E. Flower, R.G. Buckley, M.R. Presland and R.L. Davis, Physica C, 171, 61 (1990).
9. L. Pauling, "Nature of the Chemical Bond", 3rd ed, Oxford & IBH Publishing Co. (India), 1960.

CHAPTER 5

**MECHANISM FOR ENHANCED TEXTURED GRAIN GROWTH
UNDER DIFFERENT OXYGEN PARTIAL PRESSURES,
TEMPERATURES AND SUBSTITUTIONS**

CHAPTER 5

MECHANISM FOR ENHANCED TEXTURED GRAIN GROWTH UNDER DIFFERENT OXYGEN PARTIAL PRESSURES, TEMPERATURES AND SUBSTITUTIONS*

5.1 INTRODUCTION

This chapter describes the model that has been forwarded to explain the enhanced platy growth of YBCO which occurs at low oxygen partial pressure, higher processing temperature and by substitution.

As has already been described in chapter 3 and 4, the textured grain growth in YBCO depends on the temperature of processing, processing period, P_{O_2} and the nature and level of substituents incorporated.

It is well known [1] that solid state reactions which proceed through diffusion of ionic species along the reaction product layer is influenced to a great extent by parameters which affect diffusional characteristics of ions. Some of the parameters which influence diffusion of atoms in crystalline oxides are:

- a. Whether the diffusion process is controlled by cationic/anionic vacancy mechanism or interstitialcy mechanism at the chosen processing parameters.
- b. Whether it is the thermal or impurity effects that dictate the vacancy/interstitial defect concentration in the material.

* This work has been partly published in:
Solid State Commun., 81, 253 (1992).

The diffusing species which control the reaction rate are the most rapidly moving ions, or ions plus electrons, capable of arriving at a phase-boundary interface.

The general trends observed in platy grain growth of YBCO as described already in the earlier chapters are

- a. The grains grow larger as the P_{O_2} is decreased
- b. The alkali metal (Li, Na and K) substitution for various cations increases the grain size to various extents.

A simple model has been proposed in explaining these observations which is described below.

YBCO is a non-stoichiometric oxide with oxygen stoichiometry varying from 6 to 7. The ideal orthorhombic structure of YBCO is shown in Fig. 5.1. Neutron diffraction experiments on YBCO having different oxygen contents, have shown that the chain site oxygen [O(1)] becomes mobile above around 450°C and if the temperature is raised, these sites become more and more vacant [2]. Eventually, at temperatures above 700°C , structural transition from orthorhombic to tetragonal phase occurs. Creation of a few number of vacancies associated with heating was also observed at the apical oxygen site O(4) [2]. The $(1/2, 0, 0)$ sites O(5) are usually vacant, even though very small number of occupancies are observed especially when substitutions are effected. The O(2) and O(3) sites in the CuO_2 planes are found to be fully occupied in general and only above 900°C they become mobile[2].

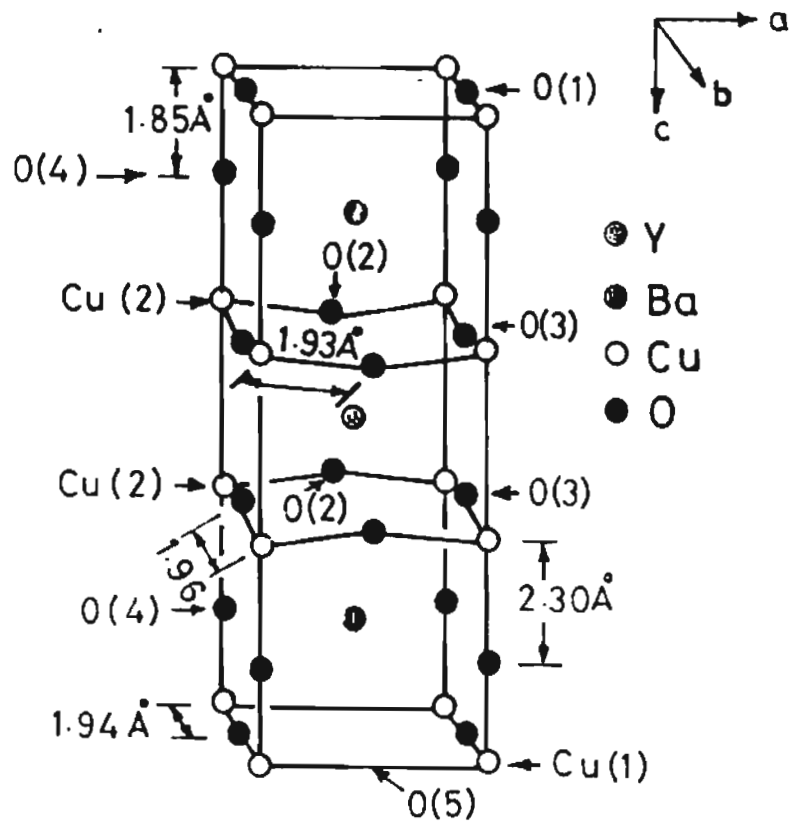


Fig. 5.1: Typical structure of $\text{YBa}_2\text{Cu}_3\text{O}_7$

5.2 DESCRIPTION OF THE MODEL

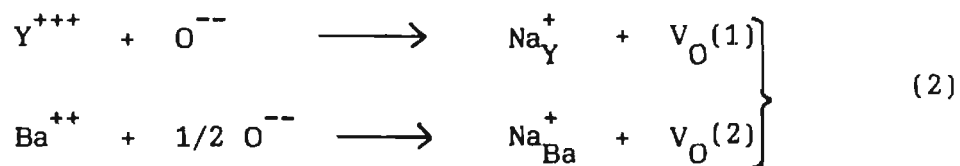
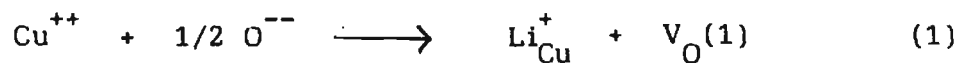
5.2.1 Effect of P_{O_2} on textured grain growth

As YBCO is a nonstoichiometric oxide, the parameters controlling the oxygen stoichiometry of the system will affect the ionic transport which depend on the oxygen vacancy concentration in the YBCO lattice. Since the grain growth depends on the ionic mobility, changes in oxygen vacancy concentration can affect the grain growth also. When the processing of YBCO is done at a low P_{O_2} , the ab-plane will have a large number of vacant oxygen sites which facilitates easy mass transport and hence an increased textured grain growth.

5.2.2 Effect of alkali metal substitutions on textured grain growth

The enhanced textured grain growth resulting from the substitution of comparatively low amounts of alkali metals for various cations in YBCO can also be accounted by the accelerated mass transport ensuing the generation of vacant oxygen sites in the lattice. When monovalent Li replaces divalent Cu, Na^+ replaces both Y^{3+} and Ba^{2+} and K^+ replaces Ba^{2+} , oxygen vacancies are generated in the lattice to maintain the charge neutrality intact.

The corresponding defect relationships can be expressed using the Kröger-Vink notations [3,4] as follows:



where $\text{V}_{\text{O}}(1)$ - oxygen vacancies at O(3) or O(2) sites of the CuO_2 planes

$\text{V}_{\text{O}}(2)$ - oxygen vacancies at O(1), O(4) or O(5) sites

The observed difference in degree of textured grain growth of the different alkali metals substituted samples under the same heat treatment schedule and substituent concentration may be due to the difference in overall vacancy formation. The importance of the site preferential vacancy creation given in equations 1, 2 and 3 can be understood, if one remembers that O(1), O(4) and O(5) sites are easily vulnerable to thermal effects compared to O(2) or O(3) sites of CuO_2 layers. Thus in the case of K substituted samples, existence of thermally generated vacancies at O(1), O(4) or O(5) sites restricts the creation of additional vacancies at these sites by substitution. But in the case of Li and Na substituted samples chemically induced vacancies add to the thermally generated ones.

Since Na^+ can replace both Y^{3+} sites and Ba^{2+} sites, the chemically induced vacancies along the CuO_2 planes $[\text{V}_\text{O}(1)]$ is less in number in Na substituted samples compared to that of Li substituted samples under the identical heat treatment schedule and substituent concentration. Thus under identical experimental conditions, the oxygen vacancy concentration will be maximum in Li substitution followed by Na and K. Therefore degree of textured grain growth also will be in the same order.

5.3 EXPERIMENTAL

As has already been emphasized, the enhanced textured grain growth - whether due to a decrease in P_O_2 or by substitution effects - is assumed as resulting from the increased oxygen vacancy concentration in YBCO. Thus it becomes a necessity to study the oxygen stoichiometry of the samples at the processing temperature in deciding the extent of validity of assumptions involved in the explanation for grain growth as detailed above.

5.3.1 Powder preparation

Carbonates, nitrates or oxides of Y, Ba, Cu and alkali metals were mixed in the appropriate molar ratio so as to get stoichiometries $\text{Y}_1\text{Ba}_2\text{Cu}_{3-x}\text{Li}_x\text{O}_{7-\delta}$, $\text{Y}_{1-a}\text{Ba}_{2-b}\text{Na}_{x=a+b}\text{Cu}_3\text{O}_{7-\delta}$ and $\text{Y}_1\text{Ba}_{2-x}\text{K}_x\text{Cu}_3\text{O}_{7-\delta}$ (where $x = 0-0.2$). The mixed precursors were heated at $920 \pm 5^\circ\text{C}$ for 12 hrs in air. The samples were then quenched from this temperature to liquid nitrogen temperature.

5.3.2 TGA

10-12 mg of the quenched powders were used for TGA in oxygen flow at a heating rate of $10^{\circ}\text{C}/\text{min}$.

5.3.3 Isothermal experiments

About 1 gm of the powders prepared by quenching were weighed accurately using an electronic balance (Mettler AE 240). These powders were then put in the furnace and heated to 430°C and kept at this temperature for 12 hrs. This temperature was chosen because the TGA experiments showed that oxygen absorption is fairly well and the oxygen desorption is fairly low at this temperature in all the cases (see section 5.4.1). The P_{O_2} inside the furnace was kept at 40% in all the cases to facilitate easier oxygen intake. After the oxygenation, the samples were weighed again and the wt% increase were calculated.

5.3.4 Iodometry

About 25 mg of powder after the isothermal oxygenation described above was taken for the determination of oxygen stoichiometry by iodometric analysis as described in chapter 2. The oxygen content of the material has been calculated as the average value obtained from 6 trials. The standard deviation has also been calculated in all the cases. From these values and the values of wt% changes obtained from the isothermal experiments, the oxygen content in the quenched materials were determined.

5.4 RESULTS AND DISCUSSION

5.4.1 TGA

The use of TG-curves in the present investigation was two fold. First of all, these curves were useful in suggesting the qualitative variation in the oxygen absorption trends of different samples. Thus a rough estimate of the temperature, at which the rate of absorption is maximum, could be determined for all the samples used in the experiment. (The TG-curves given in Fig. 5.2 clearly shows the differences in the oxygen absorption tendencies of two such samples). These estimates were helpful in deciding the temperatures for the isothermal experiments so that the samples are oxygenated to the maximum. The temperature range 420-430^oC has been found to be suitable for oxygenation of all the samples since the desorption of oxygen due to thermal effects were very small in this range.

The other purpose of using the TG-curves was in estimating the activation energy for oxygen absorption of different samples. A first order kinetic equation has been formulated for the reaction

$O_6 + O \rightleftharpoons O_7$ and Arrhenius type rate constants have been assumed. Thus the rate equation, in terms of moles of the reacting species, reads as

$$\frac{dy(t)}{dt} = r_1 e^{-E_1/kT} (N_o - y(t)) - r_2 e^{-E_2/kT} y(t)$$

where, $y(t)$ = moles of YBCO which is not yet oxygenated at time t ,

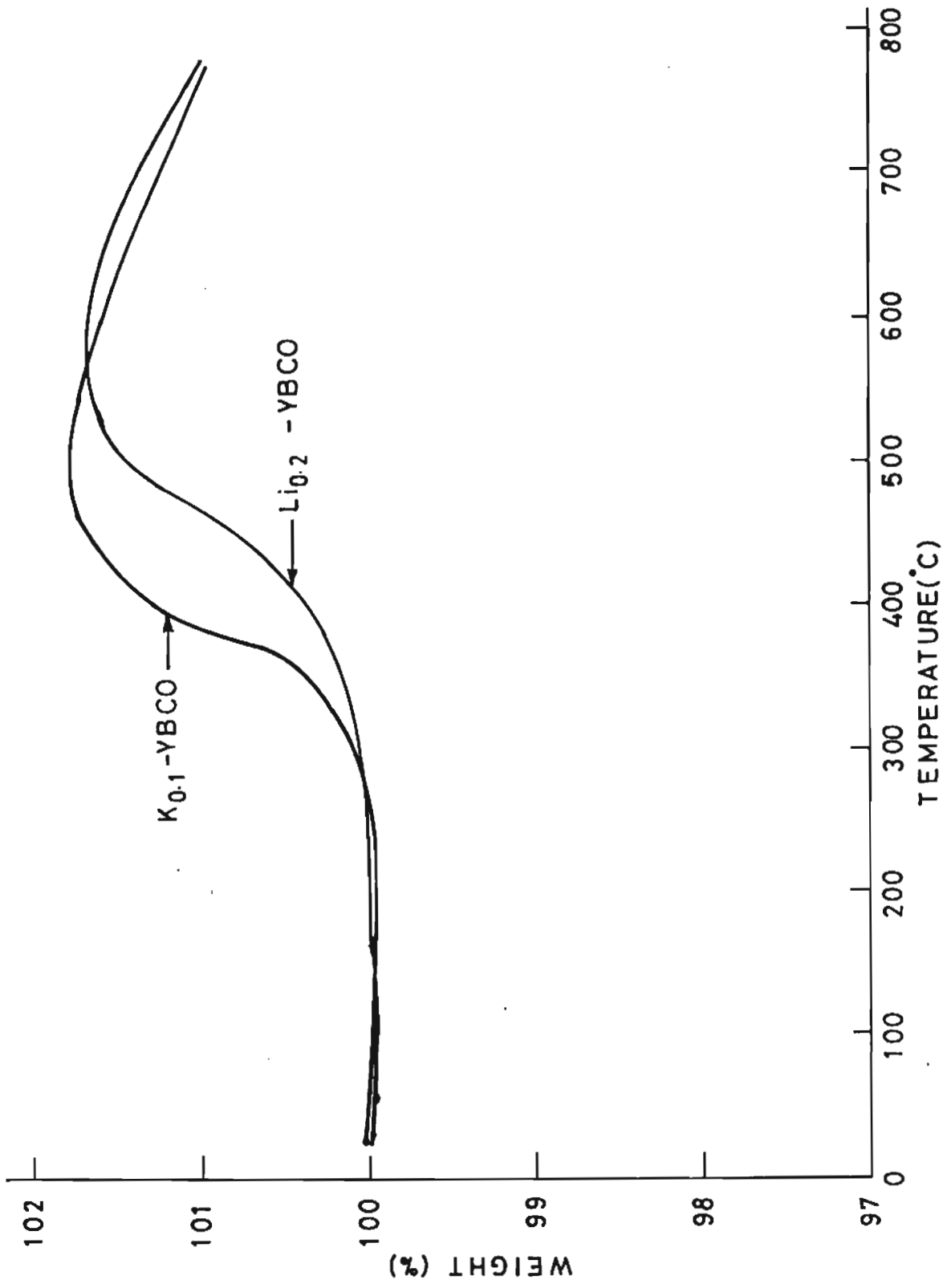


Fig. 5.2: Typical TG-curves of two samples

- N_0 = moles of YBCO present initially,
 ν_1, ν_2 = constants,
 E_1, E_2 = activation energies corresponding to oxygen absorption and desorption respectively.

The first term contains parameters related to the oxygen absorption while the second, of the desorption.

This equation was converted so that wt% changes and temperatures (rather than moles of substances and times) were incorporated and on integration, the relation connecting wt% change and temperature was obtained just as in a TG-curve. This equation was then fitted with the experimental TG-curves by keeping ν_1 and E_1 as free parameters.

To fix the values of E_2 and ν_2 , published reports on oxygen desorption studies in YBCO were looked into. There have been many reports [5,6] and the work reported by H.S. Strauven et al [5] describes the oxygen evolution trends in YBCO upto 1000^oC. Of the 5 desorption maxima observed in the entire range of temperatures, the one at the least temperature occurs at around 650^oC with activation energy = 1eV. Thus the desorption parameters in the present calculation were fixed as $E_2 = 1\text{eV}$ and $\nu_2 = 10^5/\text{s}$.

A typical TG-curve and the corresponding calculated curve are given in Fig. 5.3. The calculated activation energy parameters for oxygen absorption of Li, Na and K substituted samples with substituent

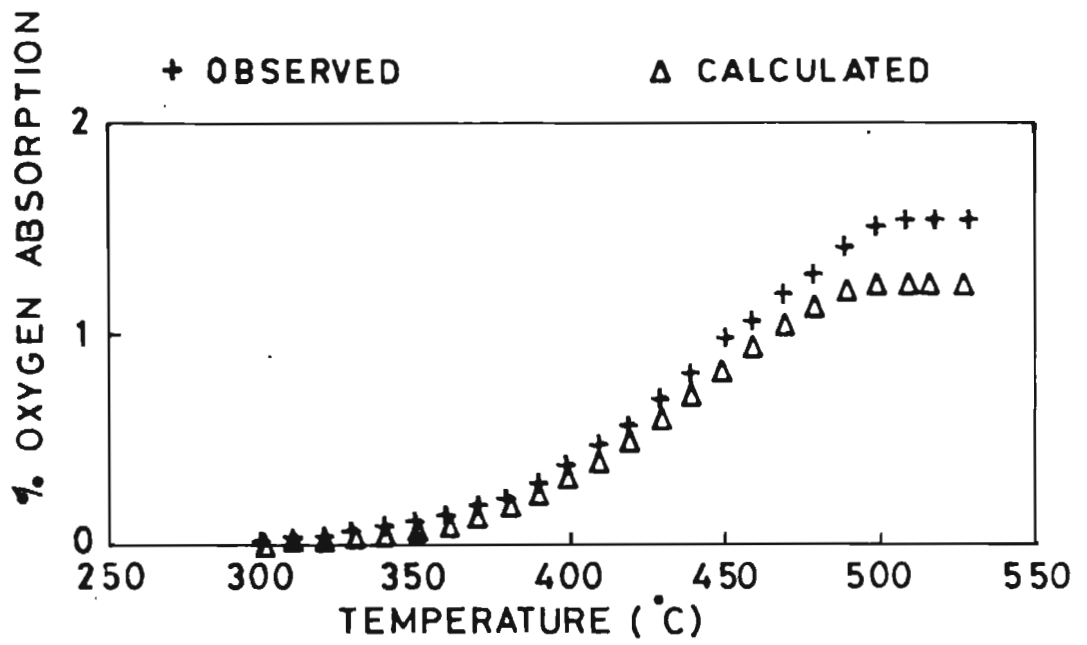


Fig. 5.3: Typical TG-curve and corresponding calculated curve

stoichiometry 0.1 along with that of undoped YBCO are given in Table 5.1.

Table 5.1: Activation energies of oxygen absorption

Sample	Activation Energy (eV)
Pure YBCO	1.42 \pm 0.03
Li _{0.1} - YBCO	1.08 \pm 0.05
Na _{0.1} - YBCO	1.39 \pm 0.03
K _{0.1} - YBCO	1.31 \pm 0.03

5.4.2 Isothermal experiments

The results of isothermal experiments carried out at 430^oC are given in Table 5.2.

From the table it is evident that in general, the oxygen stoichiometry in the alkali metal substituted YBCO at the processing temperature is less than that in the undoped YBCO. Fig. 5.4 shows the plot of oxygen content of samples at 920^oC as the substituent stoichiometry varies from 0.05 to 0.2. A dashed line corresponding to the observed oxygen content of the undoped YBCO at 920^oC also is shown as a guide to the eyes. A systematic decrease in oxygen stoichiometry at 920^oC with the increase of substituent concentration is evident in the case of Li and K substituted samples, whereas an initial increase

Table 5.2: Results of isothermal experiments done at 430°C

Stoichiometry	Final oxygen content	wt% increase	Oxygen content at 920°C	Oxygen intake per unit cell
Pure YBCO	6.8338 (0.02)	1.27	6.3137	0.52
Li _{0.05} YBCO	6.9030 (0.01)	1.82	6.1636	0.6660
Li _{0.1} YBCO	6.9282 (0.01)	1.92	6.1518	0.7764
Li _{0.2} YBCO	6.7647 (0.03)	1.642	6.1073	0.6574
Na _{0.05} YBCO	6.5686 (0.05)	1.746	5.8659	0.7029
Na _{0.1} YBCO	6.7912 (0.03)	1.914	6.0228	0.7684
Na _{0.2} YBCO	6.5615 (0.05)	1.707	5.8874	0.6741
K _{0.05} YBCO	6.6614 (0.04)	1.896	5.8986	0.7628
K _{0.1} YBCO	6.565 (0.04)	1.78	5.8551	0.7099
K _{0.2} YBCO	6.5222 (0.05)	1.696	5.8562	0.6660

(values in the brackets are the standard deviation)

is observed in the case of Na substitution. By taking the oxygen content of the samples at the substituent stoichiometry of 0.05, the subsequent depletion of oxygen has been calculated in all the cases using the defect equations (1), (2) and (3). These calculated values along with the corresponding observed values of all the three substitutions are plotted in Fig. 5.5. In the case of Li and K, the observed decrease in oxygen stoichiometry matches very well with the prediction of the model, i.e. release of one oxygen atom for every two alkali atoms

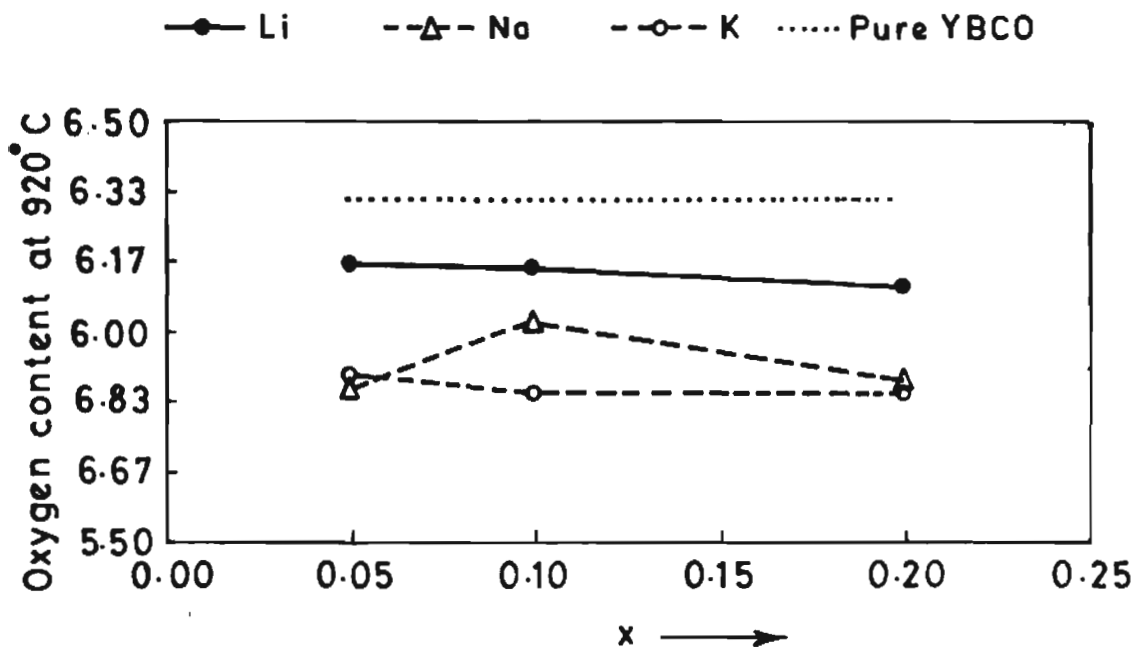


Fig. 5.4: Plot of oxygen content at 920°C vs substituent stoichiometry of the samples

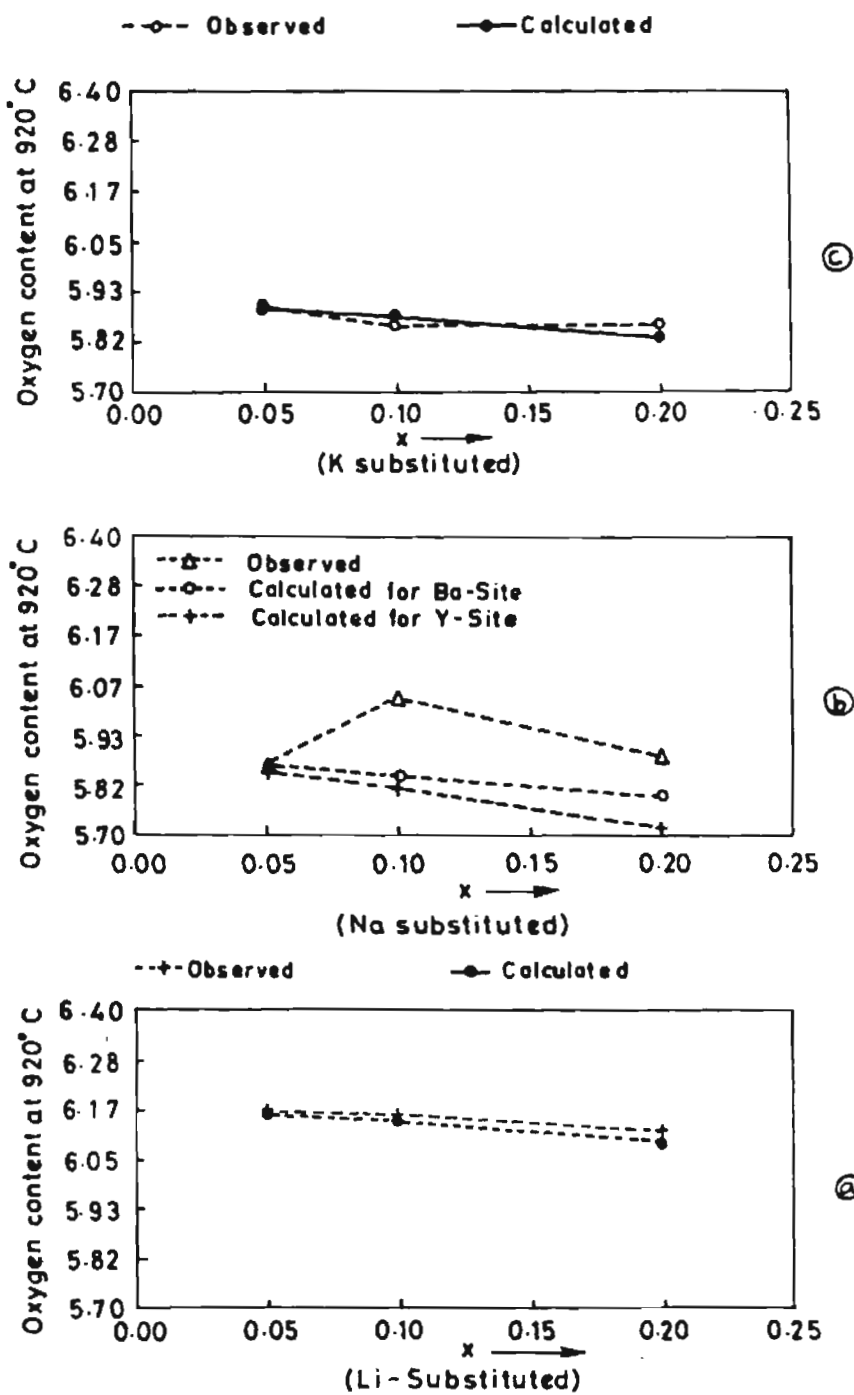


Fig. 5.5: Plots of oxygen content at 920°C by calculation and observation vs substituent stoichiometry of different samples

substituted. But in the case of Na substitution, an initial deviation from the calculated trends occurs. At the same time, if the values of initial oxygen content for the Na stoichiometry of 0.05 is exempted, the rest of the observations fits remarkably with the curve calculated on the assumption of Na substituting the Y site (Note the identical slopes in the range 0.1-0.2 in Fig. 5.5b).

Again from the table 5.2 it can be seen that the initial oxygen content is less than even 6 in all the samples with Na or K substitution except in the case of Na stoichiometry '0.1' in contrast to the values obtained in the case of samples with Li substitution. This may be because the Na or K substitution may be destabilising the YBCO structure to a greater extent so that at the processing temperature, the thermally created oxygen vacancies are much more compared to that in the Li substituted sample. If this is true, then it is evident that even if oxygen vacancy concentration in the material is high so that ionic diffusion processes are promoted, significant grain growth may not result due to the decrease in the coherence among the unit cells. In this connection, it should also be noted that in spite of low oxygen stoichiometries observed in Na and K substituted samples, the platy grain growth is maximum for Li substitution.

Thus the determination of the oxygen contents of the materials has proved beyond doubt that the alkali metal substitution increases the oxygen vacancy concentration in YBCO thus partially agreeing with the model proposed. At the same time, it has become clear that platy

grain growth is controlled not only by the oxygen vacancies but also by properties like the structural stability etc. of the substituted sample.

Another important result that has been obtained is the evidence for the increased oxygen absorption rate in alkali metal substituted samples in comparison with that of undoped YBCO. From table 5.2 it can be seen that in spite of the identical times and other parameters used in the oxygenation process, the amount of oxygen intake is more in alkali metal doped YBCO than the undoped YBCO. Fig. 5.6 in which the number of oxygen atoms absorbed per unit cell is plotted against the substituent concentration shows this clearly. This fact is also perhaps reflected by the calculated activation energies of oxygen absorption, given in Table 5.1. The activation energies for oxygen absorption is less for alkali metal substituted samples compared to that of undoped YBCO..

5.5 CONCLUSION

In this chapter a model for the textured grain growth in YBCO has been proposed which is based on the oxygen vacancy creation under different experimental conditions. When the processing of YBCO is done at a low P_{O_2} , the ab-plane will have a large number of vacant oxygen sites which facilitates easy mass transport and hence an increased textured grain growth. Similarly the enhanced textured grain growth resulting from the substitution of comparatively low amounts of alkali metals for various cations in YBCO can also be accounted by the

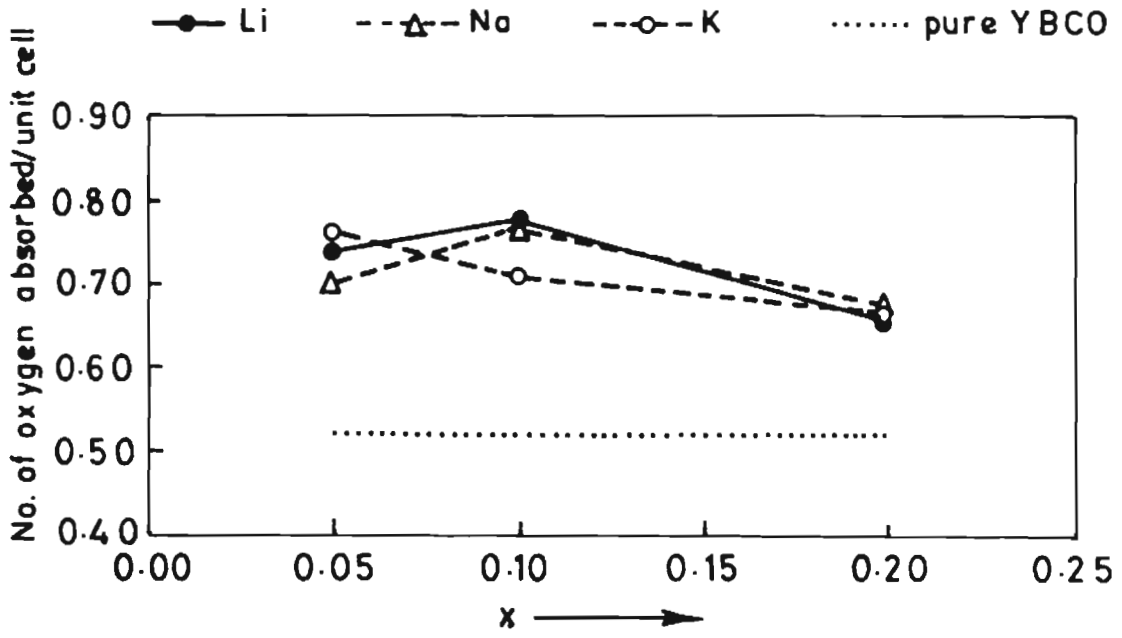


Fig. 5.6: Plots of number of oxygen absorbed/unit cell vs substituent stoichiometry of different samples

accelerated mass transport resulting from the generation of vacant oxygen sites.

In order to check the extent of validity of the proposed mechanism for textured grain growth in YBCO, oxygen stoichiometries of different samples at processing temperature were determined with the help of different thermal analyses and iodometry. The calculation of the same, using the proposed model shows that in the case of Li and K substituted samples, the observed values match very well with the prediction of the model, i.e. release of one oxygen atom for every two alkali atoms substituted. In the case of Na substitution the fit was very well except for the deviation for the Na stoichiometry 0.05.

Moreover it was observed that in the case of Li substituted samples, oxygen vacancy concentration is the main factor influencing the platy grain growth whereas in Na and K substituted samples, properties like structural stability etc. also may have to be considered.

Another important result that was obtained from this study is the evidence for increased oxygen absorption rate in alkali metal substituted samples in comparison with that of undoped YBCO.

REFERENCES

1. W.D. Kingery, H.K. Bowen and D.R. Uhlmann, "Introduction to Ceramics", 2nd edn., New York, Wiley, p.239, 1976.
2. J.D. Jorgensen, M.A. Beno, D.G. Hinks, L. Soderhol, K.J. Volin, R.L. Hitterman, J.D. Grace, I.K. Schuller, C.U. Segre, K. Zhang and M.S. Kleefisch, Phys. Rev. B., 36, 3608 (1987).
3. F.A. Kroger and V.J. Vink, "Relations between the Concentrations of Imperfections in Crystalline Solids", Solid State Physics, Vol.3, F. Seitz and D. Turnbull, Eds., Academic Press Inc., New York, 1956, p. 307-436.
4. F.A. Kröger, The Chemistry of Imperfect Crystals, North-Holland Publishing Company, Amsterdam, 1964.
5. H. Strauven, J.P. Locquet, O.B. Verbeke and I.K. Schuller, Solid State Commun., 65, 293 (1988) .
6. J.P. Locquet, J. Vanacken, B. Wyuts, Y. Bruynseraede and I.K. Schuller, Europhys. Lett., 7, 469 (1988).

CHAPTER 6

PREPARATION AND CHARACTERISATION OF SINTERED TEXTURED BULK YBCO BY COLD PRESSING AND HEAT TREATMENT

CHAPTER 6

PREPARATION AND CHARACTERISATION OF SINTERED TEXTURED BULK YBCO BY COLD PRESSING AND HEAT TREATMENT *

6.1 INTRODUCTION

As mentioned in chapter 3 it is widely recognised that the critical current density achieved in routinely processed polycrystalline YBCO are several orders of magnitude lower than what can be achieved in single crystals or thin films of the material [1-4]. The anisotropy of J_c in single crystals of YBCO and the achievement of higher J_c in oriented thin films [5-9] indicate that crystallographic alignment of grains, also called texture may be necessary to raise J_c to commercially useful levels in bulk polycrystalline materials. As described in chapter 3, several means have been reported for introducing grain alignment in bulk at the various stages of processing [10-18].

In chapters 3 and 4 we have seen the growth characteristics of platelet grains of YBCO having growth along ab-plane under different Po_2 , temperature and alkali metal substitution at the calcination stage. In this chapter, the effect of uniaxial cold pressing and sintering of these platelet grains on the intergranular orientation and corresponding J_c is described. The factors influencing the degree of orientation have been investigated and J_c of the samples was correlated with the microstructure.

*This work has been partly published in:
Solid State Commun., 71, 287 (1989)

6.2 EXPERIMENTAL

Platelet grains of YBCO having average sizes $< 15 \mu\text{m}$, $< 30 \mu\text{m}$ and $> 30 \mu\text{m}$ were synthesized by controlling the P_{O_2} , temperature and soaking period. Then the powders were sieved so that 3 batches of powders S1, S2 and S3 were prepared with average grain sizes, less than $15 \mu\text{m}$, between $15 \mu\text{m}$ and $30 \mu\text{m}$ and greater than $30 \mu\text{m}$ respectively. For the purpose of comparison, a batch of powder S4 of nearly spherical (size $\approx 5 \mu\text{m}$) is also included in the study. In order to complete the oxygenation of these powders, they were annealed at 450°C in the flow of oxygen for a period required by each sample for attaining an oxygen content more than 6.9 as evidenced by iodometric analysis described in chapter 2. A typical SEM photograph of the platy grains is shown in Fig. 6.1.

About 0.7 gms of these powders were filled in a rectangular die having dimensions of $20 \text{ mm} \times 4 \text{ mm} \times 5 \text{ mm}$ and uniaxially pressed by applying pressures in the range 50-500 MPa for 5 minutes. X-ray diffraction was performed on the pressed surface of the sample which is perpendicular to the axis of compression. These samples were sintered at 950°C in oxygen flow for 6-36 hrs. The sintered samples were oxygenated at 450°C for sufficient time. The ratio of the intensities of (005) and (113) reflections determined from XRD patterns was taken as the index for the measure of orientation introduced by pressure and heat treatment on the platy grains. J_c of these samples at 77 K were measured by D.C. transport method using $1 \mu\text{V/cm}$ criterion. Microstructure of the samples was analysed by SEM.

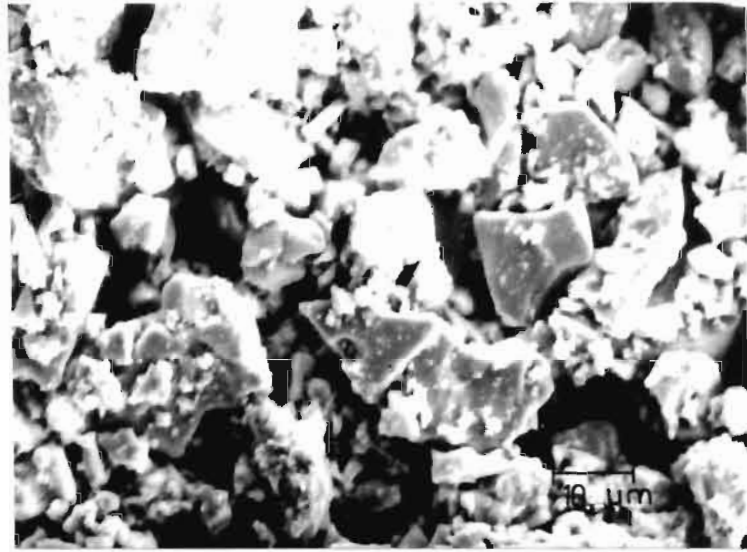


Fig. 6.1: Typical SEM photograph of the platy grains

6.3 RESULTS AND DISCUSSION

6.3.1 Effect of cold pressing

A typical SEM photograph (Fig. 6.2) of the pressed surface of the samples shows that the simple cold pressing introduces considerable orientation of platy grains. The degree of orientation was found to depend on the applied pressure as well as the grain size.

Fig. 6.3 shows the plot of orientation index of pressed surface vs applied pressure of samples of different grain sizes.

From the Fig. it is clear that in the case of S1, S2 and S3 batches as the pressure increases the orientation index also increases. But after a certain pressure, the grain orientation was found to be saturated. For a constant pressure, the orientation of grains is more for sample with larger grains. In the case of powder from S2 batch, there is a steep increase in the orientation for pressure in the range 150-200 MPa. For S4 batch sample, there is no orientation by cold pressing. Its orientation index was found to be unity.

The variation of orientation index at different depths from the pressed surface of powder from S2 batch is shown in Fig. 6.4. It is clearly seen that below 100 μm depth, there is no significant orientation induced by the application of pressure. Similar results obtained for powder from other batches as well indicate that in the uniaxial pressing set-up used in the present experiment, grain orientation can be introduced only over a thin layer of around 100 μm of the sample surface.

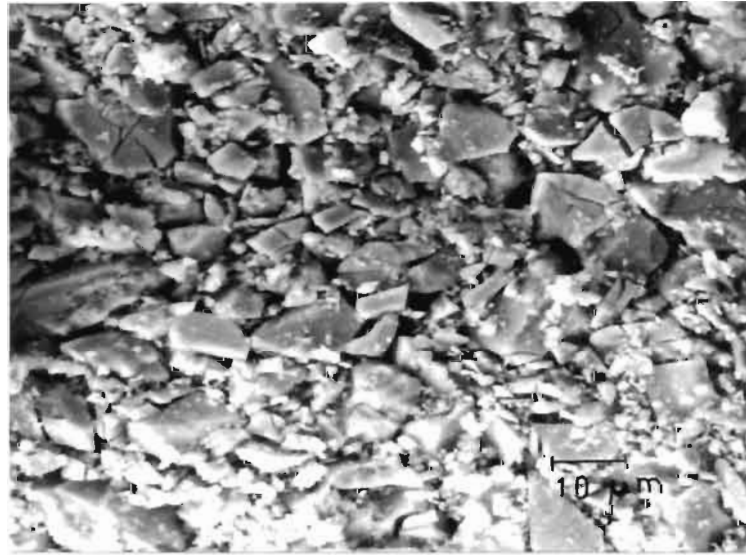


Fig. 6.2: Typical SEM photograph of the pressed surface of the sample

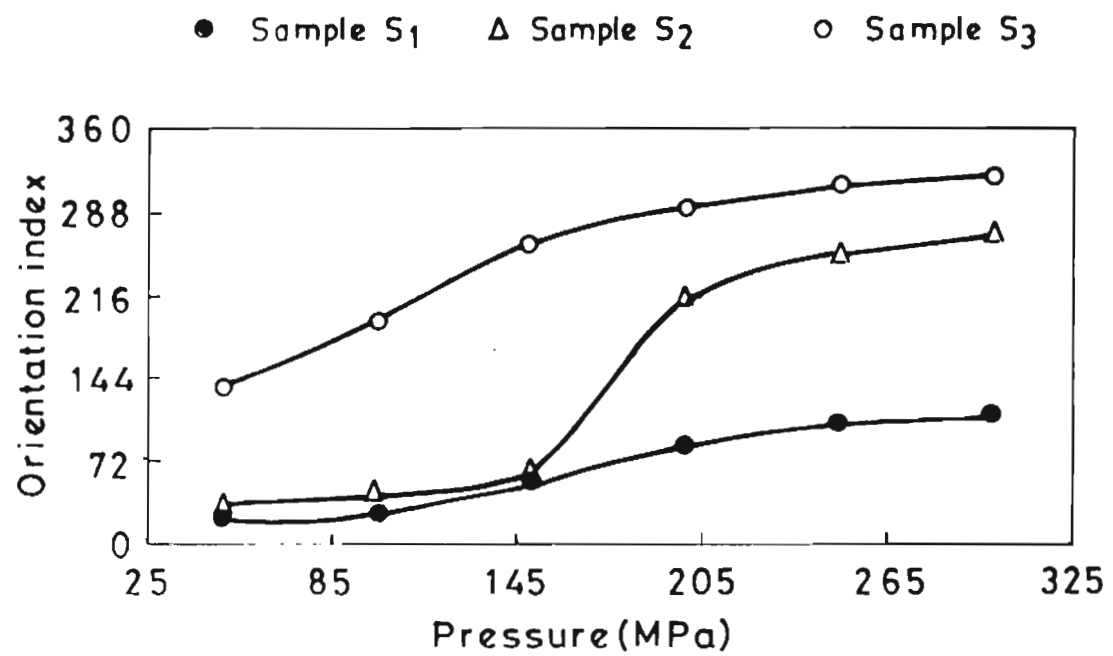


Fig. 6.3: Plots of orientation index of pressed surface vs applied pressure

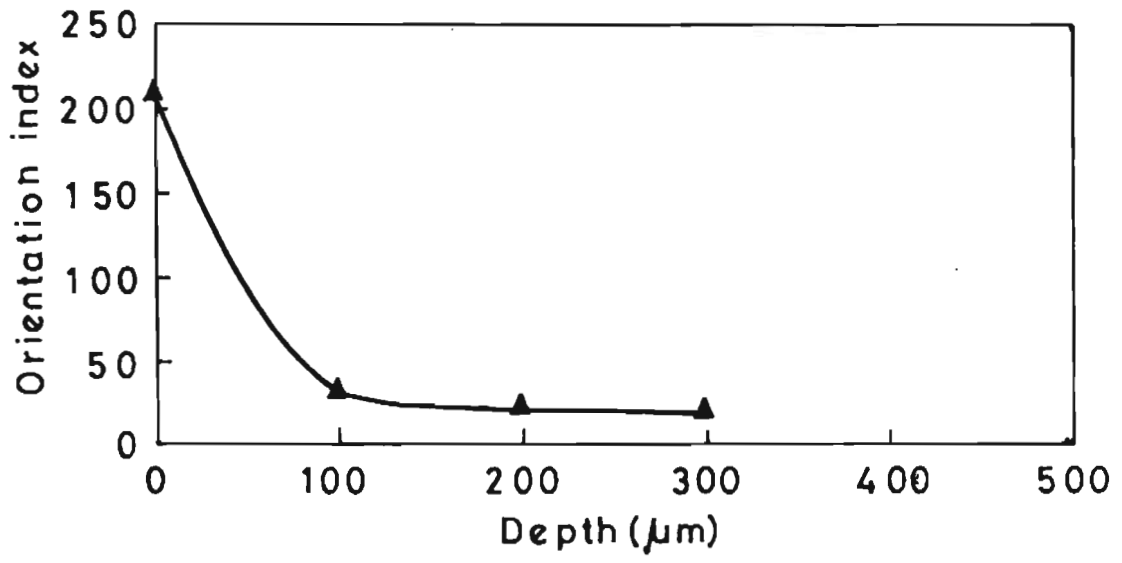


Fig. 6.4: Plot of orientation index vs different depth

6.3.2 Effect of heat treatment

Fig. 6.5 shows the typical XRD patterns of the pressed surface of as-pressed, 6 hrs sintered and 36 hrs sintered sample. Table 6.1 gives orientation index of the sintered sample made from the batch S2 powder using a pressure of 200 MPa.

Table 6.1: Orientation index of the cold pressed and sintered samples made from the batch S2 of powder

Sample	Orientation Index
as-pressed	220
6 hrs sintered	16
36 hrs sintered	78

From the XRD patterns and Table it is clear that sintering for a period of 6 hrs reduces the grain alignment. But as the sintering time increased to 36 hrs, the grain alignment is found to be increased. In the case of other samples also, the decrease of grain alignment has been observed for the initial periods of sintering and with the increase of period of sintering, the grain alignment was found to be increasing.

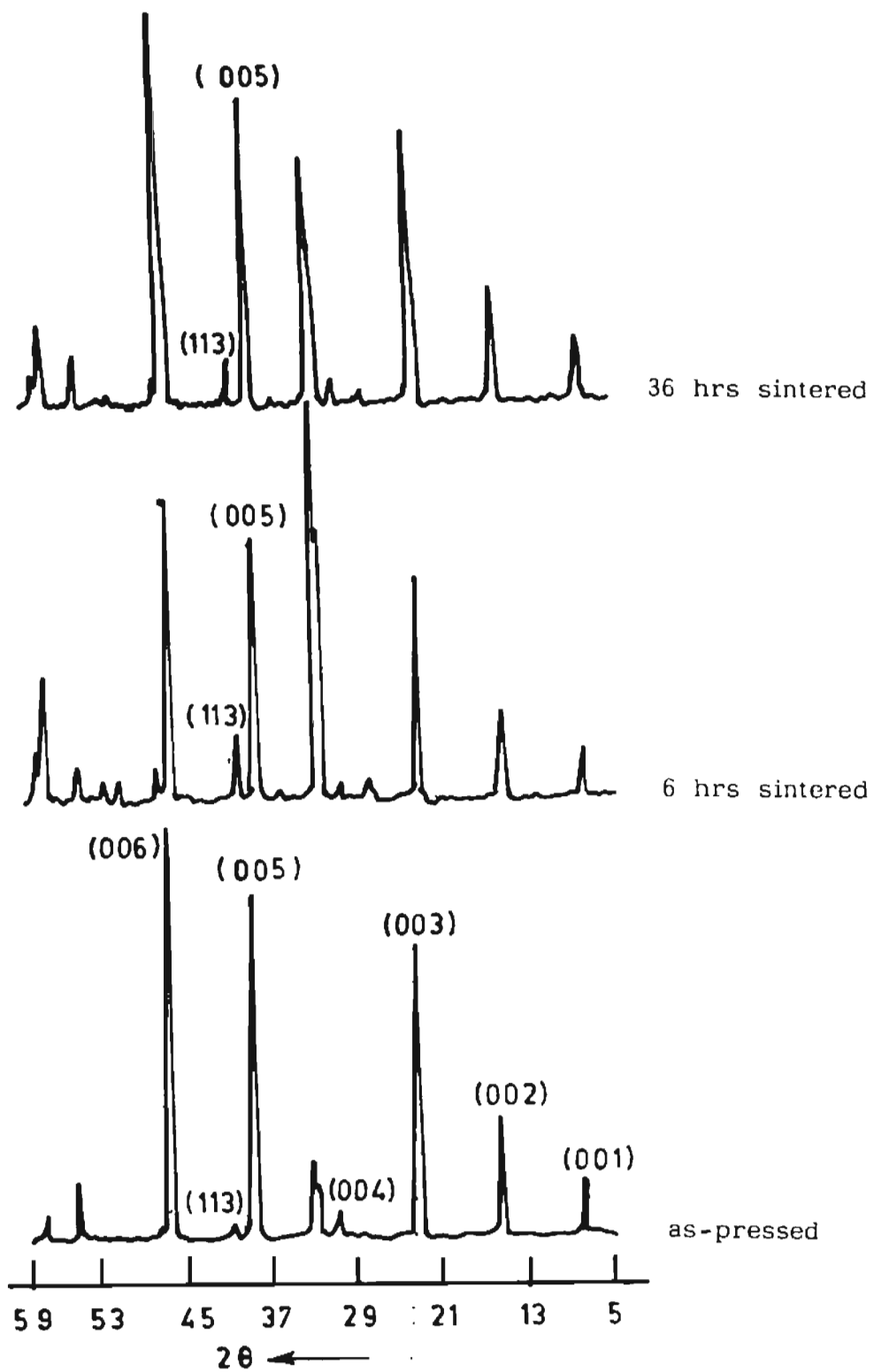


Fig. 6.5: Typical XRD patterns of the pressed surface of as-pressed, 6 hrs sintered and 36 hrs sintered sample

In contrast to the drastic decrease of grain alignment with depth in the case of as-pressed samples (Fig. 6.2), in the case of sintered samples, a deeper penetration of alignment into the interior of the sample was observed (Fig. 6.6), which increased with increasing sintering time.

6.3.3 Critical current density and microstructure

Table 6.2 gives J_c of samples sintered for 36 hrs at 950^oC in oxygen flow. The samples were prepared from all the 4 batches S1, S2, S3 and S4 of powder, pressing at a pressure of 200 MPa.

Table 6.2: J_c of the sintered samples made from different batches of powder

Batch	J_c (A/cm ²)
S1	56
S2	174
S3	110
S4	32

From the table it is clear that the sample made from the batch S2 shows higher J_c compared to others.

SEM fractographs taken near the edge of the pressed surface

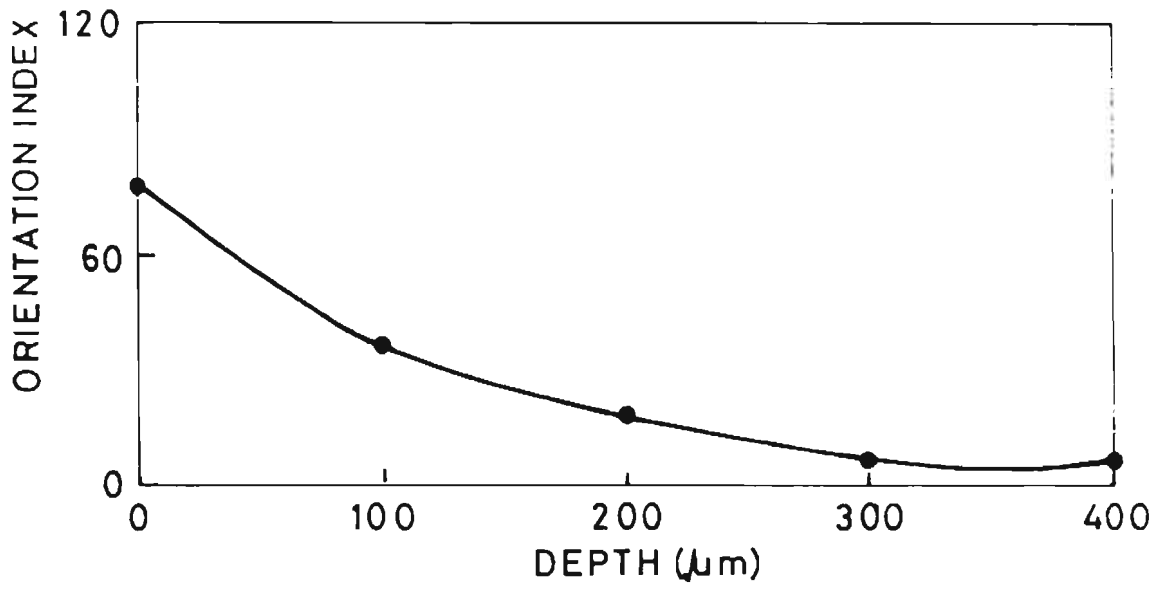


Fig. 6.6: Plots of orientation index vs different depths of sintered sample

of the sintered samples made from the batches S2 and S4 are shown in Fig. 6.7. About five fold increase in J_c in sample made from batch S2 compared to S4 can be explained only by taking account of the grain alignment as observed from the SEM fractograph.

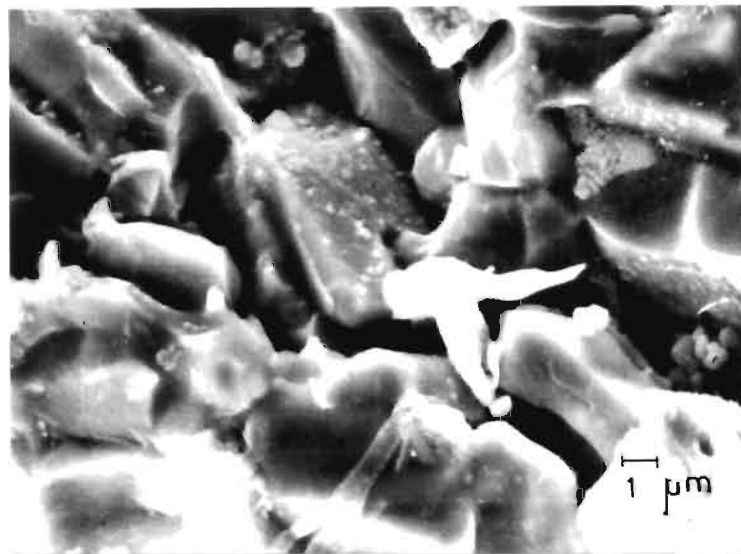
It should be remarked that compared to the J_c of 4200 A/cm^2 reported by X.G. Zheng et al [10], the J_c obtained in the present work is much less. The reason for this discrepancy may be the difference in the alignment techniques adopted. In the present work, the uniaxial compaction is found to induce alignment over a thin layer of the bulk only while the vibrational alignment and subsequent cold pressing method used in the work by X.G. Zheng succeeded in imparting grain alignment throughout the volume of the sample pressed.

6.3.4 Effect of cold pressing and heat treatment on the J_c of alkali metals substituted YBCO

In chapter 4, it was seen that the alkali metal substitution can induce platy growth of YBCO grains along a-b plane. Thus cold pressing can be applied in these grains also to see the effect of alignment and the heat treatment on the J_c . With this objective in mind, the grain size in the range 15-30 μm was synthesized as described in chapter 4 because in the case of undoped YBCO, as described above, the pressure induced alignment and subsequent heat treatment had more significant effect on J_c in this range of grain size. These grains were also subjected to a study similar to that has already been described in the case of undoped YBCO. The only difference was that in the case of alkali metal substituted samples, the heat treatment



S2



S4

Fig. 6.7: SEM photographs taken near the edge of the pressed surface of the sintered samples prepared from the batches S2 and S4

was done at a temperature of 930⁰C.

In this case also, the simple cold pressing was found to align the grains on a thin layer below the pressed surface and the depth profiles of alignment were similar to what was observed for undoped YBCO powders.

Table 6.3 gives the J_c values of alkali metal substituted YBCO samples pressed at 200 MPa and sintered for 36 hrs.

Table 6.3: J_c values of alkali metal substituted YBCO samples

Sample	J_c (A/cm ²)
Li-substituted	0.05
Na-substituted	17
K-substituted	30

From the Table it is clear that J_c values of the alkali metal substituted samples are not improved eventhough there is alignment of grains along ab-planes by cold pressing and heat treatment. In the case of Li and Na substituted samples J_c is much less than that of the undoped YBCO having no alignment (Batch S4 of Table 6.2). But in the case of K-substituted sample it is comparable.

6.4 CONCLUSION

Effect of cold pressing and heat treatment on the alignment of platy grains of YBCO of different grain sizes synthesized by controlling P_{O_2} , temperature and alkali metal substitution have been studied. Cold pressing was found to align the grains on a thin layer below the pressed surface. The degree of grain alignment was found to depend on both the pressure applied as well as the grain size.

Alignment of grains in the pressed sample was found to be decreased by short periods of sintering while for longer periods it increased. Longer periods of sintering was also found to impart deeper penetration of grain alignment into the interior of the samples. The J_c of samples prepared by pressing platy grains of undoped YBCO was found to be higher than that of those prepared from grains of nearly spherical shape. Also the J_c of the sample prepared from grains of size between 15 μm and 30 μm was found to be higher than the other samples included in this study.

The effect of cold pressing and heat treatment on the grain alignment in alkali metal substituted samples was similar to that of the undoped YBCO. Despite this, the J_c of substituted samples was found to be very low compared to that of undoped YBCO.

REFERENCES

1. V.G. Baryakhtar, V.M. Pan, V.G. Prokhorov et al, Pisma Zh Eksp Teor Fiz (Sov), 46, 168 (1987).
2. V.M. Pan, V.G. Prokhorov, C.G. Kaminsky et al, Fiz. Nizk Temp. (Sov), 13, 861 (1987).
3. R. watanabe, Y. Kasai, T. Machiku et al, Jap. J. Appl. Phys., 26, L657 (1987).
4. U. Dai, G. Deutscher and R. rosenbaum, Appl. Phys. Lett., 51, 460 (1987).
5. P. Chaudhary, R.H. Koch, R.B. Laibowitz, T.R. McGuire and R.J. Gambino, Phys. Rev. Lett., 58, 2684 (1987).
6. Y. Enomot, T. Murakami, M. Suzuki and K. Moriwaki, Jap. J. Appl. Phys., 26, L1248 (1987).
7. T.R. Dinger, T.K. Worthington, W.J. Gallagher and R.L. Sandstorm, Phys. Rev. Lett., 58, 2687 (1987).
8. G.W. Crabtree, J.Z. Liu, A. Umezawa, W.K. Kwok, C.H. Sowers and S.K. Malik, Phys. Rev. B 36, 4021 (1987).
9. S. Jin, Science, 238, 1655 (1987).
10. X.G. ZHENG, H. Kuriyaki and K. HIRAKAWA, Jap. J. Appl. Phys., 28(1), L52 (1989).
11. M.R. DeGuire, C.J. Kim, W.H. Lu, D.E. Farrel and D. Boyne, Research update, 1988, "Ceramic Superconductors II", Edited by Man F. Yan. (The American Ceramic Society, Inc., Westerville, Ohio, 1988), p.343.

12. L.C. Stearns, M.D. Vaudin, C.P. Ostertag, J.E. Blendell and E.R. Fuller, Jr., Research update, 1988, "Ceramic Superconductors II", Edited by Man F. Yan. (The American Ceramic Society, Inc., Westerville, Ohio, 1988), p.315.
13. J.J. Balducci, V.K. Seth and W.A. Schulze, Research update, 1988, "Ceramic Superconductors II", Edited by Man F. Yan. (The American Ceramic Society, Inc., Westerville, Ohio, 1988) p.367.
14. C.P. Ostertag, R.D. Shull, M.D. Vaudin, J.E. Blendell, L.C. Stearns and E.R. Fuller, Jr., Research update, 1988, "Ceramic Superconductors II", Edited by Man F. Yan. (The American Ceramic Society, Inc., Westerville, Ohio, 1988) p.332.
15. K.C. Goretta, A.J. Schultz, D.W. Capone II, T. L. Tolt, U. Balachandran, J.T. Dusek, M.T. Lanagan, R.B. Poeppel, J.P. Singh, D. Shi, R.L. McDaniel, D.S. Applegate, J.K. Degener and J.S. Kallend, Research update, 1988, "Ceramic Superconductors II", Edited by Man F. Yan. (The American Ceramic Society, Inc., Westerville, Ohio, 1988) p.323.
16. S.S. Kim, T.T. Srinivasan, T.R. ShROUT and R.E. Newnham, Research update, 1988, "Ceramic Superconductors II", Edited by Man F. Yan. (The American Ceramic Society, Inc., Westerville, Ohio, 1988) p.381.
17. L. Lynds, F. Galasso, E. Otter, B.R. Weinberger, J.I. Budnick, D.P. Yang and M. Fillipkowski, J. Am. Ceram. Soc., 71(3), C-130 (1988).
18. T. Takenaka, H. Noda, A. Yoneda and K. Sakata, Jap. J. Appl. Phys., 27, L1209 (1988).

P a r t B

CHAPTER 7

SYNTHESIS OF PHASE PURE $Y_1Ba_2Cu_3O_{7-\delta}$ BY DYNAMIC VACUUM
CALCINATION AND ITS CHARACTERISATION

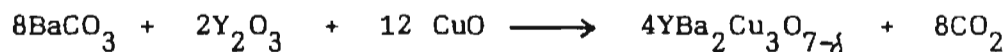
CHAPTER 7

SYNTHESIS OF PHASE PURE $Y_1Ba_2Cu_3O_{7-\delta}$ BY DYNAMIC VACUUM
CALCINATION AND ITS CHARACTERISATION

7.1 INTRODUCTION

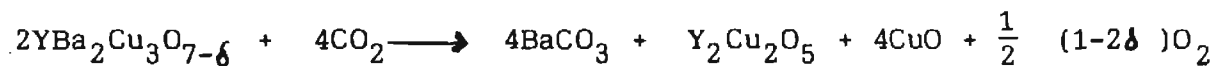
High temperature ceramic superconductors are normally prepared by solid state reaction of oxides, carbonates, nitrates etc. [1-3]. For the synthesis of $Y_1Ba_2Cu_3O_{7-\delta}$, the mixed precursors are calcined at a temperature $900-950^\circ\text{C}$ for 20-50 hrs. Intermittent grinding is also necessary to obtain relatively phase pure and homogeneous YBCO powders. The high temperatures used in the conventional methods can induce formation of liquids and nonsuperconducting phases such as Y_2BaCuO_5 and $BaCuO_2$ [1]. The presence of these nonsuperconducting phases especially at the grain boundaries lowers the critical current density. In addition to the production of undesirable phases, the conventional processes are time consuming and result in coarse particles.

If $BaCO_3$ is used during calcination of YBCO precursors, simultaneous decomposition of $BaCO_3$ to BaO and reaction among the three constituents (Y_2O_3 , BaO and CuO) forms the desired perovskite phase. The reaction can be written as follows:



However the presence of CO_2 in the processing environment can induce the undesirable back reaction with YBCO to form BaCO_3 , Y_2O_3 , CuO and $\text{Y}_2\text{Cu}_2\text{O}_5$ depending on temperature [4,5].

The reaction at 815°C , in the presence of CO_2 , can be written as follows [6].



Therefore synthesis of phase pure material which gives higher J_c by the conventional method of preparation is very difficult.

In chapter 3, describing the study of textured grain growth at different P_{O_2} and temperatures, we have seen that by the lowering of P_{O_2} , the processing temperature of YBCO phase formation can be reduced to a large extent. Similarly if the CO_2 level in the processing environment can be decreased, by pumping out the CO_2 evolved, the decomposition of YBCO through the back reaction mentioned above can also be avoided.

The synthesis route reported by U. Balachandran et al [7] ingeniously incorporates the above two considerations, in which phase pure YBCO powders have been synthesized by calcining the precursors at 800°C in flowing O_2 at reduced pressure.

In the course of present investigation, an experimental set-up has been designed and fabricated for the synthesis of phase pure YBCO powder along the lines described in the the above work [7]. The

characterisation of YBCO powders synthesized by using the set-up mentioned above was done.

7.2 EXPERIMENTAL

7.2.1 Experimental set-up

The experimental set-up fabricated for the present work is shown in Fig. 7.1. It consists of mainly a tubular furnace having provisions for applying vacuum and to pass oxygen. The pressure inside the furnace can be controlled by operating needle valves and it can be monitored through a vacuum gauge. The flow of oxygen can be controlled with the help of a flow meter, compound gauge and needle valve.

7.2.2 Processing of YBCO by dynamic vacuum calcination

Mixed precursors, weighing about 6 gms, were put inside the furnace in a platinum boat. The pressure inside the furnace was reduced to 5-10 mm of Hg by working the vacuum pump and a flow of oxygen at the rate of 0.1 litres/minute was given and this was maintained during the entire soaking period. A low rate of heating (15°C/hr) was given in the range 680°C - 800°C . A soaking period of 5 hrs and a temperature of 800°C was used during the processing. While cooling, the vacuum was discontinued and ambient-pressure O_2 was passed. To promote the oxygenation of the resulting powder, a 4 hr hold at 450°C was incorporated into the cooling schedule.

The flow rate of oxygen and heating rate are to be adjusted

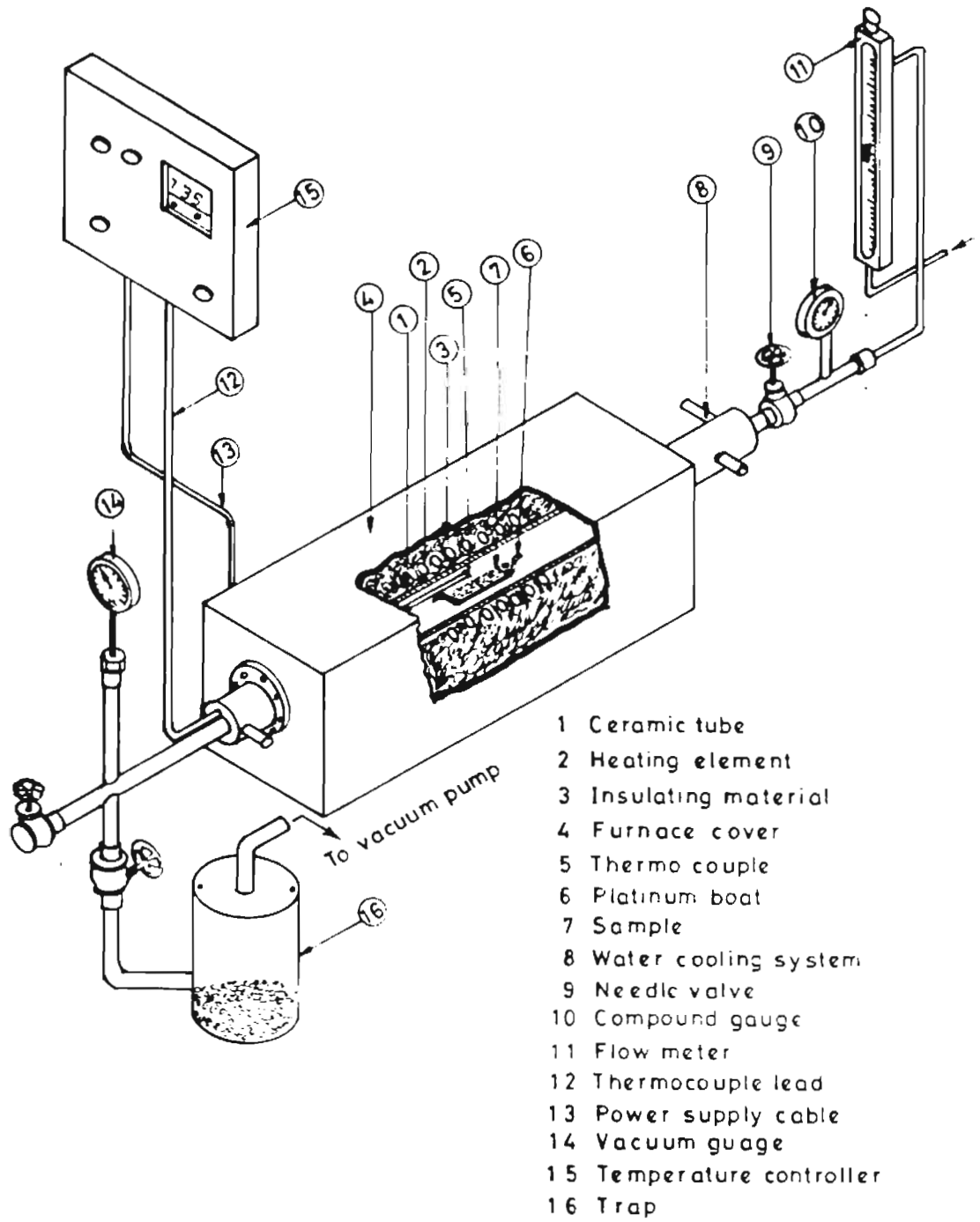


Fig. 7.1: Experimental set up for vacuum calcination

depending on the amount of samples being synthesized. Experimental parameters for the synthesis of upto 100 gm of phase pure YBCO in a single step dynamic vacuum calcination have been standardised.

The phase purity of the samples were studied by XRD, DTA and TGA.

7.3 RESULTS AND DISCUSSION

Fig. 7.2 shows the XRD patterns taken at extended scale of YBCO powders synthesized by vacuum calcination and conventional method.

The values of 2θ corresponding to two major peaks of common impurity phases, in YBCO compound are given in Table 7.1.

Table 7.1: 2θ values corresponding to two major peaks of common impurity phases in YBCO compound

Compound	2θ	
BaCuO ₂	29.282	28.44
Y ₂ BaCuO ₅	29.8	30.5
Ba ₂ Y ₂ O ₅	30.3	28.8
BaY ₂ O ₄	29.6	29.4
Ba ₄ Y ₂ O ₇	30.1	29.1
Ba ₃ Y ₄ O ₉	29.2	30.1
Cu ₂ Y ₂ O ₅	31.3	33.2

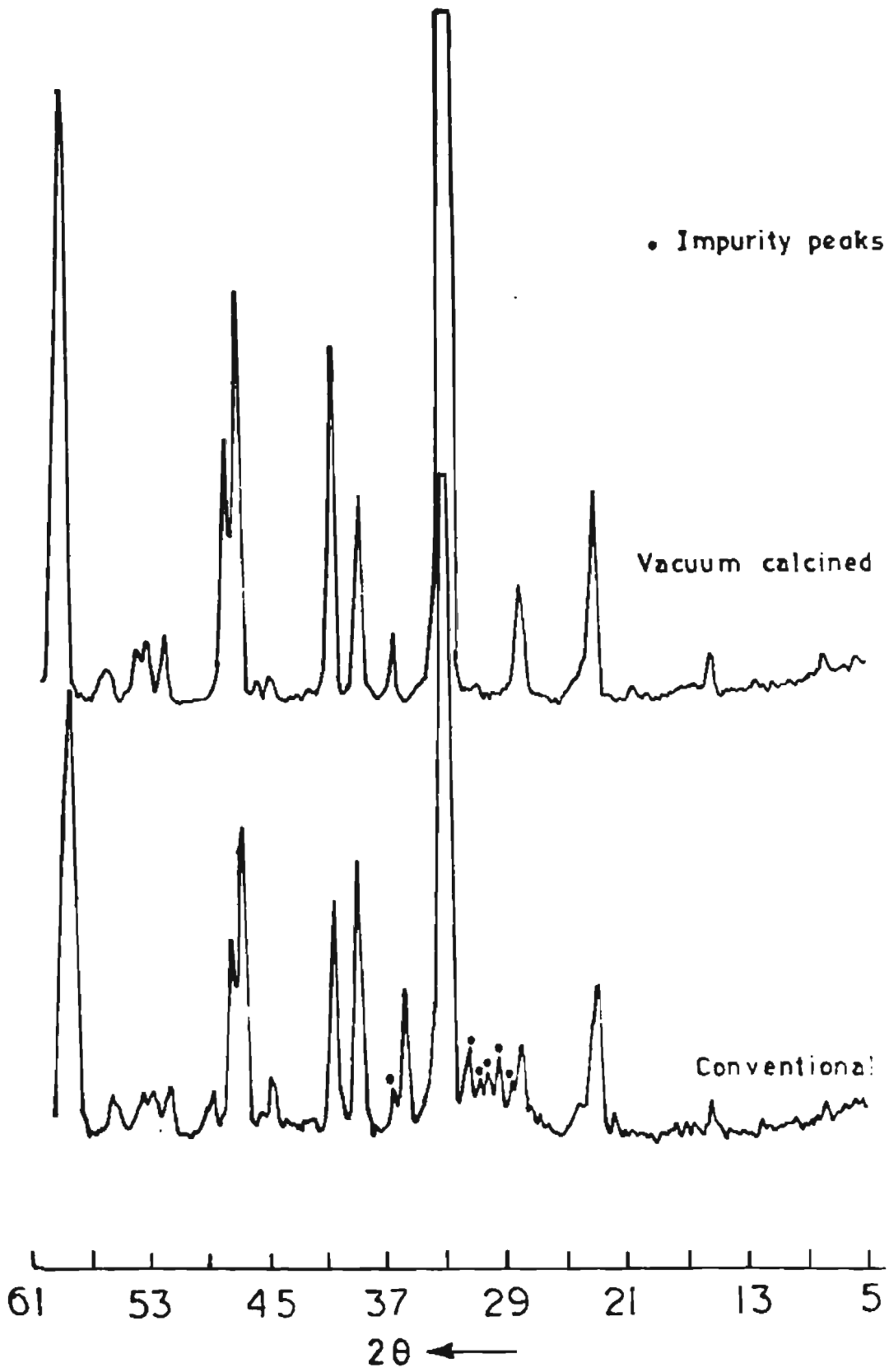


Fig. 7.2: XRD patterns of YBCO powders synthesised by vacuum calcination and conventional method

From the XRD patterns and the table it is clear that the vacuum calcined powder is more pure than the conventional one.

The DT-curves shown in Fig. 7.3 were taken in air at a heating rate of $15^{\circ}\text{C}/\text{min}$. The curve of conventionally processed powder indicates endothermic peaks at higher temperatures which may be due to the melting or reactions involving impurity phases present. On the other hand, the curve corresponding to the vacuum calcined powder is comparatively featureless in the same temperature range.

TGA was carried out on the powders at a heating rate of $10^{\circ}\text{C}/\text{min}$, in air. The TG-curves (Fig. 7.4) of vacuum calcined and conventionally synthesized powder are almost identical at all temperature ranges. But around 800°C onwards, the weight loss is more rapid in conventionally synthesized powder. This may be indicative of CO_2 loss from the BaCO_3 still present in the sample at low levels even though X-ray patterns do not indicate it. All the vacuum calcined powders showed $T_{c(0)}$ more than 90 K. After sintering, they showed J_c $1050\text{ A}/\text{cm}^2$ in self field and it was stable upto 20 oersted whereas the conventional one showed $J_c \sim 120\text{ A}/\text{cm}^2$ only and it drops drastically within 5 oersted field (Fig. 7.5).

The particle size of the vacuum calcined powder was found to be less than $5\ \mu\text{m}$ (Fig. 7.6) while that of conventionally processed samples was more than $5\ \mu\text{m}$.

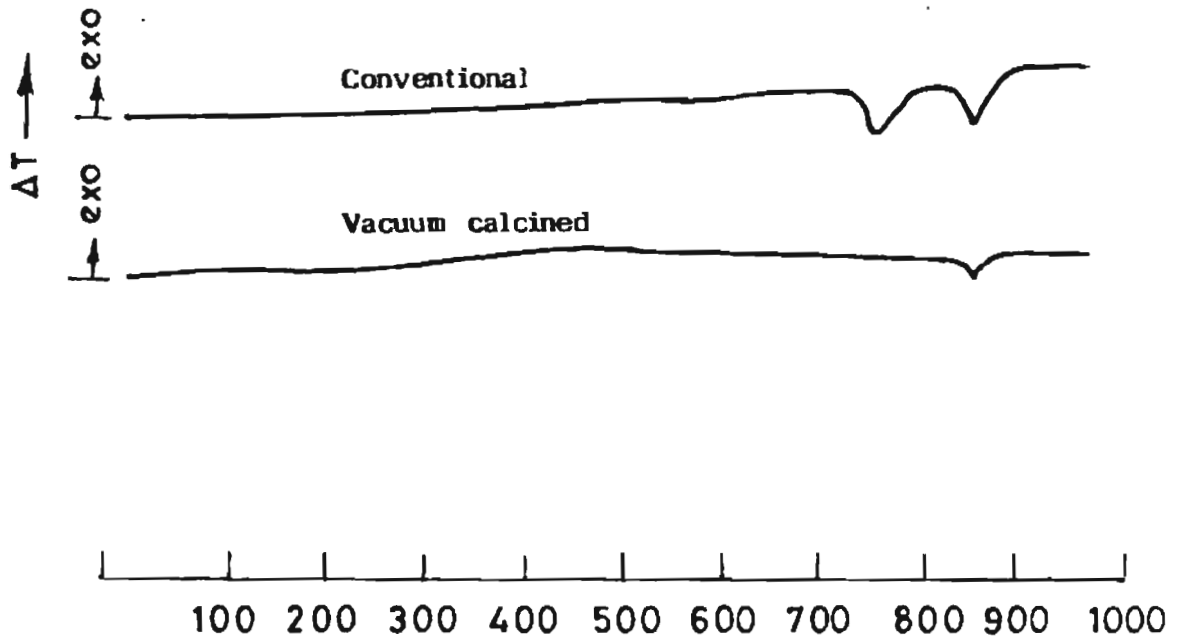


Fig. 7.3:DTG-curves of vacuum calcined and conventionally synthesized powders

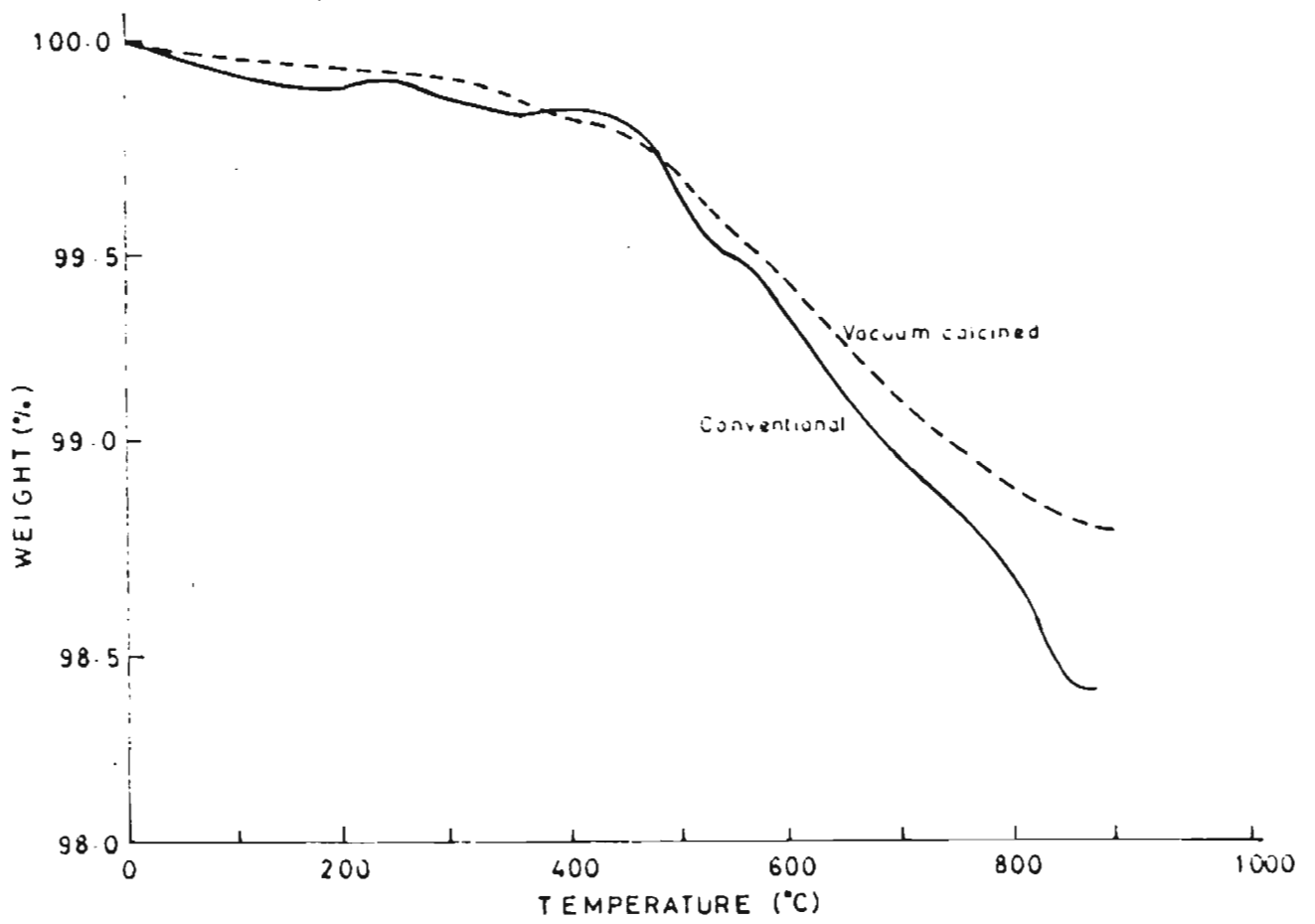


Fig. 7.4: TG-curves of vacuum calcined and conventionally synthesised powders

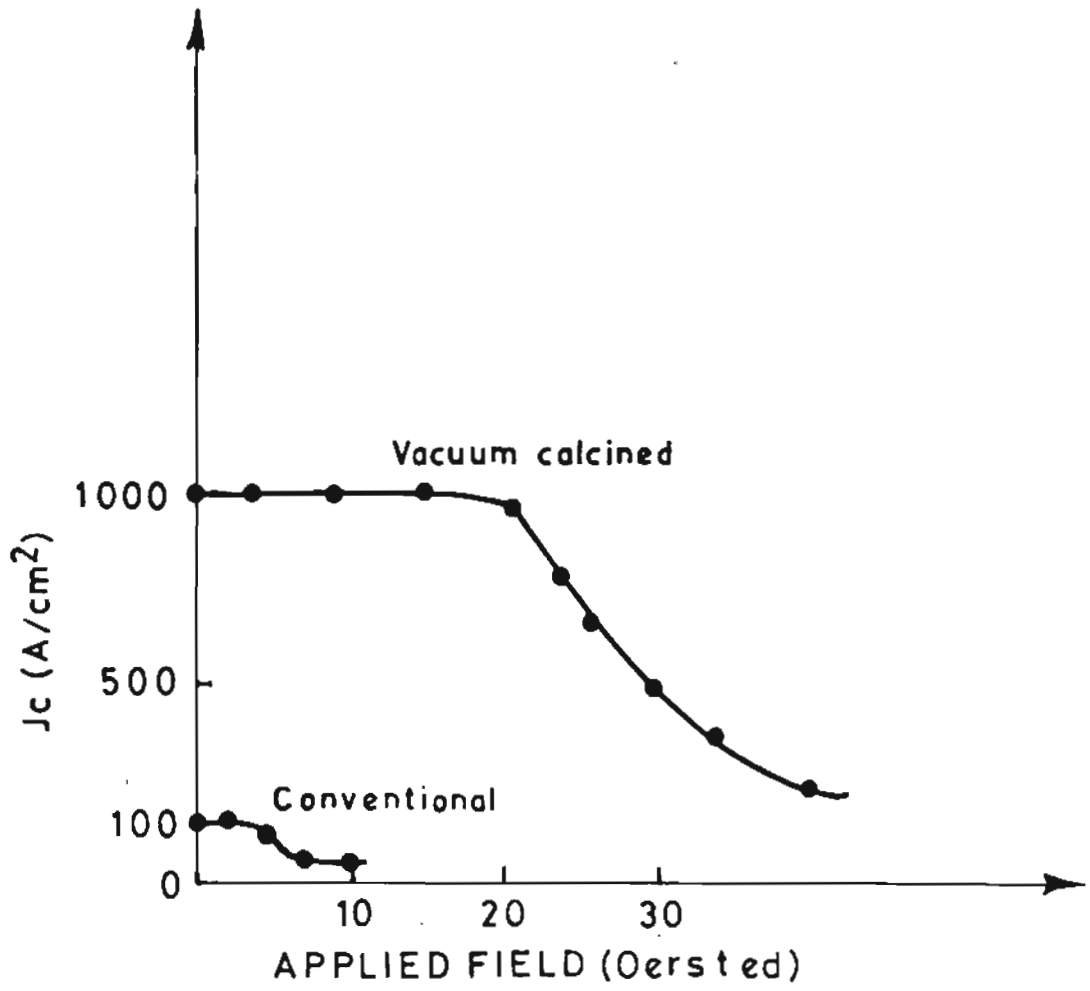


Fig. 7.5: $J_c(B)$ characteristics of samples prepared from vacuum calcined and conventionally synthesized powders

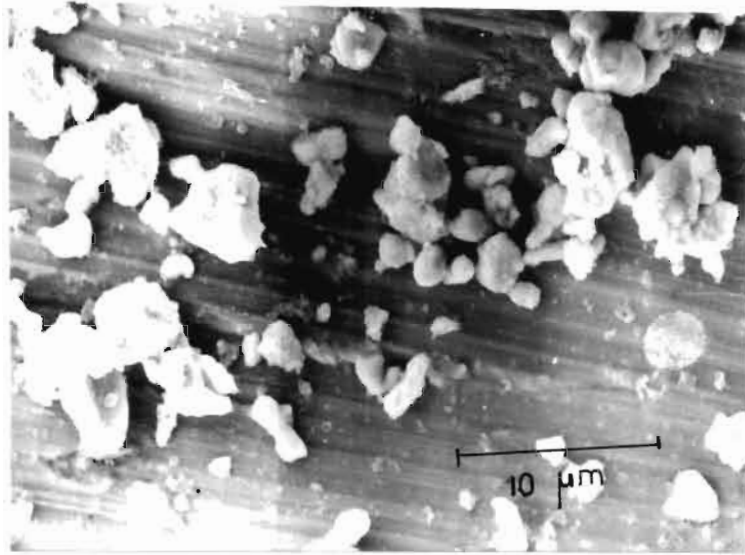


Fig. 7.6: SEM photograph of the vacuum calcined powder

The XRD patterns of vacuum calcined and conventionally processed powders kept in air for two years are shown in Fig. 7.7.

From the XRD patterns it is clear that vacuum calcined powders are more stable to the atmospheric conditions.

7.4 CONCLUSION

Experimental set-up for the synthesis of phase pure YBCO by dynamic vacuum calcination has been fabricated. Processing parameters for synthesis of phase pure YBCO powders upto 100 gms have been standardised. The merits of vacuum calcination are,

- a. Powder with higher purity
- b. Less processing temperature and soaking period
- c. Powder having less grain size
- d. Sintered samples having higher J_c and better stability against magnetic field
- e. Powder is more stable to the atmospheric conditions

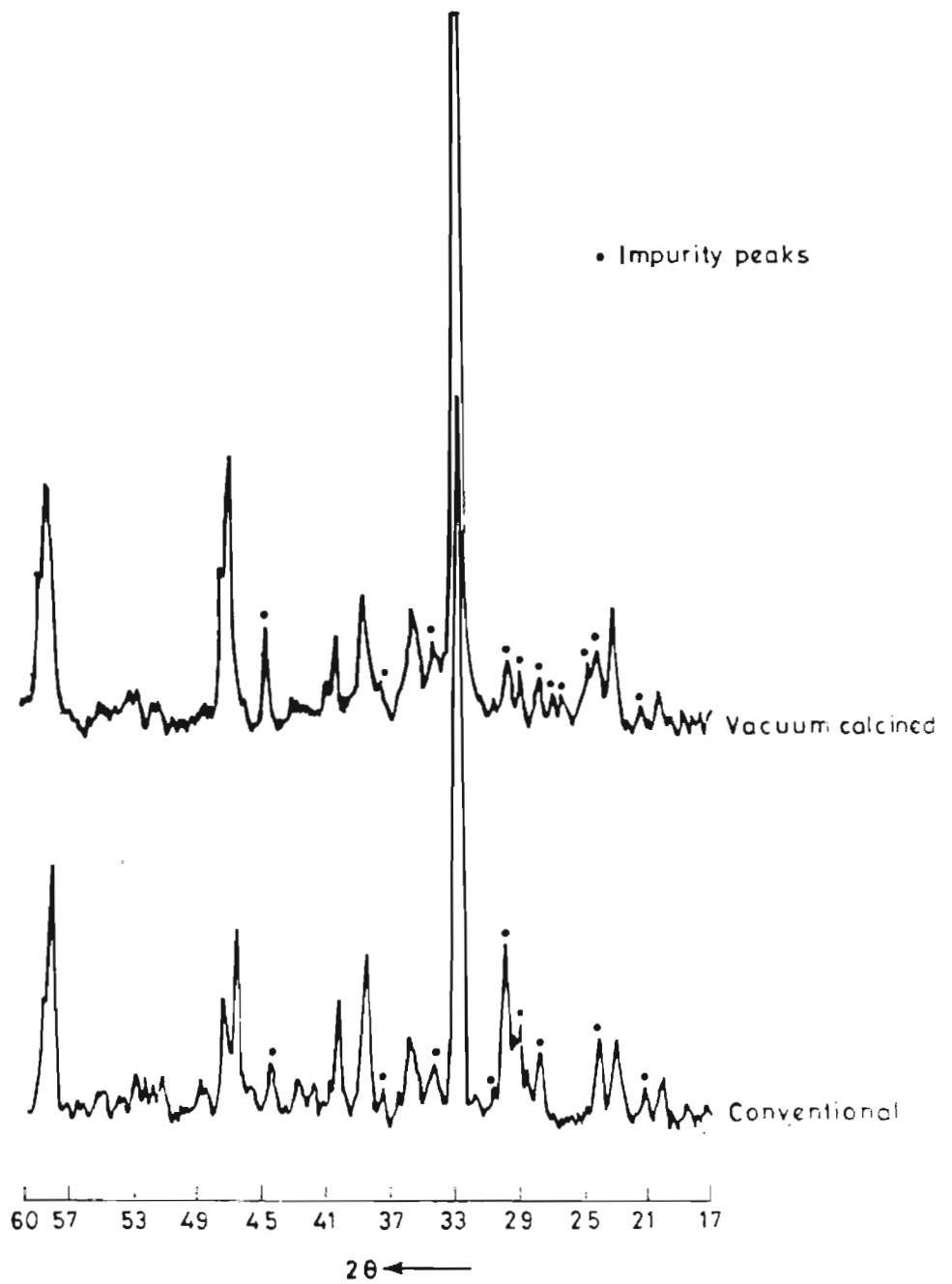


Fig. 7.7: XRD patterns of vacuum calcined and conventionally processed powders kept in air for two years

REFERENCES

1. K.C. Goretta, I. Bloom, Nan Chen, G.T. Goudey, M.C. Hash, G. Klassen, M.T. Lanagan, R.B. Poeppel, J.P. Singh, Donglu Shi, U. Balachandran, J.T. Dusek and D.W. Capone II, Mater. Lett., 7, 161 (1988).
2. R.B. Poeppel, B.K. Flandermeyer, J.T. Dusek and I.D. Bloom, "Chemistry of High Temperature Superconductors", edited by D.L. Nelson, M.S. Whittingham and T.F. George (American Chemical Society, Washington, 1987) p.261.
3. R.J. Cava, J.J. Kraewski, W.F. Peck Jr., B. Batlogg, L.W. Rupp Jr., R.M. Fleming, A.C.W.P. James and P. Marsh, Nature, 338, 328 (1989).
4. D.W.J. Smith, J. Chem. Educ., 64, 480 (1987).
5. H. Fjellvag, P. Karen, A. Kjekshus, P. Kofstad and T. Norby, Acta Chem. Scand., A42, 178 (1988).
6. Y. Gao, K.L. Merkle, C. Zhang, U. Balachandran and R.B. Poeppel, J. Mater. Res., 5(7), 1363 (1990).
7. U. Balachandran, R.B. Poeppel, J.E. Emerson, S.A. Johnson, M.T. Lanagan, C.A. Youngdahl, D. Shi and K.C. Goretta, Mater. Lett., 8, 454 (1989).

P a r t C

CHAPTER 8

**VARIATION OF STRUCTURAL AND SUPERCONDUCTING PROPERTIES
WITH INITIAL STOICHIOMETRY VARIATION IN
(Bi,Pb)-Sr-Ca-Cu-O BULK SUPERCONDUCTOR**

CHAPTER 8

VARIATION OF STRUCTURAL AND SUPERCONDUCTING PROPERTIES
WITH INITIAL STOICHIOMETRY VARIATION IN
(Bi,Pb)-Sr-Ca-Cu-O BULK SUPERCONDUCTOR

8.1 INTRODUCTION

As mentioned in the general introduction part, the two important superconducting phases in Bi-Sr-Ca-Cu-O system are $\text{Bi}_2\text{Sr}_2\text{Ca}_1\text{Cu}_2\text{O}_{8+\delta}$ (2212) with $T_c \sim 85$ K and $\text{Bi}_2\text{Sr}_2\text{Ca}_2\text{Cu}_3\text{O}_{10}$ (2223) with a $T_c \sim 110$ K. It has been found from phase equilibria studies in the quaternary system Bi_2O_3 -SrO-CaO-CuO (1) that 2212 phase is thermodynamically stable over a wide temperature range and in the presence of most of the compounds existing in this system. In contrast, the 2223 phase is stable only over a narrow temperature range and exhibits phase equilibria with fewer compounds existing in the system. Therefore the synthesis of pure 2223 phase is more difficult than the synthesis of 2212 phase. At the same time, it has been established that the partial substitution of Bi by Pb favours the formation of 2223 phase (2). The structural and superconducting properties of Pb doped Bi-based superconductor has been found to depend both on initial stoichiometry and processing conditions [3-6]. Thus the study of the effect of initial stoichiometric variation and processing conditions on the structural and superconducting properties of this system is of much significance.

In the present investigation $(\text{Bi,Pb})_2 \text{Sr}_2 \text{Ca}_2 \text{Cu}_3 \text{O}_{10}$ samples having different initial stoichiometries (variation in Bi, Pb, Sr, Ca and Cu) were synthesized by conventional ceramic route in air and changes in various structural and superconducting parameters such as high T_c (2223 phase) fraction (HTf), low T_c (2212 phase) fraction (LTf), impurity fraction (If), texturing of (001) planes (T_{001}), $T_{c(0)}$, ΔT_c , J_c , $J_c(B)$ etc. of the samples with respect to the different initial stoichiometries and soaking periods have been studied. Also an attempt has been made to differentiate the major impurity phases depending on whether they enhance the J_c or not.

8.2 EXPERIMENTAL

Samples having initial stoichiometries $\text{Bi}_{2-x} \text{Pb}_x \text{Sr}_2 \text{Ca}_2 \text{Cu}_3 \text{O}_y$, $\text{Bi}_{1.6} \text{Pb}_{0.4} \text{Sr}_{2+x} \text{Ca}_2 \text{Cu}_3 \text{O}_y$, $\text{Bi}_{1.6} \text{Pb}_{0.4} \text{Sr}_2 \text{Ca}_{2+x} \text{Cu}_3 \text{O}_y$, $\text{Bi}_{1.6} \text{Pb}_{0.4} \text{Sr}_2 \text{Ca}_2 \text{Cu}_{3+x} \text{O}_y$ (where $x = 0-0.6$) were prepared as follows. Stoichiometric amounts of $\text{Bi}_2 \text{O}_3$, PbO , SrCO_3 , CaCO_3 and CuO (Aldrich, 99.9% pure) were well mixed in an agate mortar and calcined at 800°C in air for 12 hrs. These pellets were ground and bar shaped specimen having dimensions 20 mm x 4 mm x 2 mm were prepared. These rods were sintered in air at 855°C for 80 hrs. X-ray diffraction was performed on Philips PW 1710 powder diffractometer using $\text{CuK}\alpha$ radiation under identical conditions. Critical temperature of the samples was measured by standard four probe DC technique using an APD cryostat. Direct transport method was used to determine the critical current density of the sample. $J_c(B)$ characteristics was measured at the liquid

nitrogen temperature by placing the sample axially at the centre of an electromagnetic coil.

The HTf, LTf, If as well as T_{001} [hereafter these parameters are referred as P.S. (phase and structural) parameters] were determined from the XRD patterns of the samples. Each phase viz. high T_c , low T_c and major impurities [semiconducting ($2\theta = 21.9^\circ$) and Ca_2PbO_4 ($2\theta = 17.8^\circ$) compounds] have their own characteristic x-ray reflections at different angles. Further from the XRD patterns of the samples, it was found that two types of planes viz. (001) and (111) grow preferentially during the processing period. Texturing of (001) planes is desirable because of its increased capacity of critical current density [7].

From the XRD patterns some of the reflections were chosen carefully such that they are not overlapped and have higher intensities for the quantitative estimation of P.S. parameters. The P.S. parameters have been defined as follows, where $\text{HTf} + \text{LTf} + \text{If} = 1$.

$$\text{HTf} = \frac{I_{002}(4.7^\circ) + I_{0010}(23.9^\circ)}{I_{002}(4.7^\circ) + I_{0010}(23.9^\circ) + I_{002}^*(5.8^\circ) + I_{008}^*(23.2^\circ) + I_{\text{imp}}(17.8^\circ) + I_{\text{imp}}(21.9^\circ)}$$

$$\text{LTf} = \frac{I_{002}(5.8^\circ) + I_{008}^*(23.2^\circ)}{I_{002}(4.7^\circ) + I_{0010}(23.9^\circ) + I_{002}^*(5.8^\circ) + I_{008}^*(23.2^\circ) + I_{\text{imp}}(17.8^\circ) + I_{\text{imp}}(21.9^\circ)}$$

$$I_f = \frac{I_{\text{imp}}(17.8^\circ) + I_{\text{imp}}(21.9^\circ)}{I_{002}(4.7^\circ) + I_{0010}(23.9^\circ) + I_{002}^*(5.8^\circ) + I_{008}^*(23.2^\circ) + I_{\text{imp}}(17.8^\circ) + I_{\text{imp}}(21.9^\circ)}$$

$$T_{001} = \frac{I_{002}(4.7^\circ) + I_{0010}(23.9^\circ)}{I_{002}(4.7^\circ) + I_{0010}(23.9^\circ) + I_{115}(26.2^\circ) + I_{200}(33.2^\circ)}$$

(where I and I^* refers to the intensity of the peaks corresponding to 2223 and 2212 phase resp. and I_{imp} the intensity of impurity peak). The above reflections are marked in the typical XRD pattern given in Fig. 8.1.

8.3 RESULTS AND DISCUSSION

8.3.1 Effect of Pb doping

Samples having different (Bi,Pb) stoichiometric ratio have been prepared and its various structural and superconducting properties were studied to select its better combination. The different P.S. parameters, T_c , ΔT_c and J_c of the samples after 120 + 80 hrs of heat treatment are shown in Table 8.1.

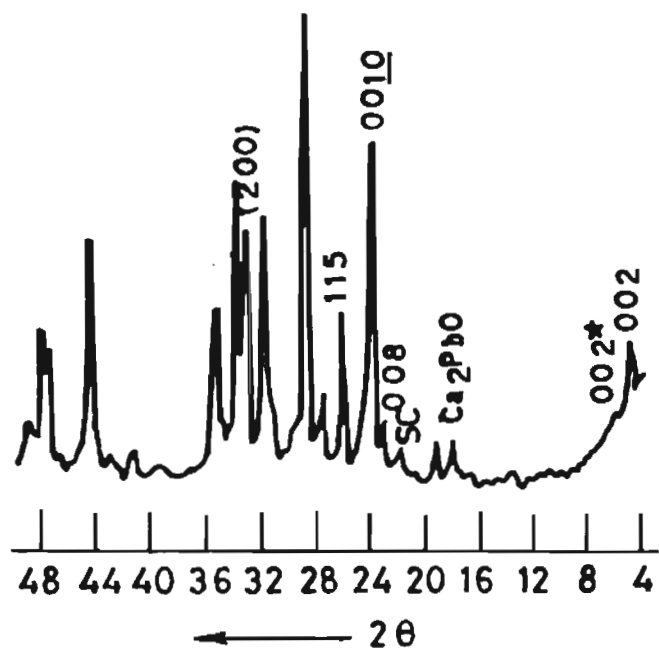


Fig.8.1: Typical XRD pattern of BPSCCO

Table 8.1: Different P.S. parameters, T_c , ΔT_c & J_c of the samples having different (Bi, Pb) stoichiometric ratio, after 120 + 80 hrs of heat treatment

Bi:Pb	HTf	LTf	If	T_{001}	$T_{c(0)}$ (K)	ΔT_c (K)	J_c (A/cm ²)
1.9:1	0.6481	0.2969	0.055	0.3888	105	7	120
1.8:2	0.7655	0.1935	0.041	0.4551	107	5	162
1.7:3	0.90	0.065	0.035	0.5663	109	4	223
1.6:4	0.92	0.06	0.020	0.75	109	4	252
1.5:5	0.741	0.211	0.048	0.542	107	6	148
1.4:6	0.621	0.34	0.65	0.3443	104	8	105

From the table, (Bi, Pb) stoichiometric ratio 1.6:0.4 is found to give better P.S. parameters and superconducting properties. Therefore in all of our next batch of experiments of varying Sr, Ca and Cu stoichiometries the (Bi, Pb) molar ratio was kept as 1.6:0.4.

8.3.2 Effect of Sr, Ca and Cu variations

Figures 8.2 and 8.3 show the variation of HTf, If, T_{001} , T_c , ΔT_c and J_c of the 120 + 80 hrs heat treated samples with x. From the figures it can be seen that, samples having following

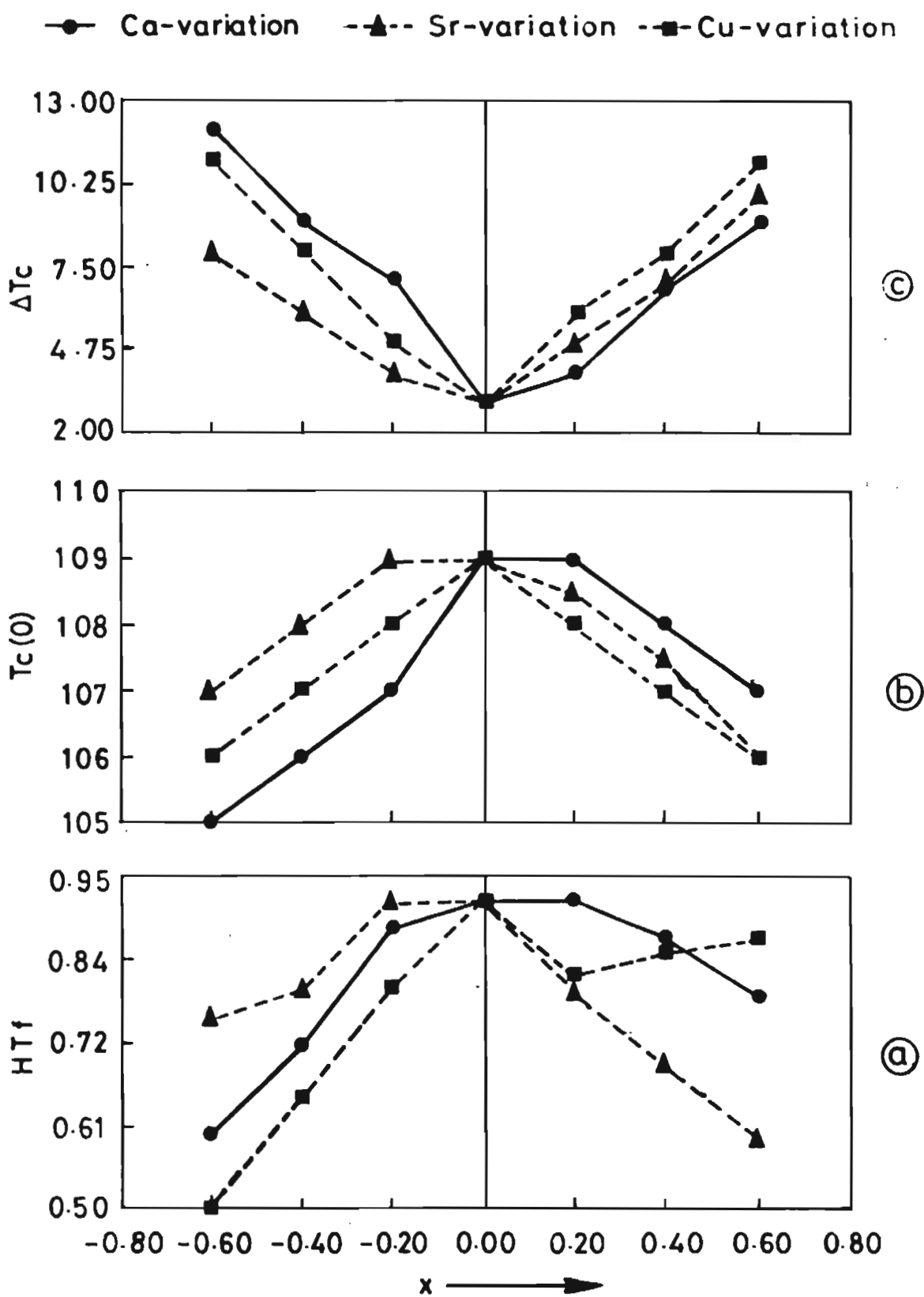


Fig. 8.2: Plots of HTf , $T_{c(0)}$, ΔT_c vs x

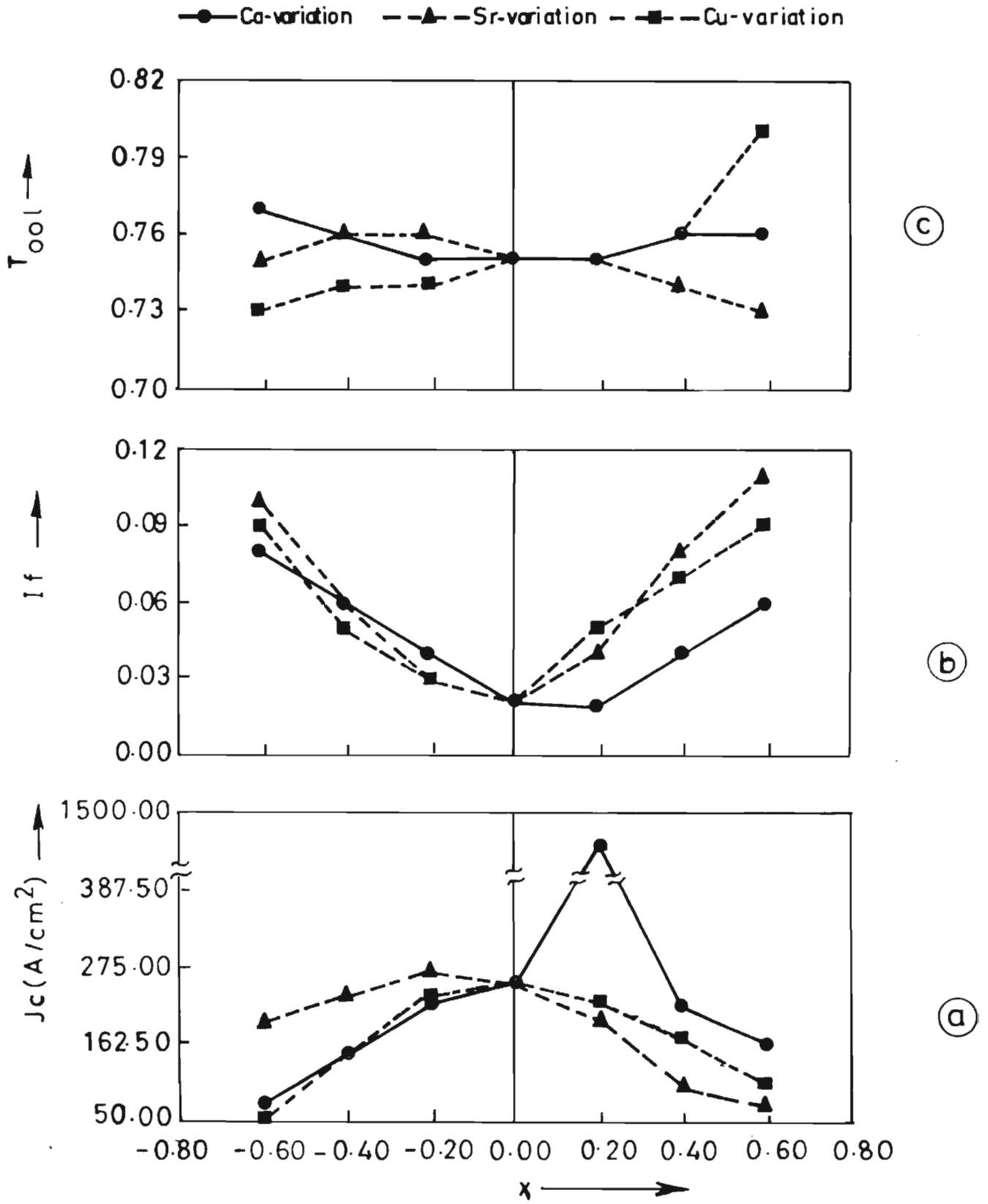


Fig. 8.3: Plots of J_c, I_f, T_{00l} vs x .

initial stoichiometries are showing better properties, i.e. highest T_c , lower ΔT_c and higher J_c .

1. $\text{Bi}_{1.6}\text{Pb}_{0.4}\text{Sr}_{1.8}\text{Ca}_2\text{Cu}_3\text{O}_y$ (sample 1)
2. $\text{Bi}_{1.6}\text{Pb}_{0.4}\text{Sr}_2\text{Ca}_{2.2}\text{Cu}_3\text{O}_y$ (sample 2)
3. $\text{Bi}_{1.6}\text{Pb}_{0.4}\text{Sr}_2\text{Ca}_2\text{Cu}_3\text{O}_y$ (sample 3)

In order to study the combined effect of stoichiometries of samples 1, 2 and 3, sample of stoichiometry $\text{Bi}_{1.6}\text{Pb}_{0.4}\text{Sr}_{1.8}\text{Ca}_{2.2}\text{Cu}_3\text{O}_y$ was prepared and its P.S. parameters, T_c , ΔT_c and J_c were determined. Table 8.2 shows the P.S. parameters, T_c , ΔT_c and J_c of this sample.

Table 8.2: P.S. parameters, T_c , ΔT_c & J_c of the sample having initial stoichiometry $\text{Bi}_{1.6}\text{Pb}_{0.4}\text{Sr}_{1.8}\text{Ca}_{2.2}\text{Cu}_3\text{O}_y$

Stoichiometry	HTf	LTf	If	T_{001}	$T_{c(0)}$ (K)	ΔT_c (K)	J_c (A/cm ²)
$\text{Bi}_{1.6}\text{Pb}_{0.4}\text{Sr}_{1.8}\text{Ca}_{2.2}\text{Cu}_3\text{O}_y$	0.854	0.112	0.034	0.74	108	6	215

None of the values given in Table 8.2 is better than that of samples 1, 2 or 3.

8.3.3 Effect of impurity phases on J_c

Among the samples 1, 2 and 3, in the case of sample 2, there is a sharp increase in J_c (Fig. 8.3a). But there is no significant increase in the texturing of (001) planes (Fig. 8.3c) or HTf (Fig. 8.2a) in sample 2 compared to samples 1 and 3.

The impurity phases which has been used in our definition of I_f are the Ca_2PbO_4 and the semiconducting phase [8]. The dependence of J_c on this factor can be seen by comparing the J_c values (Fig. 8.3a) with the I_f (Fig. 8.3b). The general trend is a decreasing J_c and an increasing I_f , as we go away from the 2223 stoichiometric initial composition. But the abrupt increase and fall of J_c as we go along the excess Ca regime is worthy of mention. A closer look at the XRD patterns taken (Fig. 8.4) at a higher scale factor for excess Ca stoichiometries revealed the presence of Ca_2CuO_3 ($2\theta = 36.7^\circ$) as an additional phase for all these compositions. Also the amount of this phase is found to increase as Ca content increases. The SEM photograph (Fig. 8.5) of this sample taken at a magnification of 6000 shows distribution of fine precipitates (which otherwise is absent in other compositions) in the superconducting matrix. These precipitates may be Ca_2CuO_3 . There is report that Ca_2CuO_3 can act as flux pinning centres [9]. Also, $J_c(B)$ characteristics of the samples 1, 2 and 3 (Fig. 8.6) shows that sample 2 has an improved magnetic performance as well. Therefore the increase in J_c in $\text{Ca}_{2.2}$ stoichiometric samples may be due to the flux pinning action of finely distributed Ca_2CuO_3 present.

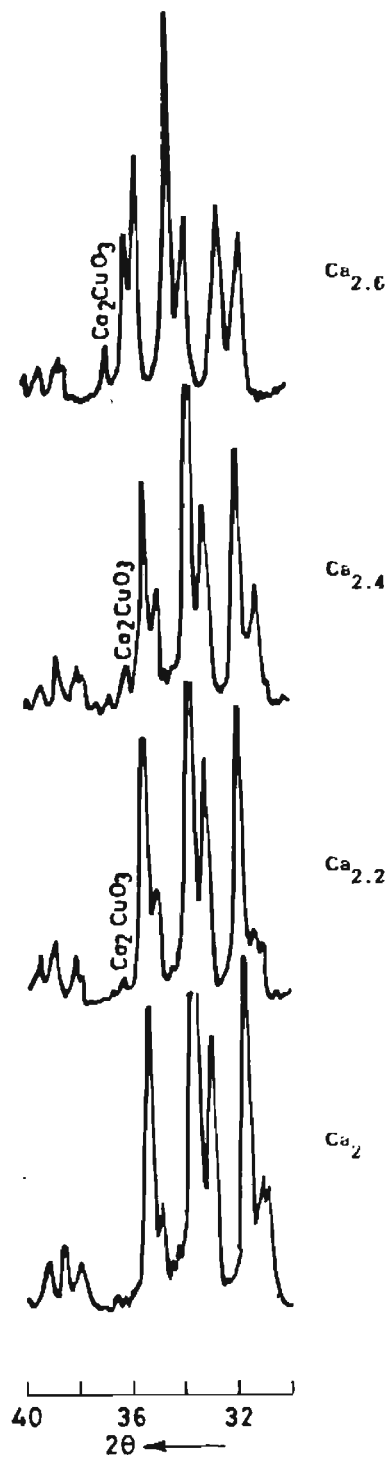


Fig. 8.4: XRD patterns of different Ca stoichiometric samples

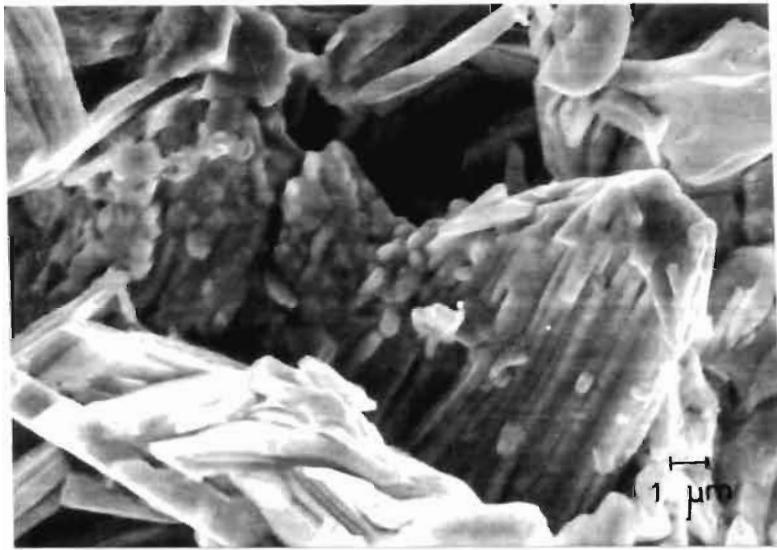


Fig. 8.5: SEM fractograph of the sample having Ca-stoichiometry 2.2

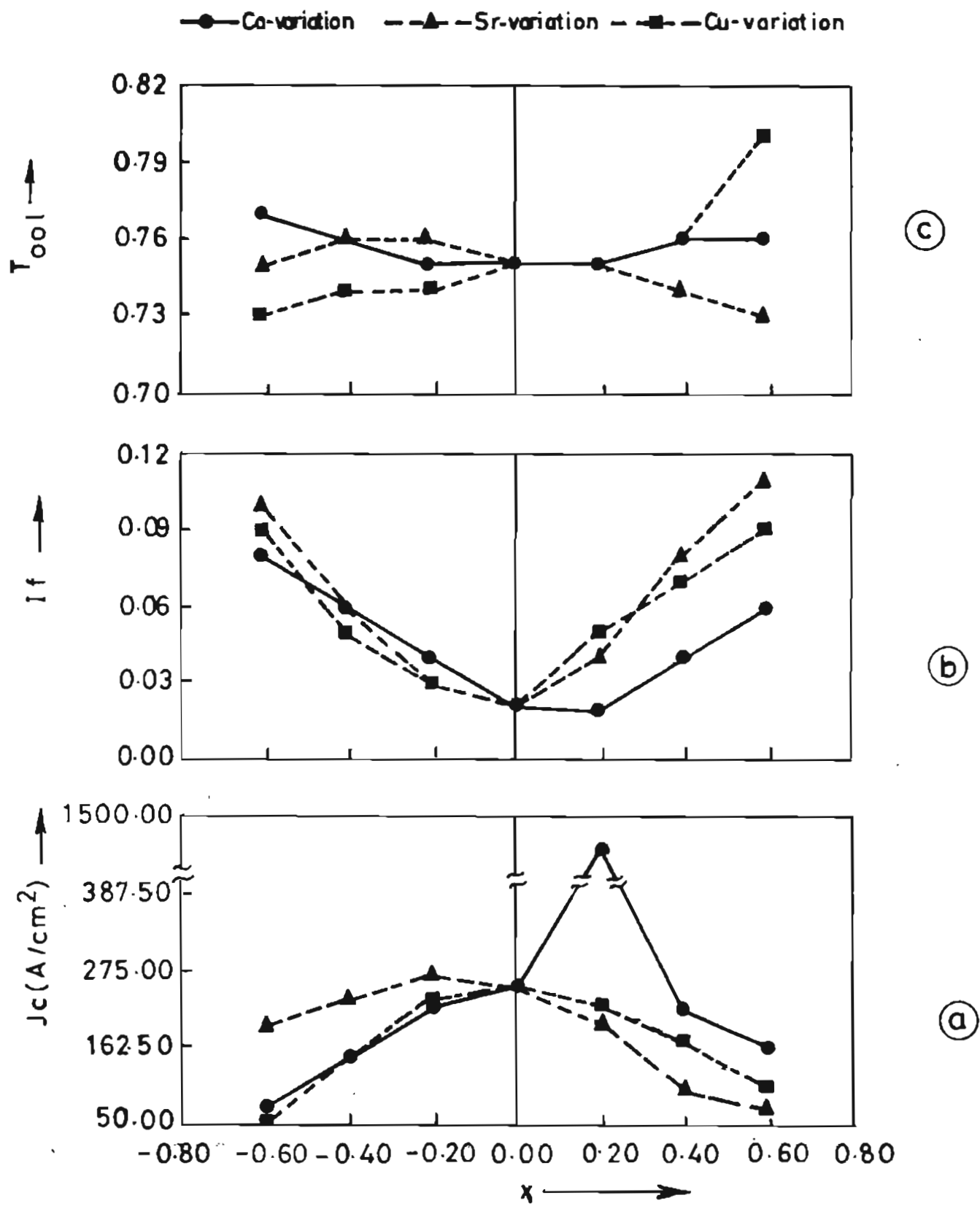


Fig. 8.3: Plots of J_c , I_f , T_{001} vs x .

initial stoichiometries are showing better properties, i.e. highest T_c , lower ΔT_c and higher J_c .

1. $\text{Bi}_{1.6}\text{Pb}_{0.4}\text{Sr}_{1.8}\text{Ca}_2\text{Cu}_3\text{O}_y$ (sample 1)
2. $\text{Bi}_{1.6}\text{Pb}_{0.4}\text{Sr}_2\text{Ca}_{2.2}\text{Cu}_3\text{O}_y$ (sample 2)
3. $\text{Bi}_{1.6}\text{Pb}_{0.4}\text{Sr}_2\text{Ca}_2\text{Cu}_3\text{O}_y$ (sample 3)

In order to study the combined effect of stoichiometries of samples 1, 2 and 3, sample of stoichiometry $\text{Bi}_{1.6}\text{Pb}_{0.4}\text{Sr}_{1.8}\text{Ca}_{2.2}\text{Cu}_3\text{O}_y$ was prepared and its P.S. parameters, T_c , ΔT_c and J_c were determined. Table 8.2 shows the P.S. parameters, T_c , ΔT_c and J_c of this sample.

Table 8.2: P.S. parameters, T_c , ΔT_c & J_c of the sample having initial stoichiometry $\text{Bi}_{1.6}\text{Pb}_{0.4}\text{Sr}_{1.8}\text{Ca}_{2.2}\text{Cu}_3\text{O}_y$

Stoichiometry	HTf	LTf	If	T_{001}	$T_{c(0)}$ (K)	ΔT_c (K)	J_c (A/cm ²)
$\text{Bi}_{1.6}\text{Pb}_{0.4}\text{Sr}_{1.8}\text{Ca}_{2.2}\text{Cu}_3\text{O}_y$	0.854	0.112	0.034	0.74	108	6	215

None of the values given in Table 8.2 is better than that of samples 1, 2 or 3.

8.3.3 Effect of impurity phases on J_c

Among the samples 1, 2 and 3, in the case of sample 2, there is a sharp increase in J_c (Fig. 8.3a) . But there is no significant increase in the texturing of (001) planes (Fig. 8.3c) or HTf (Fig.8.2a) in sample 2 compared to samples 1 and 3.

The impurity phases which has been used in our definition of I_f are the Ca_2PbO_4 and the semiconducting phase [8]. The dependence of J_c on this factor can be seen by comparing the J_c values (Fig. 8.3a) with the I_f (Fig. 8.3b). The general trend is a decreasing J_c and an increasing I_f , as we go away from the 2223 stoichiometric initial composition. But the abrupt increase and fall of J_c as we go along the excess Ca regime is worthy of mention. A closer look at the XRD patterns taken (Fig.8.4) at a higher scale factor for excess Ca stoichiometries revealed the presence of Ca_2CuO_3 ($2\theta = 36.7^\circ$) as an additional phase for all these compositions. Also the amount of this phase is found to increase as Ca content increases. The SEM photograph (Fig. 8.5) of this sample taken at a magnification of 6000 shows distribution of fine precipitates (which otherwise is absent in other compositions) in the superconducting matrix. These precipitates may be Ca_2CuO_3 . There is report that Ca_2CuO_3 can act as flux pinning centres [9]. Also, $J_c(B)$ characteristics of the samples 1, 2 and 3 (Fig. 8.6) shows that sample 2 has an improved magnetic performance as well. Therefore the increase in J_c in $\text{Ca}_{2.2}$ stoichiometric samples may be due to the flux pinning action of finely distributed Ca_2CuO_3 present.

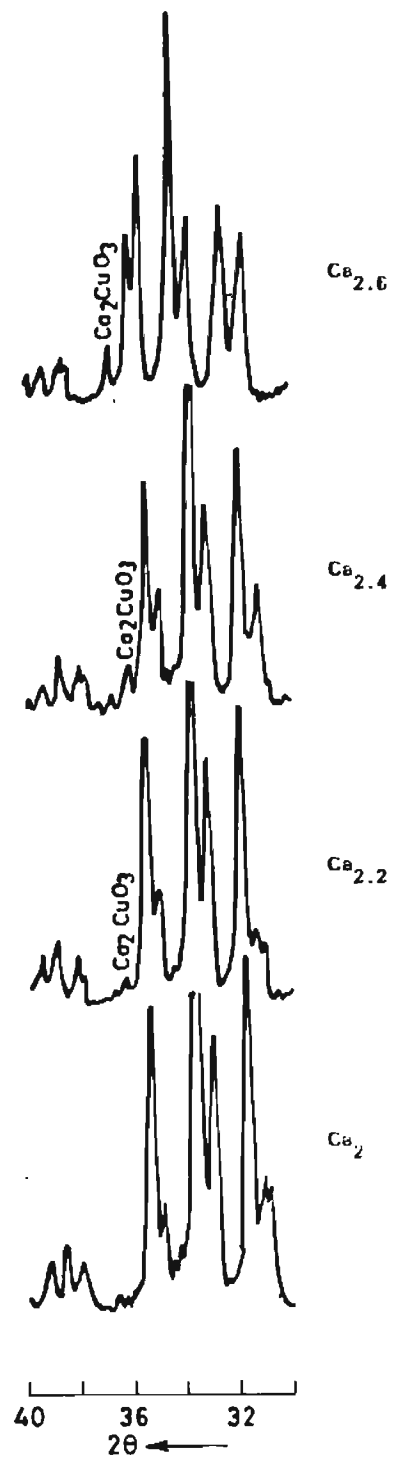


Fig. 8.4: XRD patterns of different Ca stoichiometric samples



Fig. 8.5: SEM fractograph of the sample having Ca-stoichiometry 2.2

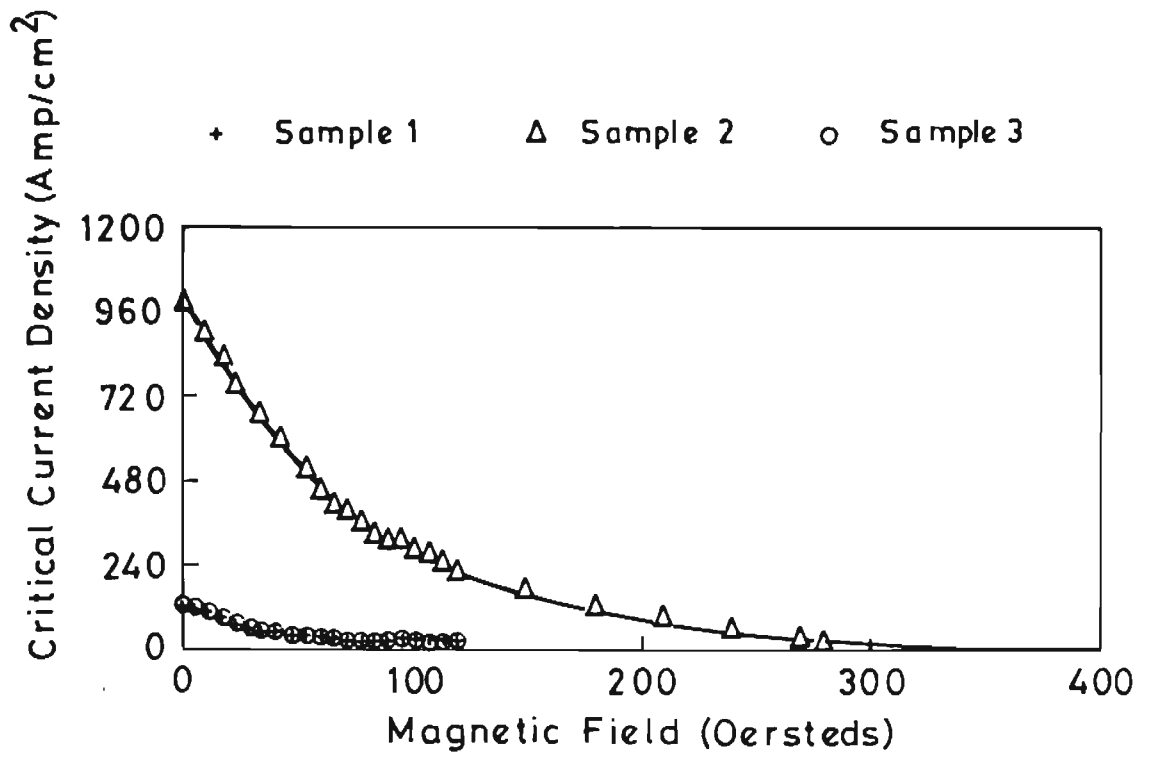


Fig. 8.6: $J_c(B)$ characteristics of samples 1, 2 and 3

But the increase in the amount of Ca_2CuO_3 in samples with Ca stoichiometries more than 2.2 does not seem to increase J_c . This may be due to the following reasons:

- a. The amount of Ca_2CuO_3 present in these samples may be higher than that is required for the flux pinning action and hence it acting as an impurity phase just like other impurity phases.
- b. From the Fig. 8.3b we see that the impurity level is significantly higher in samples with Ca stoichiometry higher than 2.2.

8.3.4 Best initial stoichiometry

From the studies, it is found that $\text{Bi}_{1.6}\text{Pb}_{0.4}\text{Sr}_2\text{Ca}_{2.2}\text{Cu}_3\text{O}_y$ is the best initial stoichiometry which gives higher T_c , J_c and better $J_c(B)$ characteristics.

8.3.5 Effect of soaking period on HTf

Fig. 8.7 shows the variation of HTf with x after 120 hrs and 120 + 80 hrs of heat treatment. In all cases HTf increases with the increase in period of heat treatment. But in the case of Cu rich stoichiometry, ($\text{Cu}_{3.4}$ and above) 80 to 90% HTf is attained within 120 hrs of heat treatment itself. However after 120 hrs, there is no further significant increase in HTf in these samples.

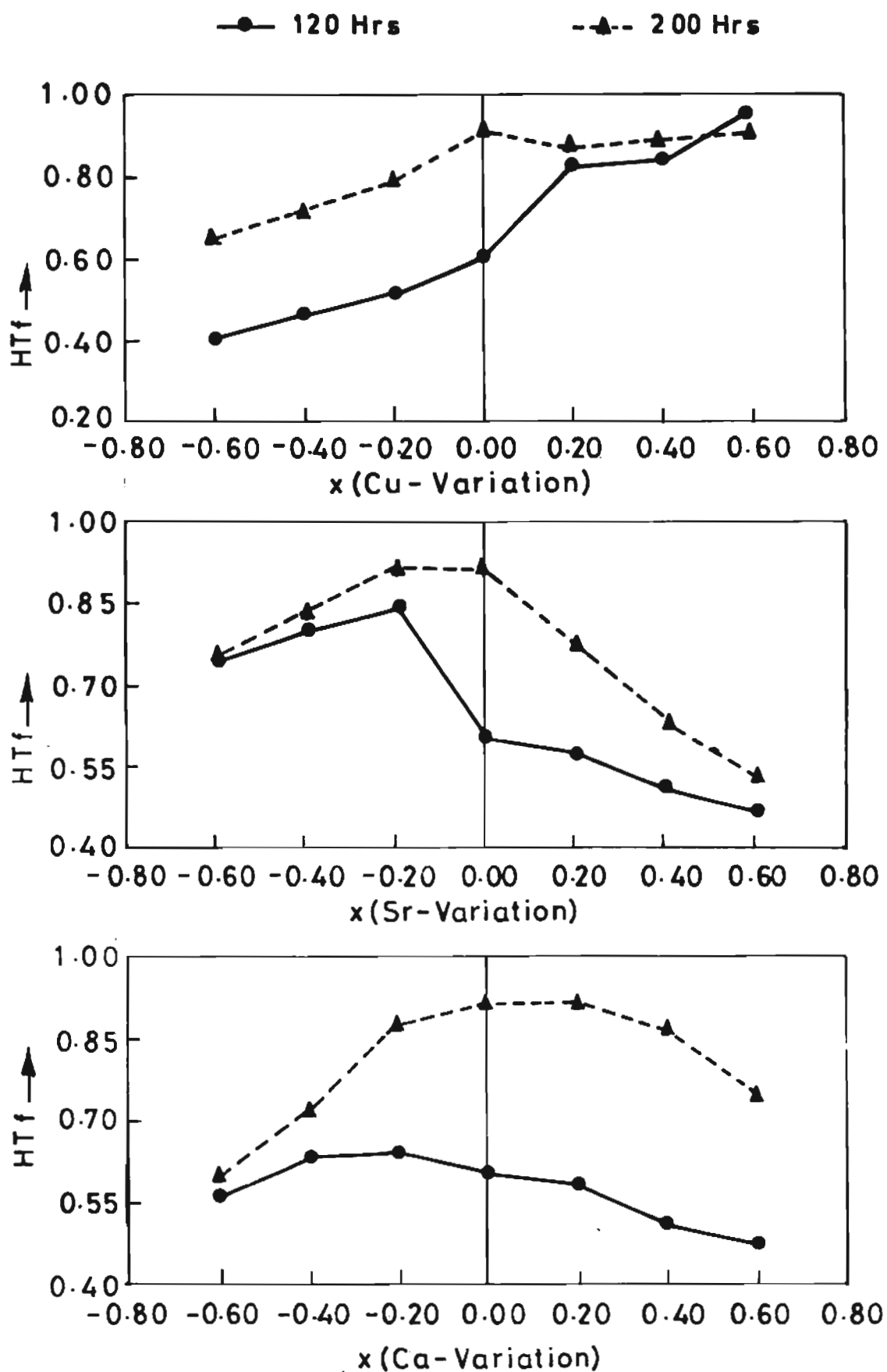


Fig. 8.7: Plots of HTf vs x of different stoichiometric samples after 120 hrs and 120 + 80 hrs of heat treatment

8.3.6 Effect of soaking period on T_{001}

Fig. 8.8 shows the variation in texturing of 001 planes with x after 120 hrs and 120 + 80 hrs heat treatment. Texturing of 001 planes also increases with the increase in period of heat treatment for all stoichiometries. Another factor improving the texturing is Cu rich stoichiometry (Fig. 8.3c). But increase in T_{001} by Cu rich stoichiometry does not improve the J_C value of the sample (Fig. 8.3a). This may be because of the higher amount of impurity phases present in the sample (Fig. 8.3b).

Table 8.3 gives the HTf and T_{001} corresponding to 120 hrs and 120 + 80 hrs heat treated Cu rich stoichiometric samples.

Table 8.3: HTf and T_{001} corresponding to 120 hrs and 120 + 80 hrs heat treated Cu-rich stoichiometric samples

Cu-stoichiometry	HTf ₍₁₂₀₎	$T_{001(120)}$	HTf ₍₁₂₀₊₈₀₎	$T_{001(120+80)}$
3.0	0.6481	0.3888	0.92	0.75
3.2	0.75	0.33	0.82	0.75
3.4	0.8	0.42	0.84	0.75
3.6	0.89	0.53	0.87	0.79

From the Table 8.3 it is clear that in the case of Cu rich

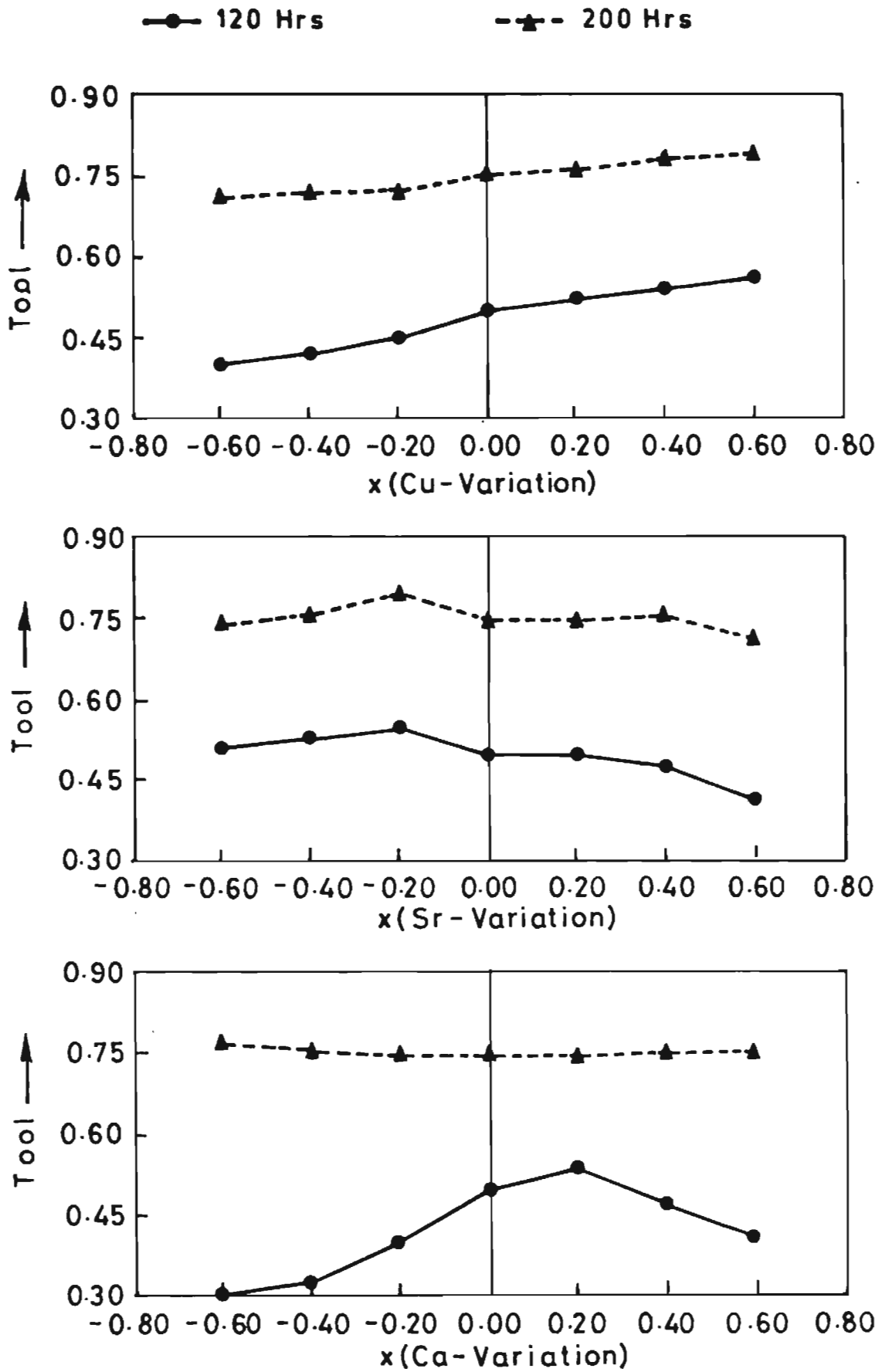


Fig. 8.8: Plots of T_{001} vs x of different stoichiometric samples after 120 hrs and 120 + 80 hrs of heat treatment

stoichiometric samples even though HTf(120) is comparable with HTf (120 + 80), T_{001} (120) is much less compared to T_{001} (120 + 80). The formation of 2223 phase can thus be accelerated by a Cu rich liquid phase reaction but for higher texturing, sufficient soaking period is needed.

8.4 CONCLUSIONS

Effect of initial stoichiometry variation (variation in Bi, Pb, Sr, Ca and Cu) on various structural and superconducting properties of the Pb doped Bi-based superconductor has been studied. From the studies the following conclusions can be drawn:

- a. The sample having initial stoichiometry $\text{Bi}_{1.6}\text{Pb}_{0.4}\text{Sr}_2\text{Ca}_{2.2}\text{Cu}_3\text{O}_y$ gives the best structural and superconducting properties. It has been found that the most important factors affecting J_c in this sample are the type of impurity phases present, its amount and its distribution in the superconducting matrix.
- b. Cu-rich stoichiometry enhances the formation of 110 K phase by Cu rich liquid phase reaction but the large amount of impurities present in the sample decreases J_c .
- c. The formation of 110 K phase and texturing of 001 planes in a (Bi, Pb)-Sr-Ca-Cu-O sample depend on the period of heat treatment and stoichiometry.

REFERENCES

1. P. Majewski, B. Hettich, H. Jaeger and K. Schulze, *Adv. Mater.* 3(1), 67 (1991).
2. P. Bordet, C. Chaillout, J. Chenavas, J.L. Holdean, M. Marezio, J. Karpinsk and E. Kaldis, *Nature*, 334, 596 (1988).
3. S.X. Dou, H.K. Liu, M.H. Apperley, K.H. Song and C.C. Sporrel, *Supercond. Sci. technol.*, 3, 138 (1990).
4. Y. Hayashi, H. Kogure and Y. Gondo, *Jap. J. Appl. Phys.*, 28(12), L2182 (1989).
5. K. Konstantinov, S. Karbanov, A. Souleva and D. Kovacheva, *Supercond. Sci. Technol.*, 3, 309 (1990).
6. M. Pissas, D. Niarchos, C. Christides and M. Anagnostou, *Supercond.Sci. Technol.*, 3, 128 (1990).
7. C.M. Gilmore, *Mat. Sci. Eng.*, B1, 283 (1988).
8. S. Koyama, U. Endo and T. Kawai, *Jap. J. Appl. Phys.*, 27(10), L1861 (1988).
9. S.X. Dou, S.J. Guo, H.K. Liu and K.E. Easterling, *Supercond. Sci. Technol.*, 2, 308 (1989).

CHAPTER 9

**STUDIES ON TEXTURED GRAIN GROWTH IN BPSCCO AND PREPARATION
AND CHARACTERISATION OF TEXTURED SINTERED
BULK BPSCCO BY SUSPENSION METHOD**

CHAPTER 9

STUDIES ON TEXTURED GRAIN GROWTH IN BPSCCO AND PREPARATION AND CHARACTERISATION OF TEXTURED SINTERED BULK BPSCCO BY SUSPENSION METHOD*

9.1 STUDIES ON TEXTURED GRAIN GROWTH IN BPSCCO

9.1.1 Introduction

We have already seen that the synthesis of 2223 phase in Bi-Sr-Ca-Cu-O system is more difficult than the 2212 phase [1]. Also it is well known that substitution of Pb for Bi in small amounts enhances the formation of 2223 phase and it grows from the initially formed 2212 phase and several impurity compounds such as Ca_2PbO_4 and CuO [2,3]. This process requires a long annealing time (100-300 hrs) because of slow kinetics of formation of 2223 phase [4,5].

In the course of present investigation mixed precursors of oxides or carbonates of Bi, Pb, Sr, Ca, Cu corresponding to the 2223 stoichiometry were prepared and the preferential growth of various crystallographic planes in this material during the different annealing periods has been studied.

9.1.2 Experimental

Precursor powders corresponding to 2223 stoichiometry were prepared by mixing appropriate amounts of Bi_2O_3 , PbO, SrCO_3 , CaCO_3 and CuO in an agate mortar in acetone medium. These powders were

*This work has been partly published in:
Solid State Commun., 76, 477 (1990).

heated at 800°C for 12 hrs and then furnace cooled. These samples were then ground and pressed into pellets of 13 mm diameter and 5 mm thickness. These pellets were then heated at $850 \pm 5^{\circ}\text{C}$ for 24 hrs (sample S1), 48 hrs (sample S2), 72 hrs (sample S3) and 120 hrs (sample S4) in a closed muffle furnace. X-ray diffraction patterns of these samples were taken under identical conditions using $\text{CuK}\alpha$ - radiation.

9.1.3 Results and discussions

Fig. 9.1 shows the XRD patterns of the different samples.

From the XRD patterns, reflections from (001) and (111) are found to be more prominent, which indicates preferential growth of (001) and (111) planes.

Table 9.1 shows the ratio of the intensities of (0012) and (119) reflections ($2\theta = 28.8^{\circ}$ and 32° respectively) from the XRD patterns and high T_c fraction (HTf) determined using the definition given in chapter 8.

Table 9.1: Ratio of the intensities of (0012) and (119) and HTf of different samples

Samples	Annealing time (hrs)	I_{0012}/I_{119}	HTf
S1	24	0.67	0.52
S2	48	0.86	0.66
S3	72	0.99	0.74
S4	120	1.43	0.81

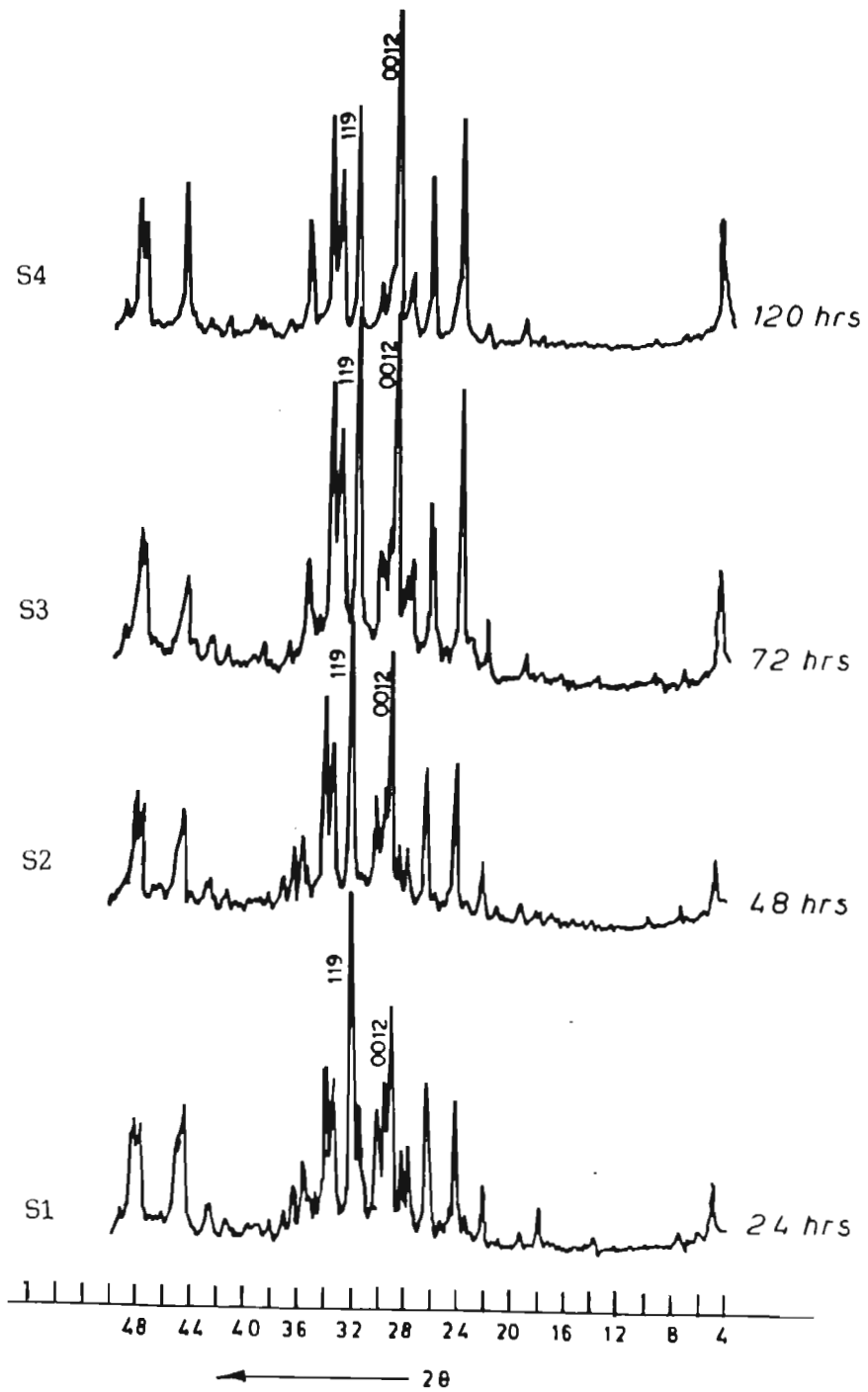


Fig. 9.1: Typical XRD patterns of samples having different annealing period

A comparison of the intensity ratio, given in the table, at different annealing periods shows that this increases with annealing time. This indicates that (001) planes grow faster compared to (111) planes with processing time. High T_c fraction also increases correspondingly.

SEM fractographs of the samples S1, S2, S3 and S4 are shown in Fig. 9.2 (a, b, c, d).

From the SEM photographs, the platy growth of grains in 2223-rich samples is clear. This increases with the increase in HTf. This indicates that in a 2223-rich sample, the grains are of platelet in nature having growth along ab-plane.

9.2 PREPARATION AND CHARACTERISATION OF TEXTURED SINTERED BPSCCO BULK BY SUSPENSION METHOD

9.2.1 Introduction

From the above studies it is clear that 2223 grains are platy in nature having growth along ab-plane. From single crystal studies, it has been established that ab-plane can carry orders of magnitude higher J_c than along c-axis [6]. Therefore if the platelet grains of 2223 grains can be aligned or textured so that their ab-planes lie in the same direction, their J_c can be improved a lot.

In the present work, platelet grains of 2223 have been synthesized and their alignment by the suspension through a dense liquid has been studied. J_c of the samples was correlated with microstructure.

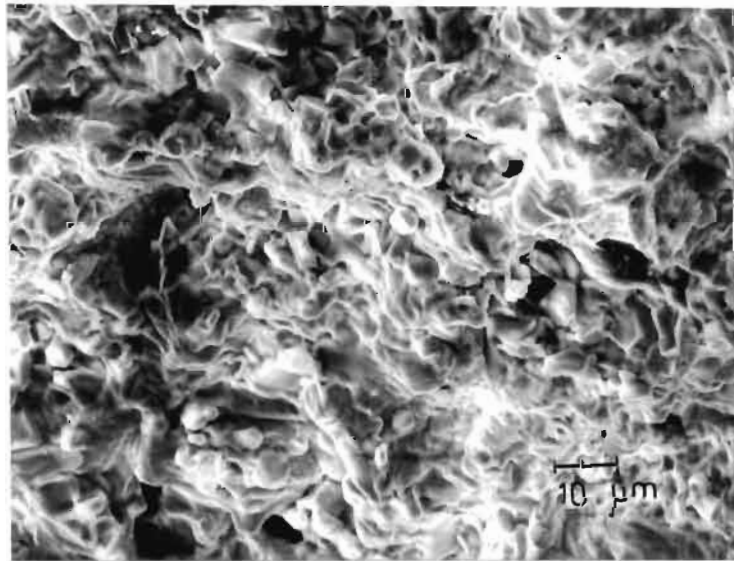


Fig. 9.2: (a) SEM fractograph of the sample S1

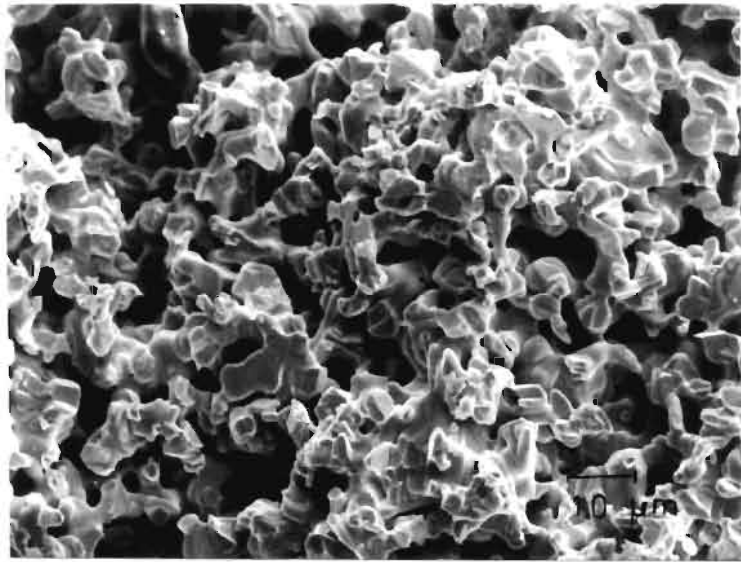


Fig. 9.2: (b) SEM fractograph of the sample S2

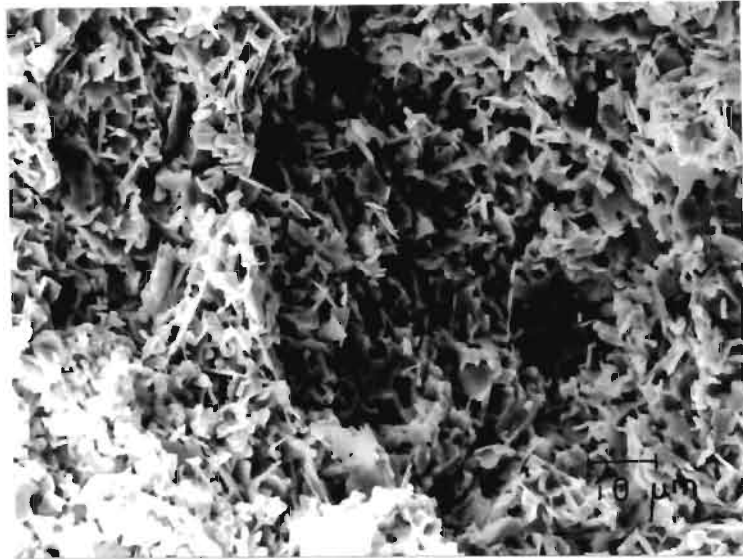


Fig. 9.2: (c) SEM fractograph of the sample S3

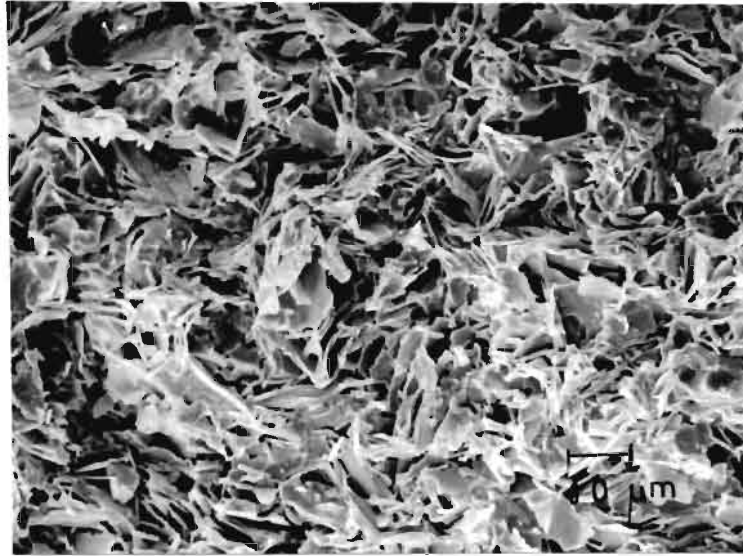


Fig. 9.2: (d) SEM fractograph of the sample S4

9.2.2 Experimental

Powders containing about 90% of 2223 phase were synthesized by the method described above where the annealing time was about 200 hrs. These powders were sieved so that particles of size less than 20 μm could be isolated for the purpose of the present experiment.

Bromoform has been used as the suspension medium because it was found to be sufficiently dense and nonreactive with the superconducting powder.

The experimental set-up (Fig. 9.3) consists of a glass column attached to the female part of the mould of dimensions 20 mm x 4 mm x 5 mm. Bromoform was filled in it to about 15 cm height. Superconducting powder was gently introduced into the bromoform by small amounts (about 0.05 gms each time) and the top portion of the column was stirred well. Sufficient time was given so that the powder settled in the mould. This process was repeated till the mould contained about 1 gm of powder. After this the bromoform was taken out gently, using a syringe and the glass column was removed. The powder with the mould was then slowly heated upto 120^oC and kept at this temperature for 12 hrs so that evaporation of bromoform was complete. After this, the powder was uniaxially pressed under a pressure of 200 MPa without disturbing the settled platelet grains. These samples were then sintered at 855 \pm 5^oC for 80 hrs in air. J_c of the samples were measured at 77 K by DC transport method using 1 $\mu\text{V}/\text{cm}$ criterion.

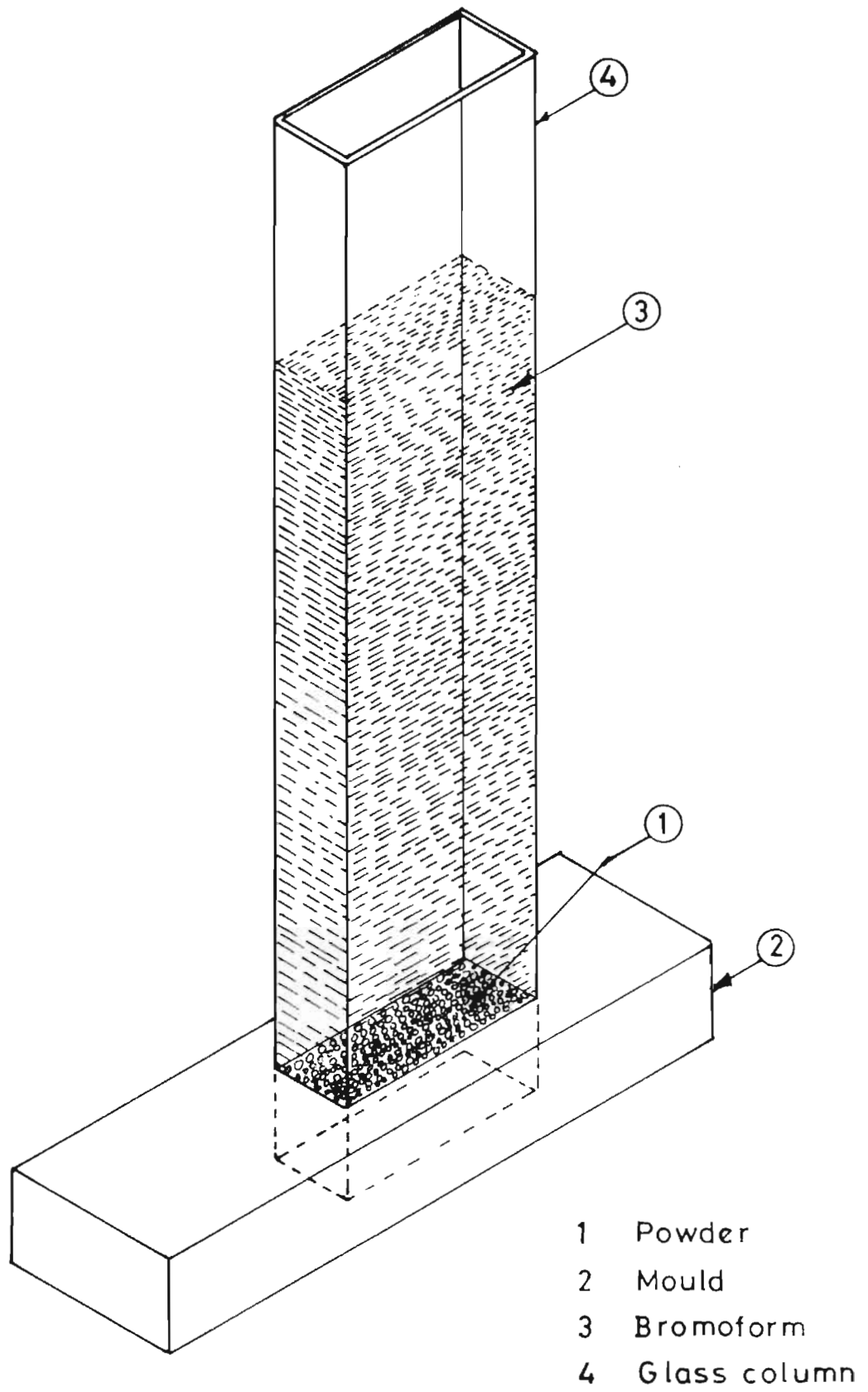


Fig. 9.3: Experimental set up for suspension

9.2.3 Results and discussion

Table 9.2 gives the $T_{c(0)}$ and J_c of the samples prepared conventionally and by suspension methods.

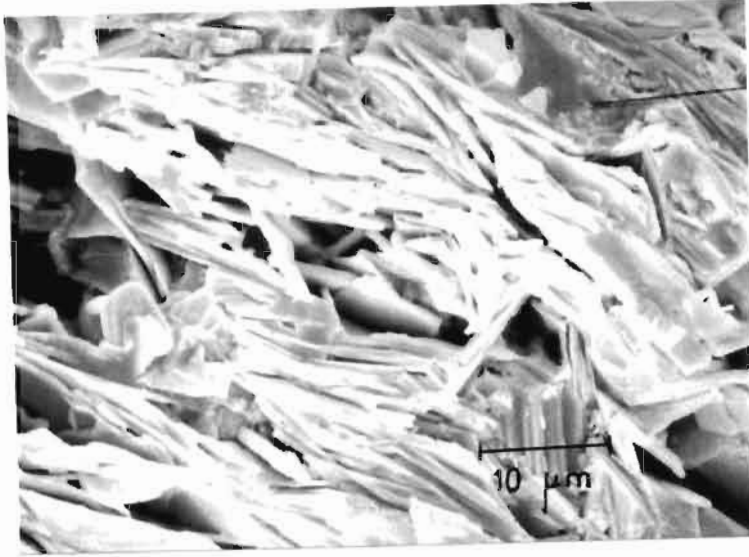
Table 9.2: $T_{c(0)}$ and J_c of samples prepared conventionally and by suspension method

Method of preparation	$T_{c(0)}$ (K)	J_c (A/cm) ²
Conventional	109	246
Suspension	109	716

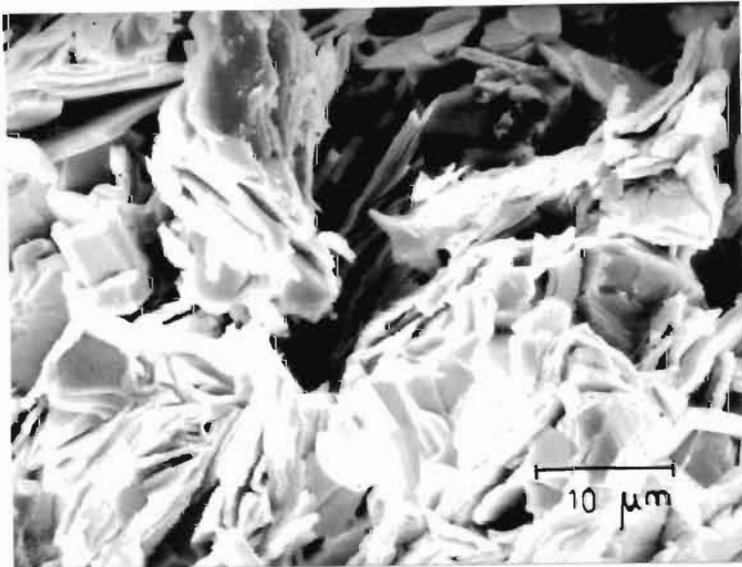
From the table it is clear that there is no change in $T_{c(0)}$ of the conventionally prepared and suspended samples whereas a significant improvement in J_c has been obtained by the suspension method.

Fig. 9.4 shows the SEM fractographs of the conventionally prepared and suspended samples.

About three fold increase in J_c in the sample prepared by suspension method compared to the conventional one can be explained only by taking account of the grain alignment as observed by the SEM photographs.



Suspension method



Conventional method

Fig. 9.4: SEM fractograph of the samples prepared conventionally and by suspension method

9.3 CONCLUSIONS

Preferential growth of planes and formation of 2223 phase in a 2223 stoichiometric precursor during the different annealing periods have been studied. (001) and (111) planes are found to grow preferentially. The growth of (001) planes was found to be much faster compared to (111) as the period of annealing increases. Moreover the increased growth of (001) planes was associated with the corresponding increase in the high T_c fraction. Thus it can be concluded that in a 2223-rich sample, the grains are platy in nature with grain growth along ab-plane.

Platy grains of BPSCCO were aligned so that their ab-planes lie in the same direction, by the suspension method by the use of bromoform. A three fold increase in J_c was found in the sample prepared by suspension method compared to that of the conventionally prepared one. Microstructure of these samples revealed the enhanced grain orientation in the sample prepared by the suspension method.

REFERENCES

1. P. Majewski, B. Hettich, H. Jaeger and K. Schulze, *Adv. Mater.*, 3(1), 67 (1991).
2. P. Bordet, C. Chaillout, J. Chenavas, J.L. Hodean, M. Marezio, J. Karpinski and E. Kaldis, *Nature*, 334, 596 (1988).
3. K. Aota, H. Hattori, T. Hatano, K. Nakamura and K. Ogawa, *Jpn. J. Appl. Phys.*, 28(12), L 2196 (1989).
4. H. Nobumasa, K. Shimizu, Y. Kitano and T. Kawai, *Jpn. J. Appl. Phys.*, 27, L 846 (1988).
5. S. Kobayashi, Y. Saito and S. Wada, *Jpn. J. Appl. Phys.*, 28, L 772 (1989).
6. S. Jin, *Science*, 238, 1655 (1987).

CHAPTER 10

**SUPERCONDUCTING AND MECHANICAL PROPERTIES OF
(Bi, Pb)-Sr-Ca-Cu-O/Ag COMPOSITE**

CHAPTER 10

SUPERCONDUCTING AND MECHANICAL PROPERTIES OF (Bi, Pb)-Sr-Ca-Cu-O/Ag COMPOSITE*

10.1 INTRODUCTION

High temperature superconductors are generally very brittle with unacceptably low strength [1,2]. The use of these materials in bulk application thus requires improvement of their mechanical properties. High yield strength is required to withstand the forces of magnetic fields and considerable ductility is necessary to fabricate wires and cables from the superconducting material. In order to resist crack initiation and propagation, the fracture toughness of these materials has also to be increased. These desired mechanical properties may be achieved by the addition of a ductile metal to the brittle superconductor to form a metal matrix composite. Apart from improving the load bearing characteristics, the presence of a metal can improve the deformability characteristics and avoid brittle fracture.

In the case of YBCO it has been established that Ag upto 50 wt% can be added without adversely affecting the T_c , while there is a considerable improvement in their mechanical properties [3-5]. The nonpoisoning effect of Ag addition in Bi-Sr-Ca-Cu-O system has also been reported by S. Jin et al [6]. But it has been reported by S.X. Dou et al [7] that Ag addition has a poisoning effect on

* This work has been partly published in:
a. Solid State Commun., 76, 659 (1990)
b. J. Mat. Sci. Lett., 11, 1437 (1992)

Bi-system doped with Pb(BPSCCO) when processed in air. According to them $T_{c(0)}$ has been found to be depressed to as low as 60 K for 30 wt% Ag when sintered in air.

In the course of present study, Ag composites of BPSCCO having Ag content upto 40 wt% have been synthesized by adding $AgNO_3$ and processing in air. Their superconducting and mechanical properties such as $T_{c(0)}$, J_c , flexural strength, % deflection at breakage, hardness etc. have been studied.

10.2 EXPERIMENTAL

Ag composites of BPSCCO were prepared by mixing Bi_2O_3 , PbO , $SrCO_3$, $CaCO_3$, CuO (stoichiometric ratio = 0.8/0.2/1/1/1.5), $AgNO_3$ (which was added to include the required wt% of Ag in the compound) and calcining at $800^\circ C$ for 12 hrs and $840^\circ C$ for 120 hrs in air with intermittent grinding. The resulting powder was pressed into rods having dimensions 40 mm x 3 mm x 2 mm and sintered at $840^\circ C$ for 80 hrs in air. X-ray diffraction was performed using $CuK\alpha$ radiation. Flexural strength and % deflection at breakage were measured in an Instron testing machine employing a span of 35 mm and depth of 2 mm. Sample hardness was measured using a Leitz micro hardness tester employing a load of 16.625 kg.

10.3 RESULTS AND DISCUSSION

10.3.1 Superconducting properties of BPSCCO/Ag composite

Table 10.1 gives the variation of room temperature resistivity,

contact resistance, $T_{c(0)}$ and J_c with wt% Ag in the composite.

Table 10.1: Room temperature resistivity, contact resistance, $T_{c(0)}$ and J_c of the composites

Wt% Ag	Room temp. resistivity (m Ω .cm)	Contact resistance (m Ω)	$T_{c(0)}$ (K)	J_c (A/cm ²)
0	1.68	0.15	110	147
5	0.56	0.18	108	155
10	0.56	0.13	108	162
20	0.52	0.12	107	267
40	0.52	0.12	107	191

From the table it is clear that Ag addition upto 40 wt% does not have any poisoning effect on the superconducting properties of BPSCCO system when processed under the present experimental conditions in air. The resistivity has been found to decrease with the addition of a small amount (4 wt%) of Ag itself. Addition of Ag has also been found to reduce contact resistance by an order of magnitude. Also, J_c is maximum for sample having 20 wt% of Ag as reported elsewhere [8].

The XRD patterns of various samples are shown in Fig. 10.1.

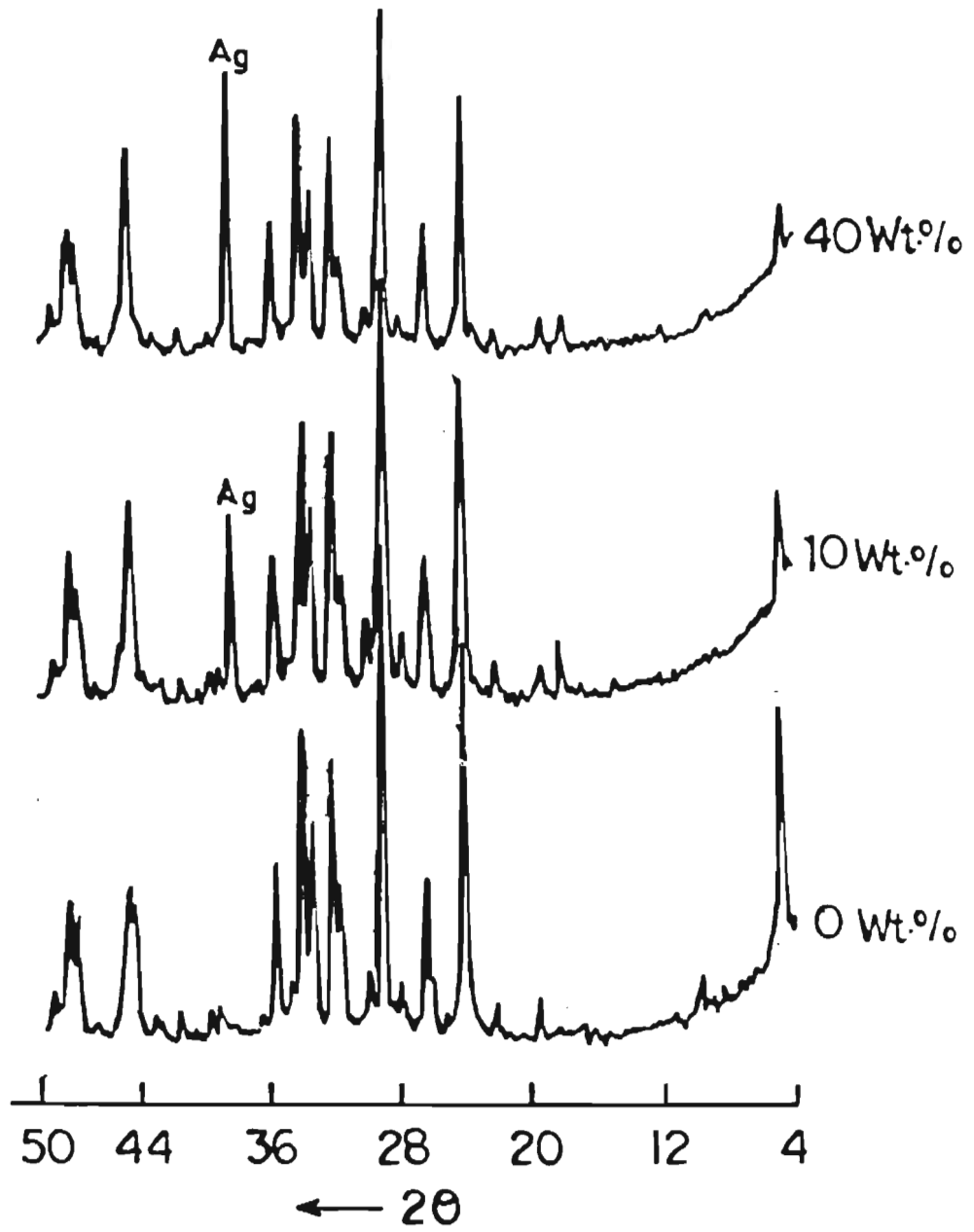


Fig. 10.1: XRD patterns of samples having different wt% Ag

Fig. 10.2 shows the optical micrograph of the polished surface of the sample containing different wt % Ag (X 400).

From the XRD patterns of the samples, the formation of $(\text{Bi, Pb})_2\text{Sr}_2\text{Ca}_2\text{Cu}_3\text{O}_{10}$ phase and the presence of Ag is clear. Also, there is a relative increase in the intensities of Ag peaks in the XRD patterns ($2\theta = 38.2^\circ$ and 44.4°) with wt% Ag. No significant change in the cell parameters were observed with Ag addition. The optical micrograph, (Fig. 10.2), shows the distribution of Ag in the superconducting matrix (where the white shining particles are Ag, the gray and black portions are superconducting phase in which the colour difference may be resulting from the difference in alignment of the platy grains). It shows that Ag particles are distributed uniformly in the continuous matrix of superconductor as observed in the case of superconducting Ag composites prepared by adding metallic Ag [9]. XRD patterns of the samples taken at different depths also showed that there is no change in the intensities of Ag peaks and thereby confirming the uniformity of the Ag distribution in the bulk. These observations show that the role of Ag is likely to be that of a second phase material in the superconductor which gives better connectivity between grains and reduces resistivity and contact resistance.

From the intensities of various X-ray reflections (Fig. 10.1), high T_c (2223 phase) fraction (HTf), impurity fraction (If) and texturing of (001) planes (T_{001}) were determined using the definitions already given in chapter 8. Table 10.2 gives the variation of these three parameters with wt% Ag added.



Fig. 10.2(a): Optical micrograph of the polished surface of the sample containing 5 wt % Ag (X 400)



Fig. 10.2(b): Optical micrograph of the polished surface of the sample containing 10 wt. % Ag (X 400)

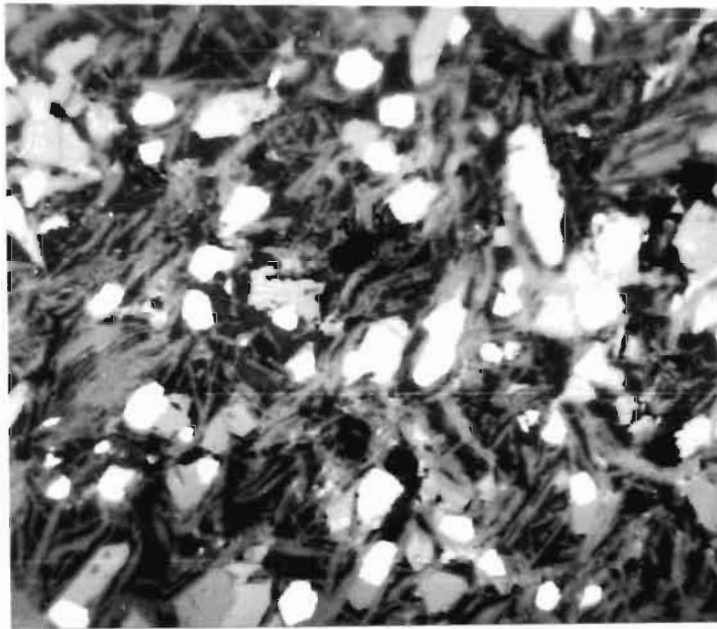


Fig. 10.2(c): Optical micrograph of the polished surface of the sample containing 20 wt. % Ag (X 400)

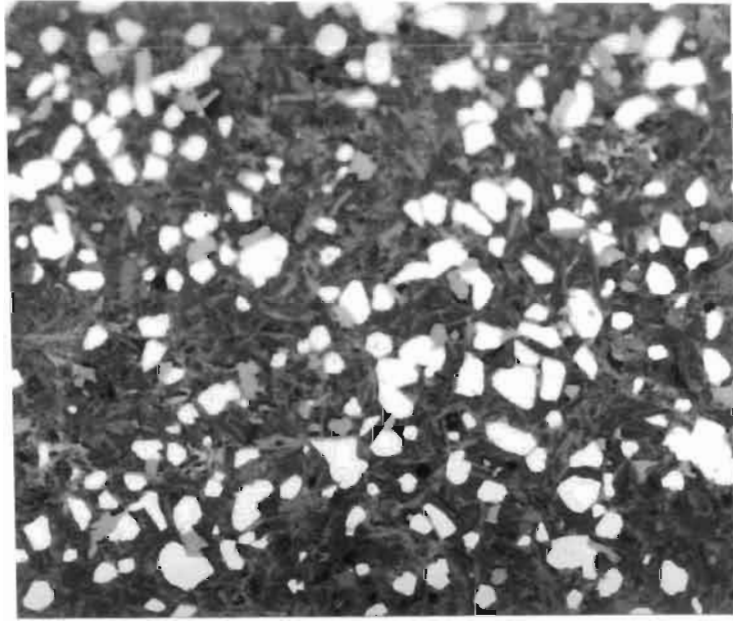


Fig. 10.2(d) : Optical micrograph of the polished surface of the sample containing 40 wt % Ag (X 400)

Table 10.2: HTf, If and T_{001} of the composites

Wt% Ag	High T_c fraction	Impurity index	Texture index
0	0.91	0	0.64
5	0.69	0.19	0.57
10	0.74	0.14	0.55
20	0.82	0.10	0.53
40	0.83	0.06	0.52

From the table, it is clear that texturing of (001) planes decreases by the Ag addition in BPSCCO system. But in the case of YBCO it has been reported that it is increasing [10]. Ag addition decreases high T_c fraction and increases impurity fraction in general. However with higher content of Ag, there is an increase in high T_c fraction as compared to the lower content with a simultaneous decrease in impurity fraction.

10.3.2 Mechanical properties of BPSCCO/Ag composite

Fig. 10.3 shows the variation of flexural strength and % deflection at breakage with wt% Ag in the composite.

From the figure it is clear that there is a considerable

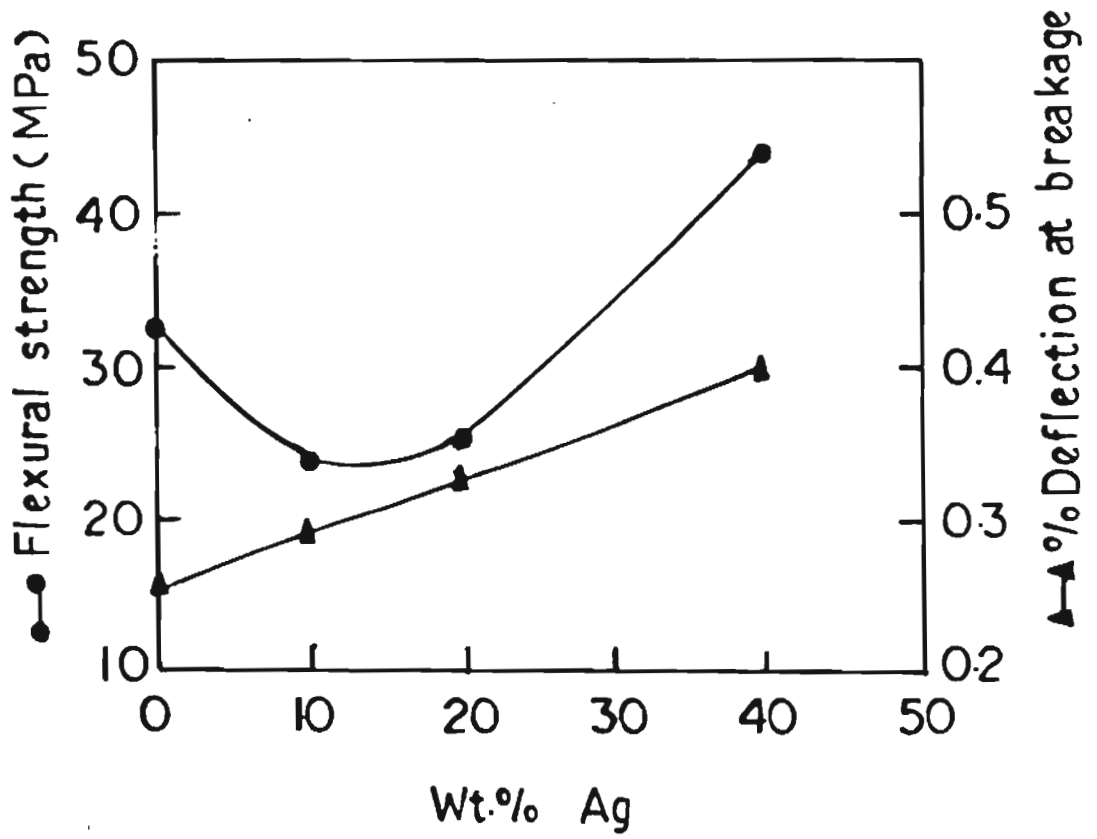


Fig. 10.3: Plots of flexural strength and % deflection at breakage vs wt. % Ag

improvement in these properties by the addition of Ag between 20-40 wt%. There is an initial drop in flexural strength upon addition of 10 wt% Ag. This is because, at low volume fraction of reinforcements in composites, stress concentration effect due to the presence of reinforcement particles is more, than the reinforcement effect. This causes premature failure of the composite and resulting in drop of ultimate failure of stress.

The plots of porosity and hardness vs wt% Ag are given in Fig. 10.4. The hardness values do not show any appreciable change between 20-40 wt% Ag. Porosity is found to be decreased significantly by the addition of Ag in the superconductor.

However the observed mechanical properties are unacceptably low for practical applications eventhough addition of Ag above 20 wt% showed remarkable improvement in the properties. One of the main reasons for this may be the high porosity (Fig. 10.4).

10.4 CONCLUSION

Superconducting Ag composite of Bi-Pb-Sr-Ca-Cu-O system having Ag content upto 40 wt% was synthesized by adding AgNO_3 and processing in air, without any considerable decrease in $T_{c(0)}$. J_c was found to be maximum for samples having ~20 wt% Ag. Also, the role of Ag was found to be that of a second phase material distributed uniformly in the superconducting matrix which gives better connectivity between grains and thus reduces both resistivity and contact resistance. Texturing of (001) planes was seen to be decreased

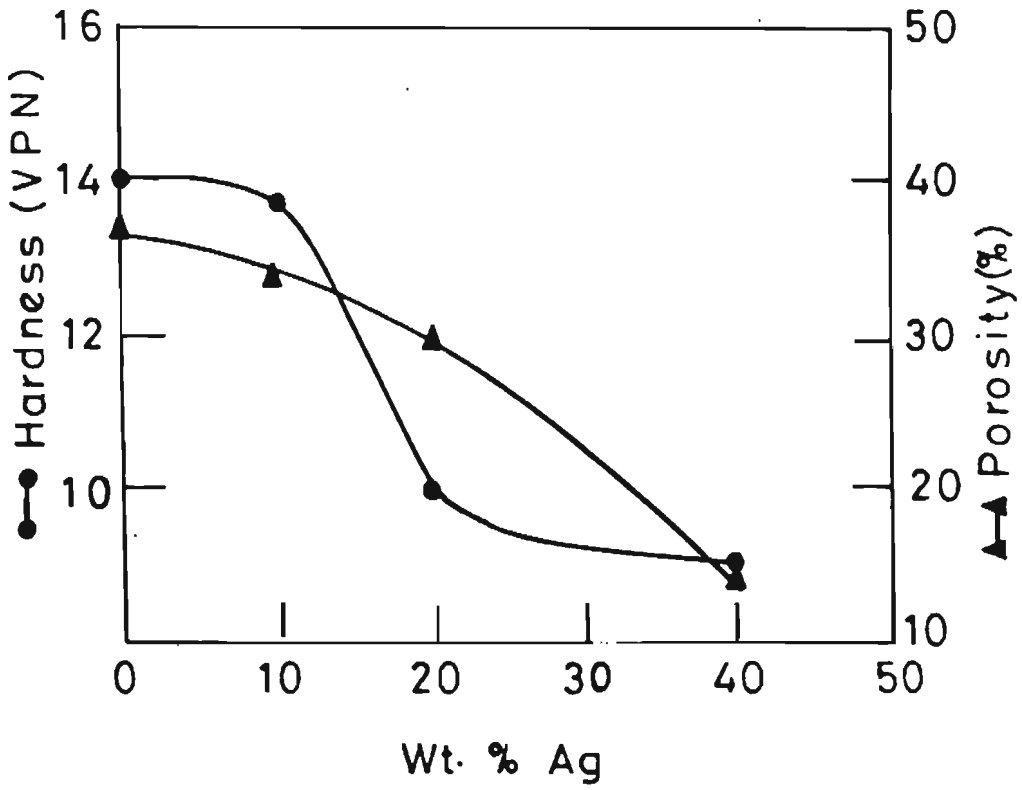


Fig. 10.4: Plots of hardness and porosity vs wt. % Ag

by the Ag addition in BPSCCO system.

There is considerable improvement in flexural strength and % deflection at breakage by the addition of Ag between 20-40 wt%. The hardness do not show any appreciable change between 20-40 wt%. Porosity is found to be decreased significantly by the addition of Ag in the superconductor.

REFERENCES

1. G.W. Crabtree, J.W. Downey, B.K. Flandermeyer, J.D. Jorgensen, T.E. Klippert, D.S. Kupperman, W.K. Kwok, D.J. Lam, A.W. Mitchell, A.G. Mckale, M.V. Nevitt, L.J. Nowicki, A.P. Paulikas, R.B. Poeppel, S.J. Rothman, J.L. Routbort, J.P. Singh, C.H. Sowers, A. Umezawa, B.W. Veal and J.E. Baker, *Adv. Ceram. Mater.*, 2, 444 (1987).
2. R.F. Cook, T.M. Shaw and P.R. Duncombe, *Adv. Ceram. Mater.*, 2, 606 (1987).
3. D. Pavuna, H. Berger, M. Affronte, J. Van der Maas, J.J. Capponi, M. Guillot, P. Lejay and J.L. Tholence, *Solid State Commun.*, 68, 535 (1988).
4. R. Prasad, N.C. Soni, A. Moham, S.K. Khera, K.V. Nair, C.K. Guptha, C.V. Tomy and S.K. Malik, *Mater. Lett.*, 7, 9 (1988).
5. C. Laubschat, M. Domke, M. Prietsch, T. Mandel, M. Bodenbach, G. Kaindl, H.J. Eichenbusch, R. Schoellhorn, R. Miranda, E. Moran, F. Gracia and M.A. Alario, *Europhys. Lett.*, 6, 555 (1988).
6. S. Jin, R.C. Sherwood, T.H. Tiefel, G.W. Kammlott, R.A. Fastnacht, M.E. Davis and S.M. Zahurak, *Appl. Phys. Lett.*, 52, 1628 (1988).
7. S.X. Dou, K.H. Song, H.K. Liu, C.C. Sorrell, M.H. Apperley, A.J. Gouch, N. Savvides and D.W. Hensley, *Physica C*, 160, 533 (1989).
8. K.H. Song, H.K. Liu, S.X. Dou, C.C. Sorrell, N. Savvides and G.J. Bowden, *J. Mat. Sci. - Materials in Electronics*, 1, 30 (1989).
9. J.P. Singh, H.J. Leu, R.B. Poeppel, E. Van Voorhees, G.T. Goudey, K. Winsley and D. Shi, *J. Appl. Phys.*, 60, 3154 (1989).
10. M.K. Malik, V.D. Nair, A.R. Biswas, R.V. Raghavan, P. Chaddah, P.K. Mishra, G. Ravikumar and B.A. Dasanacharya, *Appl. Phys. Lett.*, 52, 1525 (1988).

SUMMARY

The main objective of the work reported in this thesis is to study the ways and means of imparting desirable properties to high temperature superconductors so that they can be considered for practical applications in bulk form. With this objective, studies were conducted and the results obtained are summarized below.

The effect of varying the processing parameters like P_{O_2} , temperature and soaking period during the calcination stage of YBCO show that (i) grain growth along ab-plane is accelerated by the decrease of P_{O_2} , if the processing temperature is kept constant, (ii) if the P_{O_2} is kept constant, the grain growth along ab-plane is accelerated as the processing temperature increases, (iii) if P_{O_2} , processing temperature and soaking period are suitably selected, platelet grains of desired size (within a range of 5-100 μm) can be synthesized.

Apart from establishing the dependence of growth of platy grains of YBCO on the processing parameters, this study has also indicated that YBCO phase formation in the conventional ceramic route commences at lower temperatures if the oxygen partial pressure is reduced.

Studies on comparatively low amounts (upto 20 at. wt%) of Li, Na and K substituted YBCO have shown that textured grain growth is maximum for Li substitution followed by Na and K for the same

amount of substituents. In all the cases, with the increase in substituent concentration, textured grain growth is also found to be increased. Li-substitution severely affects $T_c(0)$ whereas the effect of Na and K are less pronounced.

A model for the textured grain growth in YBCO has been proposed which is based on the oxygen vacancy creation under different experimental conditions. When the processing of YBCO is done at a low P_{O_2} , the ab-plane will have a large number of vacant oxygen sites which facilitates easy mass transport and hence an increased textured grain growth. Similarly the enhanced textured grain growth resulting from the substitution of alkali metals for various cations in YBCO can also be accounted by the accelerated mass transport resulting from the generation of vacant oxygen sites. The calculation of oxygen stoichiometries at processing temperature using the proposed model shows that in the case of Li and K substituted samples, the observed values match very well with the prediction of the model, i.e., release of one oxygen atom for every two alkali atoms substituted. In the case of Na substitution the fit was very well except for the deviation for the Na stoichiometry around 0.05.

Moreover it was observed that in the case of Li substituted samples, oxygen vacancy concentration is the main factor influencing the platy grain growth whereas in Na and K substituted samples, other properties also may have to be considered. Another important result that was obtained from this study is the evidence for increased oxygen absorption rate in alkali metal substituted samples in comparison with

that of pure YBCO.

Cold pressing was found to align the grains on a thin layer below the pressed surface. The degree of grain alignment was found to depend on both the pressure applied as well as the grain size. Longer periods of sintering was found to impart deeper penetration of grain alignment into the interior of the samples. The J_c of samples prepared by pressing platy grains of undoped YBCO was found to be higher than that of those prepared from grains of nearly spherical shape. Also the J_c of sample prepared from grains of size between 15 μm and 30 μm was found to be higher than the other samples included in this study.

The effect of cold pressing and heat treatment on the grain alignment in alkali metal substituted samples was similar to that of the undoped YBCO. Despite this, the J_c of substituted sample was found to be very low compared to that of undoped YBCO.

Experimental set-up for the synthesis of phase pure YBCO by dynamic vacuum calcination has been fabricated. Processing parameters for synthesis of phase pure YBCO powders upto 100 gms have been standardized. The merits of vacuum calcination are, (i) powder with higher purity, less grain size, (ii) less processing temperature and soaking period, (iii) sintered samples having higher J_c and better stability against magnetic field and (iv) powder is more stable to the atmospheric conditions.

From the studies of initial stoichiometry variation in

(Bi,Pb)-Sr-Ca-Cu-O system, it was observed that the sample having initial stoichiometry $\text{Bi}_{1.6}\text{Pb}_{0.4}\text{Sr}_2\text{Ca}_{2.2}\text{Cu}_3\text{O}_y$ gives the best structural and superconducting properties.

X-ray diffraction studies revealed that in a 2223-rich sample, the grains are platy in nature with grain growth along ab-plane. These platy grains of BPSCCO were aligned by the suspension method using bromoform. A three fold increase in J_c was found in the sample prepared by suspension method compared to that of the conventionally prepared one. Microstructure of these samples revealed the enhanced grain orientation in the sample prepared by the suspension method.

Superconducting Ag composite of Bi-Pb-Sr-Ca-Cu-O system having Ag content upto 40 wt% was synthesized by adding AgNO_3 and processing in air, without any considerable decrease in T_c . J_c was found to be maximum for samples having 20 wt% Ag. Also, the role of Ag was found to be that of a second phase material distributed uniformly in the superconducting matrix. There is considerable improvement in flexural strength and % deflection at breakage by the addition of Ag between 20-40 wt%. The hardness do not show any appreciable change between 20-40 wt%. Porosity is found to be decreased significantly by the addition of Ag in the superconductor.